Acoustic Design of Super-light Structures

Christensen, Jacob Ellehauge; Hertz, Kristian Dahl; Brunskog, Jonas; Kjær, Martin V.

Publication date:
2013

Document Version
Publisher's PDF, also known as Version of record

Acoustic Design of Super-light Structures

- DTU Byg Ph.D. thesis

J.E. Christensen

Ph.D. Thesis

Department of Civil Engineering
Technical University of Denmark

2013

Supervisors:

Professor K.D. Hertz, Technical University of Denmark, Denmark
Associated Professor J.Brunskog, Technical University of Denmark, Denmark
Marketing Director M. V. Kjær, Aarhus Grontmij A/S, Denmark

Assesment Committee:

Professor L.C. Hoang, University of Southern Denmark, Denmark
Professor K. Virdi, University of Aarhus, Denmark
Professor A. Ågren, Luleå University, Sweden

Acoustic Design of Super-light Structures
-DTU Byg Ph.D. thesis

Printed by DTU-Tryk
Department of Civil Engineering
Technical University of Denmark
ISBN: 0000000000000
ISSN: 0000-0000

Preface

This thesis is submitted as a partial fulfilment of the requirements for the Danish Industrial Ph.D. degree. The work has been carried out as a collaboration between at the Department of Civil Engineering at the Technical University of Denmark and the Grontmij Consulting Engineers Inc. at the Department of Structural and Fire Engineering at the Glostrup (Copenhagen) Office. The main supervisor is Kristian Dahl Hertz from The Department of Civil Engineering and Associate Professor Jonas Brunskog from the Department of Electrical Engineering as co-supervisor. From Grontmij Consulting Engineers Inc, Marketing Director Martin Venning Kjær, Chief Advisor Poul Erik Haurbæk, Head of the Department of Structural and Fire Engineering Karen Gaarden, Per Alan Olsen and Claus Møller Petersen, has all been a part of a co-supervising team.

Four papers are appended as a part of this thesis.

- Paper I: Airborne and impact sound transmission loss in super-light structures.
- Paper II: Simulation of flanking transmission in super-light structures.
- Paper III: Super-light concrete decks.
- Paper IV: Super-light precast deck elements integrated in a traditional concrete precast element construction.

The acoustics tests have been designed by the author who also has made the acoustical experiments and simulations. Likewise the analyses of the acoustical results have been made by the author. The static and fire tests have been designed, carried out and analysed in collaboration with the main supervisor Kristian Dahl Hertz, phd-student in super-light structures Niels Andreas Castberg and two M.Sc. students as a part of their master thesis. The design of the super-light elements used for indoor pedestrian bridges has been made by the author, as a part of the industrial Ph.D. project, at the Department of Structural and Fire Engineering, Grontmij Consulting

Engineers Inc.

Lyngby, the 24th February 2013

J.E. Christensen

Abstract

Super-light structures is a newly developed and patented construction principle for concrete structures. It combines some of the desirable properties of normal strong concrete and lightweight aggregate concrete in order to improve the utilization of the materials and to design improved concrete structures and elements.

The super-light slab element in the present research is developed as a holistic design including all relevant disciplines. The element is based on well-known technologies and materials, which have been used for millenniums, namely compression arches and lightweight expanded clay aggregate (leca) along with a newly developed technology called pearl-chain reinforcement, which is a system for post-tensioning. Here, it is shown how to combine these technologies within a precast super-light slab element, while honoring the requirements of a holistic design.

Acoustic experiments in a controlled laboratory environment have been conducted with the element in order to evaluate its performance in airborne and impact sound insulation. These results have been employed in simulations of the flanking transmission to estimate the in-situ performance of the super-light slab element. The flanking transmission has been done both in a standard room consisting of precast concrete elements and as a parametric study in order to estimate the accuracy of the used model.

Experiments on the ultimate limit state regarding moment, shear and pull-out resistance is carried out for the super-light element. As a part of the same test series elastic behaviour of the super-light element is also investigated. This is done to verify that requirements and methods supplied by design codes can be applied to the element with sufficient accuracy. In addition, the super-light slab element has been exposed to a standard fire test.

A demo project, where a variation of the super-light element is included as indoor pedestrian bridges, has been designed and constructed. The support system was complicated and included a high amount of point supports. This required a high degree of versatility of the super-light element, as sev-

eral known technologies were integrated and developed for the super-light element, in order to construct the pedestrian bridges.

Resumé

Super-lette konstruktioner er nyudviklet og patenteret konstruktionsprincip for betonkonstruktioner. Det kombinerer nogle af de gode egenskaber af normal stærk beton og letklinkerbeton så materialerne kan blive bedre udnyttet og gør det muligt at designe forbedrede betonkonstruktioner og elementer

Det super-lette dæklelement i den nærværende forskning er udviklet som en holistisk design, ved at inkluderer alle relevante discipliner. Elementet er baseret på velkendte teknologier og materialer, der har været brugt i årtusinder, det drejer sig om trykbuer og letvægtsbeton (LECA) sammen med en nyudviklet teknologi kaldet perle-kæde aremering, som er et system for efterspænding . Her er det vist hvordan man kan kombinere disse teknologier i et præ-fabrikeret super-let dækelement, mens kravene til et holistisk design er honoreret.

Akustiske målinger er blevet udført med elementet i et kontrolleret laboratorie miljø for at evaluere dets præstation i luftlydsisolering og trinlydsisolering. Disse resultater er blevet anvendt til simuleringer af flanketransmission af et super-let dækelement for at vurdere dets in-situ præstation. Flanketransmission er blevet undersøgt i både et standard rum, der består af præ- fabrikerede betonelementer og ved en parametrisk undersøgelse for at vurdere præstationen i et ukendt rum og for at vurdere nøjagtigheden af den anvendte model.

Forsøg af brudgrænsetilstanden mht. moment-, forskydnings- og forankrings bæreevner er udført for det super-lette element. Som en del af den samme eksperimentelle testserie er de elastiske strukturelle egenskaber af det superlette element også undersøgt. Dette gøres for at kontrollere, at kravene og fremgangsmåderne der er specificerede i design standarderne kan anvendes til dækelementet med tilstrækkelig nøjagtighed. Desuden har det super-lette dækelement succesfuldt været udsat for en to timers lang standard brandprøvning.

En modificeret udgave af det superlette element er blevet brugt til et demo-project, hvor indendørs gangbroer er blevet designet og bygget. Understøtnings betingelserne er komplicerede da der er stor mængde punkt un-

derstøtninger. Dette krævede en høj grad af tilpasning af det super-lette dækelement, hvor flere kendte teknologier er blevet integreret, samt udviklet til det super-lette dækelement med henblik på at kunne konstruere gangbroerne.

Contents

Part I

Introduction and summary

Chapter 1

Introduction

Pre-fabricated concrete elements are used throughout the building industry in Denmark and similar countries, where high labour cost favours prefabricated elements rather than the labour-intensive in-situ cast method for concrete structures (Jensen 1991). Additionally, the geographical location of Denmark favours concrete rather than steel as building material since the natural resources of Denmark can supply a self-sustained cement production but not a steel production. Pre-fabricated building elements have been used through history of time and dates back till 3000 B.C., e.g., the sweet track, an ancient causeway is constructed from pre-fabricated timber elements (Cunliffe 2005). However, the modern technology of pre-fabricated concrete building elements, in particular for residential multi-storey housing, was invented in the late 19th century and early in the 20th century in England (Sutherland et al. 2001). The speed of development was greatly increased after the second world war, where large parts of the infrastructure needed to be rebuild quickly and cheaply (Bullock 2002). In Denmark the pre-fabricated concrete elements were developed as an industry in the 1950s with the development of the hollow core slab, and from that time they have more or less been the preferred choice for the building industry in Denmark (Jensen 1991).

Since the 1960s demands of general living conditions and structures have increased steadily. This is expressed in standards and in the Danish building regulations (Bygningsreglementet 2008). Here a sharpening of the requirements in relation to the performance of structures and the quality of living in general, constitute a basis of a new version of the regulations. In many ways these new building regulations have acted as a motivation for developing the super-light slab element as an alternative to patching of older known solutions, so that they comply with newer regulations. This includes fire safety, where the structure at last should be able to allow for evacuation,

before the structural safety is compromised, and demands to both building and room acoustics. In addition, the level of vibration should be limited for personal comfort, although this is not required by the building regulation. The acoustic standards have likewise been developed in the 1960s, where the first requirements were formulated, and they have since regularly been tightened. Something else which has not yet been specified by any standard, but regardless receives a lot of attention from media and public in general is the influence on the environment caused by CO_2 emission.

To meet these trends of current and future expected requirements a super-light slab element has been developed and designed as a holistic design, which integrates and fulfil all functional requirements with respect to load-bearing capacity, energy consumption, material consumption, acoustics, indoor climate, fire safety, economy, applicability, and aesthetics. One of the biggest challenges in the design is to make the super-light slab element as light as possible in relation to the goal of achieving an acceptable acoustical performance, as this is traditionally associated with high mass. It is expected that it is the acoustical properties, namely sound insulation, which will suffer most from the reduction of mass, and therefore carries the main emphasis of the design. The design is carried out in order to save material and thus reducing the cost of production and transportation along with the CO_2 emission (Hertz and Bagger 2011).

Super-light slab element

The super-light element is developed from the general super-light technology. Due to requirements of a maximum element height, set to 215 mm, it is not possible to utilize all the features of super-light structures, which are described in Chap. 2. The height is limited in order to be compatible with the existing pre-fabricated concrete element scheme. The original principle of pearl-chains has been omitted in single elements, but the principle can be applied to several elements as it is discussed n Chap. 2. If the design of the element was based solely on statics, it would have been possible to utilize the super-light principles so that the element would be lighter compared to the present design of a super-light slab.

In order to save weight compared to comparable concrete elements the super-light slab element is constructed from two different concrete materials, namely a normal concrete and a lightweight aggregate concrete based on expanded clay. In order to save material and achieve acceptable acoustics properties the function of the slab element depends on interaction between the two concretes. In addition, the two different concrete parts are geometrically

formed, so that the element will behave isotropic in regards to optimizing the acoustic properties of the plate. The use of porous lightweight expanded clay aggregate concrete with a high thermal insulation greatly improves the thermal insulation performance of the element and provides good insulation of the pre-stressed reinforcement in regards to structural fire safety. The porous structure of the lightweight aggregate structure also provides increased sound absorbing qualities compared to normal concrete (McElroy 1990).

The statics of the element has been investigated for both the ultimate and the serviceability limit state and the results are presented in Chap. 4 and the accompanying paper (Hertz et al. 2013) with a main emphasis on validating known design formulas in relation to codes for actions on structures (Eurocode 1-1-1 2002) and (Eurocode 1-1-2 2002) and codes for concrete structures (Eurocode 2-1-1 2004) and (Eurocode 2-1-2 2004). A demo project with a variation of the super-light deck element has been constructed and built in practice. Here the element is used for indoor pedestrian bridges serving as access routes. This project and the deck element is presented in Chap. 5 and the accompanying paper (Christensen and Hertz 2013).

Acoustics

One of the main problems in relation to present standards of living is the acoustic comfort. This is especially true for apartments, where both noise coming from neighbours and the restraint of not being able to do noisy activities in order to not annoy neighbours, are reducing the living quality for inhabitants of apartments. In addition, the acoustical requirements, which were formulated in the 1960s, are based on speech and footfall as the main noise sources. This is no longer the case. Especially hi-fi equipment has changed the average power spectral density of noise produced by households to include more noise in the lower and higher frequency range (Hopkins 2007, Chapter 1). This means that even when the acoustical standards are obeyed, the acoustical performance can still be rated individually as dissatisfactory, since the regulations are based on the building acoustic frequency range limited to $100 - 3150$ Hz. Traditionally acoustical ratings of building elements are done by a single number rating for both airborne and impact sound insulation. This is based, and dates back to the 1960s, on a reference curve (ISO 717-1 1996) and (ISO 717-2 1996). Single number ratings can be obtained by laboratory measurements (ISO 10140-2 2010) and (ISO 10140-3 2010) where flanking often is excluded. Single number ratings can also be obtained through calculations (EN12354-1 2000) and (EN12354-2 2000) where flanking can be included if the flanking partitions

is known. Later a correction term called the spectral adaption term has been introduced to address problems with the limited frequency range for building acoustics. This is done by supplying methods to obtain metrics on an extended frequency range to 50 Hz to 5000 Hz (ISO 717-1 1996) and (ISO 717-2 1996).

Legislation concerning sound insulation in the various European countries is documented by (Rasmussen 2010) and (Rasmussen and Rindel 2010), where the difference in evaluation metrics regarding sound legislation is discussed. The analysis covers 24 European countries and reveals great inhomogeneous legislation across Europe for both requirements to the single number rating and the metrics used to evaluate the acoustics. For airborne sound insulation 9 different description are used with a difference in single number rating requirements for multi-storey housing up to 5 dB. For impact sound insulation 5 different descriptors is used and a maximum difference of 15 dB is found in the various countries legislation. In addition only one country (Sweden) has included low-frequency adaption terms in its legislation. The many different descriptors in use make it hard to compare legislation between different countries. Nine of the 24 countries have introduced a classification scheme where buildings and buildings elements can be rated, (DS490 2007) is valid for Denmark.

In the Nordic countries the sound insulation is rated from A to D in a classification scheme, A being the best, C being the requirement and D the worst only applicable in special cases. The pre-mentioned spectral adaption term is for most countries only applied in class A and B as it is also the case for Denmark. A survey shows that more than 90% of inhabitants are satisfied with the insulation supplied by rating A and 50%-65% are with the insulation supplied by rating C (DS490 2007). In Denmark the latest edition of building regulations came in 2008 (Bygningsreglementet 2008). Here, vertical airborne sound insulation was increased in terms of the single number rating from 53 dB to 55 dB and impact sound insulation was increased in terms of the single number rating from 58 dB to 53 dB. These new requirements are identical with the classification C, but as the results of the survey show for class C, which is identical to the new requirements, less than two-thirds of the population is satisfied (DS490 2007). This leaves space for further tightening of the legislation as a very realistic possibility in the future. The super-light slab element is already partly prepared to such changes by e.g. increasing the density of the lightweight aggregate concrete blocks, changing the geometry of the lightweight aggregate concrete or developing an element with a height of 265 mm, which is equivalent to the next tier of element height in the pre-fabricated concrete elements construction scheme.

For the acoustic development of the super-light slab element the main em-

phasis has been on the airborne sound insulation, based on the idea that the impact sound insulation is handled by an external floor. The acoustic measurements, simulations and analysis of the super-light element is described in Chap. 3 and the accompanying papers (Christensen et al. 2013a) and (Christensen et al. 2013b).

Chapter 2

Super-light technology

A super-light structure is developed in order to optimize concrete structures, so that the strong concrete is only applied, where it is needed, which is usually in arches. A lighter weaker concrete fills out the shape and stabilizes the strong concrete. The name *super-light* is derived from the original first principle, which is also explained later in this section for a beam in Fig. 2.1. Utilizing a high-strength concrete ($f_c > 80\,\text{MPa}$) to construct the beam in the example it can be made lighter than an equivalent steel beam. As steel structures are generally considered lightweight structures compared to concrete structures, the super-light structures was named in a provoking fashion. However, due to the need for a high surface mass when considering acoustic requirements, the first thought was to develop a super-light element $10 - 20\%$ lighter than a hollow-core element which typically has a surface mass of $340\,\text{kg/m}^2$, (Betonelement 2010) and (Spæncom 2010), by utilizing the combination of the two concretes. The very first super-light slab element design, which is the one described in the end of this chapter, had a surface density of $289\,\text{kg/m}^2$.

The main concept of super-light structures is elaborated and described by (Hertz 2010) and (Hertz 2009). Here those concepts are shown by a simple tall beam. Several iterations of the principle where the complexity increase are shown in Fig. 2.1. The first beam shows a normal reinforced concrete beam where a full section of normal heavy concrete is present. The second part shows an arch of normal concrete accommodating in shape both the internal and external load, but the supports must be able to take the horizontal forces from the arch. The arch is surrounded by lightweight aggregate concrete in order to protect the load-bearing normal concrete against buckling and fire. To further expand about the idea of minimal structures the load-bearing concrete could be a high strength concrete of 100 MPa or more. The third iteration adds reinforcement in the shape of prestressed high strength

concrete taking the tension as unloaded compression. This is placed in the bottom of the beam to deal with the horizontal forces associated with the forces in the arch. Finally, the last iteration is statically equal to the third, but here the arch is made from straight segments of concrete along with segments shaped as wedges to angle the straight segments in order to create the arch. This concept is called pearl-chain reinforcement and it is elaborated on in Sec. 2.3.

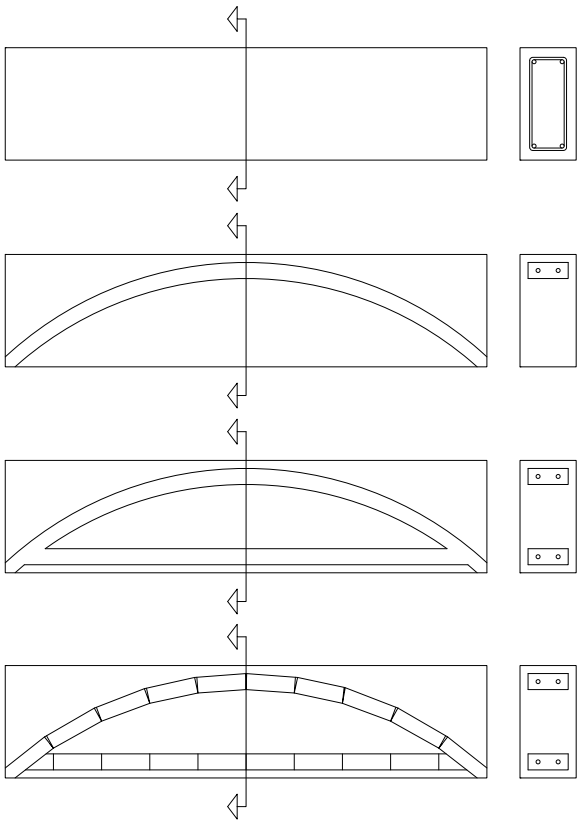

***Figure 2.1**: The overall principle of super-light structures explained in a beam*

By minimizing the material consumption by use of compression arches it is possible to make the super-light element lighter than similar concrete elements in analogy to the iterations in Fig. 2.1. In other words the main feature of a super-light structure is to place the load-bearing high-strength concrete where it is most useful. With the good compression strength of concrete, this will often be as arches or vaults, but it could also be arranging the load-bearing concrete in truss-formations using prestressed pearl-chain

reinforcement in tension elements. In all cases, the lightweight aggregate concrete will be present for stabilizing against buckling, protecting against fire, and in some cases for utility such as shaping the element to comply with architectural features.

2.1 Materials

The super-light deck elements are made from two different concretes in addition to reinforcement. One of the concretes is a normal concrete with a relatively high characteristic strength 55 MPa and density 2300 $\mathrm{kg/m^3}$, the other is a lightweight expended clay aggregate with low characteristic strength 3 MPa and density 600 $\mathrm{kg/m^3}$. The characteristic stiffness of the concretes are 38 GPa for the normal concrete and 3 GPa for the lightweight aggregate concrete. Loss factors for the concretes are $0.004 - 0.008$ for normal concrete and approximately 0.01 for the lightweight aggregate concrete, (Cremer and Heckl 1973). For the prototype elements used for the experiments another normal concrete was used with a characteristic strength of 50 MPa and characteristic stiffness of 37 GPa.

The plasticity of a concrete used for e.g. hollow core elements is limited so that the hollow cores can be created by an extruder without collapsing. This consideration is not needed for the normal concrete used in the super-light structures. Here it is desirable to have a high plasticity to ensure that the connection between the lightweight aggregate concrete and the normal concrete is strong by letting the normal concrete penetrate the surface of the porous lightweight aggregate concrete. The increased plasticity also ensures that the normal concrete reaches all corners which can be created by the geometry of the lightweight aggregate concrete, which is important in order to create a proper cover layer of the normal dense concrete at the reinforcement in relation to steel corrosion.

2.2 Arches

The static properties of an arch combine well with the material properties of concrete. If an arch is carefully constructed according to its load e.g. catenary for self-weight, parabola for an uniformly distributed load or straight lines between point loads, a cross-section in full compression can be archived and the arch resembles the simple statics of a column.

In the general concept of super-light structures arches are widely employed as the load carrying mechanism. This is exemplified in a couple of

projects where the arches in super-light structures have been used as cornerstones of the design (Castberg and Hertz 2012a), (Castberg and Hertz 2012b).

An investigation of the influence of the shape of arches in a concrete beam as the ones shown on Fig. 2.1 has been carried out and is documented in (Bagger and Hertz 2010). The main results were that sharp bends of an arch would create locally concentrated stresses and that the forces would follow the overall shape of the arch, whether it was shaped as part of a circle, spline or straight segments adjusting the flow of compression forces to the cross-section of normal concrete. This result has been used in the super-light slab element, where the lightweight aggregate is cast with straight lines, rather than a curved shape, while compression arches are still emerging in the normal concrete over the of the shape of lightweight aggregate concrete.

2.3 Pearl-chain reinforcement

Pearl-chain technology is described by (Hertz 2011) and has been developed in 2008, shortly after the actual concept of super-light structures was developed. The main purpose of pearl-chain reinforcement is to support super-light structures by an alternative method to create arbitrary shapes of the strong concrete of super-light structures without the need for expensive and time consuming curved scaffolding and moulds.

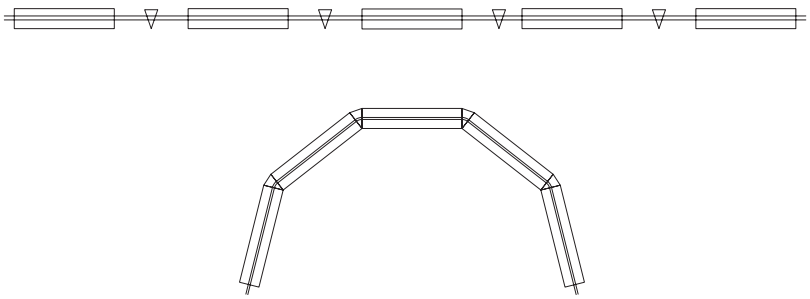

***Figure 2.2**: The concept of pearl-chains in super-light structures, at the top the shapes on a line, at the bottom after reinforcement have been post-tensioned and an arch is established.*

The general principle of pearl-chains is shown on Fig. 2.2, where segments of straight and angled, easy to shape and cast, concrete elements are shown and a vault is created by combining the linear straight blocks with the wedges or by application of straight elements with inclined ends. More advanced

shapes can be created if so desired. Several super-light slab elements may be combined as a pearl-chain to create an arch with a long span. The pearl-chain segments are provided with a steel wire in a duct. The wire will be post-tensioned and compresses the segments together, which then will shape the curved structure they are intended to, and can serve by taking tension stresses as unloaded compression.

2.4 Super-light slab element

The super-light element is developed utilizing the above mentioned technologies when applicable. Developing a super-light slab element is an iterative process, where many factors influence the direction of the design/redesign. The first edition of the pre-fabricated element had a width of 1.2 m and the testing described here has been done with that design. The latest design has a standard width of 2.4 m, other parameters such as the geometry of the lightweight aggregate blocks have also been changed. The changes are due to numerous issues including demands and needs from manufactories, which introduce limits for the geometry of the design, production cost also influence some of the parameters, while other parameters are influenced by design requirements. The various lab tests discussed in Sec. 3 and Sec. 4 have influenced the design along with the demo project discussed in Sec. 5 where an earlier edition of the element has been used. The changes to the element and their influences are discussed in Sec. 6.

The element described in the following is the edition on which most of the work in this thesis is based. The super-light element is made from the two concretes described in Sec. 2.1. The lightweight aggregate concrete is cast in a special custom-made mould so it constitutes a block. The block and its measurements are shown in Fig. 2.3. This geometry creates grooves between the lightweight aggregate blocks which are as deep as possible without compromising the thermal insulation property of the lightweight aggregate concrete in relation to fire and the ability to cast the block. Moreover, still deep and wide enough to place reinforcement strands in bundles in them with a reasonable internal moment lever arm and concrete cover to protect against corrosion and taking the prestress forces without cracking. A total of three blocks are placed in the width of a 1.2 m wide element.

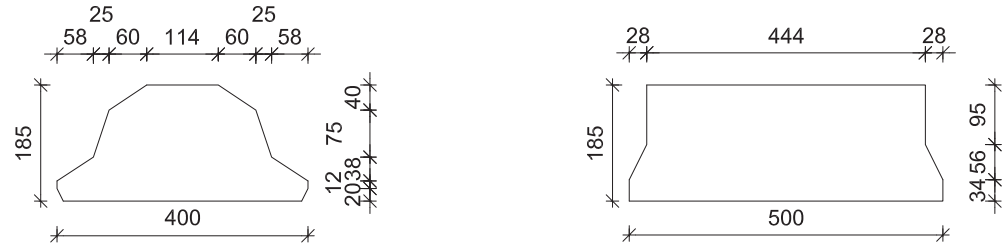

***Figure 2.3**: The lightweight aggregate block, dimensions and shape.*

After the lightweight aggregate blocks are cast the prestressed reinforcement is placed in the grooves. The 1.2 m wide element can accommodate up to 8 strands with a nominal diameter of 12.5 mm. One at each side of the element and three in a bundle in the grooves between the lightweight aggregate concrete blocks. Between the blocks in the secondary direction slack rebars with a diameter of 6 mm is placed to counteract the horizontal part of the arch forces over each block and to stabilize the element and prevent longitudinal cracking. This is of importance if the width increases beyond 1.2 m, where longitudinal cracking becomes a bigger risk. The reinforcement arrangement in the element is shown on Fig. 2.4.

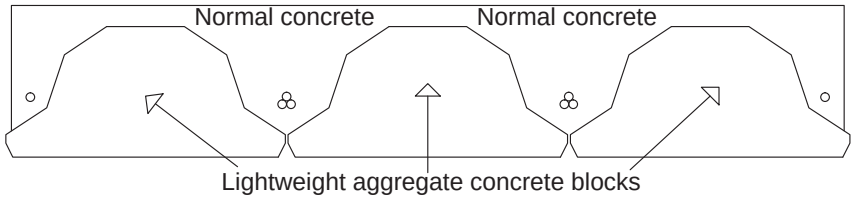

***Figure 2.4**: Reinforcement in a 1.2 m wide super-light element.*

Normal concrete is cast on top of the lightweight aggregate blocks to create the rectangular form of the cross-section, as it can be seen on Fig. 2.5. At any place in the element the top layer of normal concrete is at least 30 mm, enough to fully constitute a maximum compression zone depth of 22 mm, when the element is fully reinforced with 8 prestressed rebars for a plastic calculation of the moment capacity. The increased plasticity of the normal concrete ensures that it penetrates the open pores of the lightweight aggregate concrete blocks as shown on Fig. 2.6 and a strong connection between the two concretes is created.

***Figure 2.5**: A slice of the completed rectangular cross-section of the super-light element.*

***Figure 2.6**: On the left cross-section of a fully cast element, on the right comparison with the block without cast concrete.*

Arches are locally created within the element due to the shape of the lightweight aggregate concrete blocks. The arches span from one groove to another where the main load carrying lines in the element are found. The arches bring the distributed load to these grooves. Apart from having the static influence on the element, the arches are shaped so that material consumption and weight of the element are reduced.

Statically, the super-light element comes with the possibility to be clamped at its supports. This is done by casting the element with grooves in the top surface near the support along the grooves between the lightweight aggregate concrete blocks. When installing the element, slack reinforcement is placed in the grooves in the top surface across the support and concrete is cast into the grooves. A concept drawing of this is shown in Fig. 2.7. The clamped support of a beam element will greatly enhance its performance in the serviceability limit state. Cracking will first occur at a higher load. Maximum deflection at midspan is reduced compared to the simple supported case and the natural frequency of the element will be approximately 2.25 times higher than if the element was acting as a simple supported beam this is greatly

reducing the acceleration of the vibration in the comfort related frequency range.

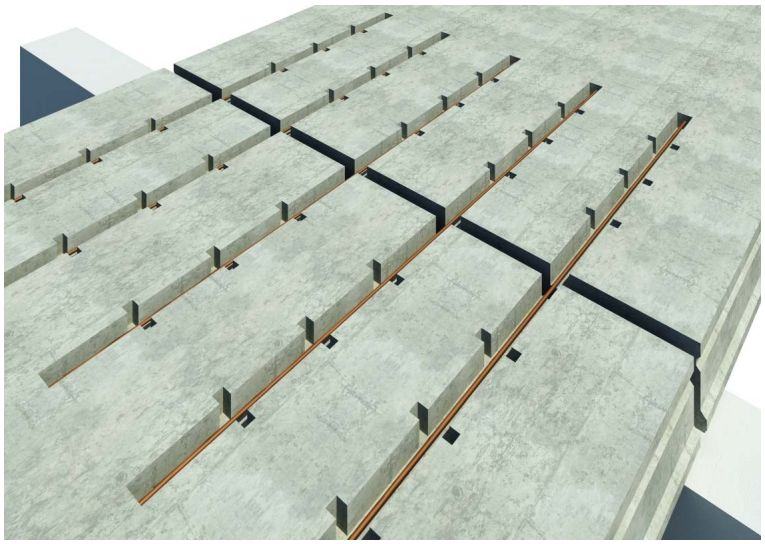

***Figure 2.7**: Example on how to create a restraining moment at the support in order to clamp the super-light slab.*

The pearl-chain technology is not directly applied within a single super-light deck element. The limited element height of 215 mm and the cost of production means that it is not feasible to use it. Instead it can be used to combine multiple elements. A space between two rows of lightweight aggregate concrete blocks can be added to make room for a hollow duct for the post-tensioning cable. Application of this across the deck element opens up for possibilities of load-bearing in two directions yielding a further reduction of deflections and vibrations.

Chapter 3

Acoustic design

The super-light element is developed acoustically in regards to newly changes in acoustic legislation in Denmark, which was discussed in Chap 1. In the introduction it was also implied that the legislation is still insufficient to provide an optimal acoustical environment for large parts of the population. Therefore, the element is also prepared so that it is able to adapt for future changes to the legislation.

The main idea behind the acoustic development of a super-light element is an even stiffness distribution in the two principal directions in order for the element to be considered isotropic along with a beneficial interacting between the normal concrete and the lightweight aggregate concrete. The focus is placed on the airborne sound transmission; this means that certain requirements exist to the type of flooring, which should be used in combination with the super-light element. Moreover, the floor should be able to compensate for the increased sound transmission coming from flanking when comparing in-situ simulations to the laboratory measurements. For heavy elements as, e.g., concrete floors, a rule-of-thumb is that this can be estimated approximately to be 3 dB (Kristensen and Rindel 1989). Furthermore and most importantly, the floor should account for fulfilling the requirements to impact sound insulation.

Traditionally, hollow core slabs with a surface mass of $320\,\mathrm{kg/m^2}$ has been sufficient in regards to building acoustic performance when using concrete elements (Kristensen and Rindel 1989). After the acoustic part of the building code was changed a new recommendation was published where $440\,\mathrm{kg/m^2}$ was recommended for the pre-fabricated building scheme (Rasmussen et al. 2011). Impact sound insulation is the cause for the steep increase to the requirement of surface mass, and therefore development of floors has led to a new analysis (Christensen 2012), where the results is that a surface density of $370\,\mathrm{kg/m^2}$ is needed to achieve $R_w \geq 55\,\mathrm{dB}$ and $L_{n,w} \leq 53\,\mathrm{dB}$. In (Simmons 2004) are

several measurements of concrete hollow core slabs available. The surface mass of the included elements cover the range $255-(480+90)\,\mathrm{kg/m^2}$, where $480\,\mathrm{kg/m^2}$ is the surface density of the hollow core slab and $90\,\mathrm{kg/m^2}$ is the surface density of an additional in-situ cast layer of concrete. All of these measurements has been modified in order to be used as input data for Bastian software, the method which the result has been modified is available within the report. Some of the modified results of the sound insulation for the hollow core slabs are $R'_w = 51\,\mathrm{dB}$ and $L'_{nw} = 89\,\mathrm{dB}$ for a hollow core slab with a surface density on $255\,\mathrm{kg/m^2}$, $R'_w = 53\,\mathrm{dB}$ and $L'_{nw} = 86\,\mathrm{dB}$ for a hollow core slab with a surface density on $290+25\,\mathrm{kg/m^2}$ comparable to the super-light element in terms of surface density, $R'_w = 55\,\mathrm{dB}$ and $L'_{nw} = 84\,\mathrm{dB}$ for a hollow core slab with a surface density on $255+90\,\mathrm{kg/m^2}$ and $R'_w = 57\,\mathrm{dB}$ and $L'_{nw} = 83\,\mathrm{dB}$ for a hollow core slab with a surface density on $365\,\mathrm{kg/m^2}$.

The present acoustic investigation consists of a test element specially designed for the acoustic test facilities. Here airborne sound insulation has been measured along with impact sound insulation and the input mobility of the super-light element, which is also the topic of the accompanying paper (Christensen et al. 2013a). These results have been applied with the acoustical simulation software Bastian to investigate flanking performance in a room setup based on current partitions and methods in the Danish prefabricated concrete element industry. In addition, a parametric study with a wide array of partitions is also investigated, in order to obtain a more general assessment of the flanking transmission; additional details regarding the study of flanking transmission can be found in the accompanying paper (Christensen et al. 2013b).

3.1 Test setup

The measurements were all carried out in the reverberation chamber at the Technical University of Denmark. For the airborne transmission loss measurements, the guidelines in (ISO 10140-2 2010) has been used. The impact transmission measurements were made in accordance to (ISO 10140-3 2010). The standard tapping machine was used in five different positions on the slab. Different angles and positions related to the rib structure of the super-light element created by the lightweight aggregate blocks was used for the tapping machine. For the impact transmission the influence of external floors was not measured, but as discussed later they have instead been simulated.

***Figure 3.1**: Test setup fin the receiver room*

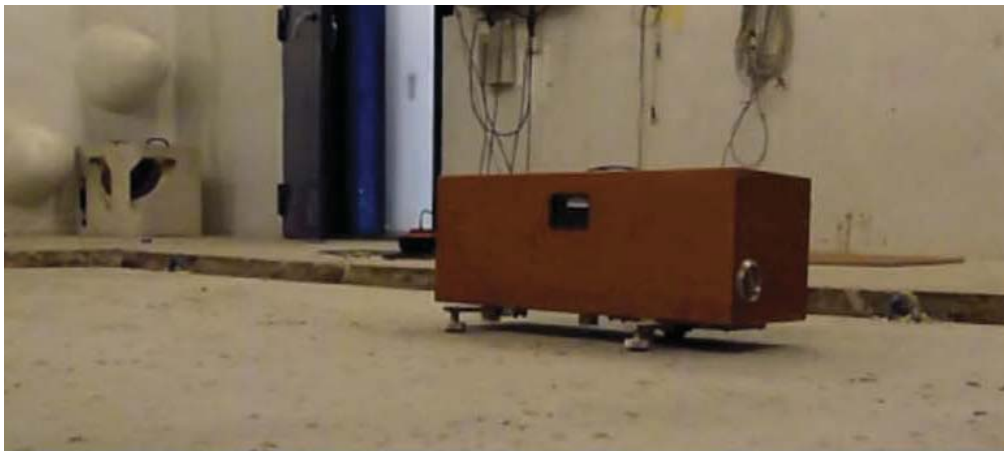

***Figure 3.2**: Standard tapping machine for impact sound insulation measurements.*

The mobility of the slab has been measured after three weeks, in order to establish the boundary condition and explain the uneven mode-dominated transmission of the slab at lower frequencies compared to the more even transmission in the rest of the frequency range. Three positions have been used, two above ribs and one above the centre of a lightweight aggregate concrete block. Due to limitations in the setup, where some of the equipment was suspended from a crane locked in a rail in the ceiling, it was not possible to avoid one of the main nodal lines in the element. In the case of a nodal line in the centre of the element which was the case here half the nodes will have no vibration along this line making it is impossible to identify all modes in the mobility measurements.

***Figure 3.3**: Setup mobility measurements.*

The flanking transmission analysis is made with the acoustic software Bastian (Metzen 2010). Bastian is based on the standards (EN12354-1 2000) and (EN12354-2 2000) for airborne and impact sound insulation respectively. The standard EN12354 was developed as an energy flow prediction model based on work by (Gerretsen 1979) and (Gerretsen 1994). The model is also equivalent to a first order SEA model as shown by (Nightingale and Bosmans 2003). Gerretsen combine measured data for direct sound insulation with an average between transmission in one direction and reciprocal transmission in the opposite direction; this means that radiation efficiencies can be ignored and the model is simplified. In general the model has limitations regarding accuracy at low frequencies and for lightweight elements, note that the super-light element investigated here, is despite of its name, not considered lightweight in relation to the flanking transmission model in Bastian.

Accuracy of measurements and simulations

The nature of the calculation and measurements methods, including both the laboratory and the in-situ, in general for acoustic problems introduce

uncertainties in the results which is typically expressed in and evaluated by standard deviations and confidence intervals or probability quantiles. These uncertainties are further enhanced by the randomness of workmanship, which could be caused by different traditions in construction methods, small cracks or holes in the element, etc.

For the laboratory measurements, which the sound insulation measurements of the super-element is based on, the uncertainties are based on two things, variations in the sound fields in the source and receiver rooms and by variations of different testing facilities. Studies on various laboratories are used to create the repeatability and reproducibility values listed in Annex A (ISO 140-2 1992). For the single measurement of the super-light element, with one determination y, 95 % confidence intervals for the true mean of the measurements can be established by the reproducibility values R as,

$$y - \frac{R}{\sqrt{2}} < \mu < y + \frac{R}{\sqrt{2}} \tag{3.1}$$

The reproducibility values are higher at the lower frequencies increasing the confidence interval on the measurements, for airborne measurements the confidence intervals range are from ±6.36 dB at lower frequencies to ±2.47 dB at higher frequencies, for impact measurements the confidence intervals range are from ±3.54 dB at lower frequencies to ±1.77 dB at higher frequencies. Another type of measurement errors are for in-situ measurements, these are reported by (Craik and Evans 1989). Here, the exact same measurement was carried out 7 times, the result of an average residual standard deviation was found on this basis to $\sigma = 0.83$ dB, which was also concluded to be lower than other uncertainties such as workmanship.

The uncertainty in the lab measurements is shown in Fig. 3.4, where also the accompanying 95% confidence interval of the measurements is shown. For the airborne measurements the data is based on 10 measurements as specified by ISO 10140-2 and 20 impact measurements as specified in 10140-3.

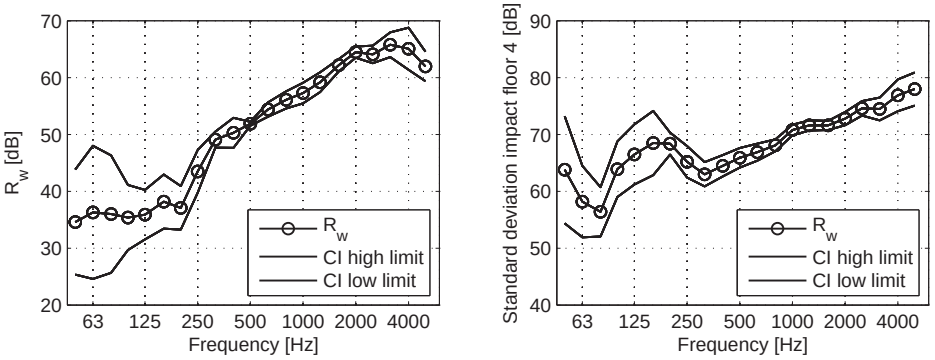

***Figure 3.4**: Confidence intervals for the laboratory measurements .*

The confidence intervals are very large at low frequencies, up to values of 20 dB is observed. At the middle frequencies the interval is narrow with values below 3 dB, while the spread of the measurements are increased at higher frequencies.

Both EN 12354-1 and EN 12354-2 acknowledge the lack of accuracy of the model used for prediction flanking transmission and list the following factors as the reason: accuracy of the input data, the fitting of the situation to the model, the type of elements and junctions involved, the geometry of the situation and the workmanship. They give estimate of the total accuracy for the airborne sound insulation calculations for homogenous elements in terms of a standard deviation of 1.5 dB for situations where everything in the model is accounted for and 2.5 dB for more complex situations. For the impact sound insulation the standard deviation is given as 2 dB for a vertical analysis.

The accuracy of the flanking transmission model in EN 12354 has been investigated by (Mahn and Pearse 2009). This is done by an analysis of the uncertainty regarding input data, and includes structural reverberation time, in-situ resonant sound reduction index, in-situ direction averaged velocity level difference and flanking transmission sound reduction index. The main finding is a standard deviation in each of the one-third octave bands, ranging from 0.9 dB to 2.4 dB with the largest uncertainties at the lower frequencies. This corresponds to an average confidence interval of ± 2.5 dB when uncertainty regarding workmanship is omitted from the analysis. Another analysis on the uncertainties regarding the flanking transmission model in EN 12354 has been conducted by (Simmons 2005); here it is suggested to apply a safety margin of 2 dB for R_w and 2 dB for L_{nw} when designing acoustic solutions by means of EN12354. This recommendation is based on measurements according to ISO 140 and calculations according to EN 12354.

The uncertainty of EN 12354 for lightweight constructions is greater than for homogenous, monolithic elements, especially at the lower frequencies. In analogue the uncertainty of the model at lower frequencies is also an issue for the super-light element where requirements for a good accuracy of the SEA model are not meet for the lower frequencies, i.e. the amount of modes in a one-third octave band is below 5 and the modal overlap factor is below 1 (Hopkins 2005). (Öqvist et al. 2012) conduct a case study on a lightweight timber floor. It is concluded, in agreement with the findings of (Craik and Evans 1989), that the uncertainty regarding measurements are small compared to other uncertainties, it is also indicated that uncertainty regarding workmanship may be reduced for pre-fabricated elements compared to in-situ constructions.

The workmanship of the entire constructions is also known to cause uncertainties. This has been investigate by measuring ten identical floors, (Craik and Steel 1989). The uncertainty regarding workmanship is found to be $1.5 - 2$ dB for each of the one-third octave bands and 1.3 dB for the single number rating.

In general the statistic regarding the uncertainties has been carried out in the domain of dB and all means and standard deviations are reported by dB. This corresponds to the geometrical mean rather than the arithmetical mean. The variances associated with the uncertainties are small, which means that the geometrical means has been used as a good approximation.

3.2 Test element

A special test element has been designed for the acoustic experiments to accompany the facilities where the super-light element was tested. The element is designed to mimic the original idea both statically and geometrically as it is described in Sec. 2.4. Its cross-sections for both principal directions are shown in Fig. 3.5. The element has a surface density of 315 kg/m^2 comparable to the element it was modelled after of 289 kg/m^2.

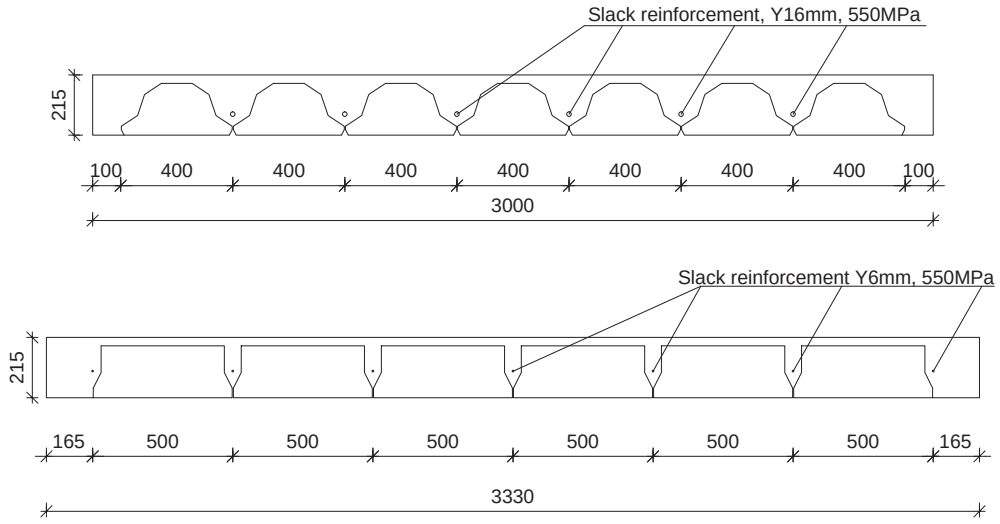

***Figure 3.5**: Cross-sections of the super-light element used in acoustic tests.*

The odd geometry of the hole separation the two floors, when compared to the modular pre-fabricated concrete element, is causing that the size of the lightweight aggregate concrete blocks does not align perfectly with the hole. The hole is 3.3×3 m. The difference is accounted for by having full sections of concrete at the edges of the element where, at least for the lower frequency range, the amplitude of the vibration is less than at the middle of the element. The size of the element is further controlled by a custom made steel frame designed for the hole separation the two floors which the concrete element has been cast in.

The boundary condition is established as shown in Fig. 3.6. It is important as it determines the natural frequencies of the element and the lowest of these will be dependent on the boundary condition, possible leading to peaks in the sound transmission for certain frequencies. The connection between the test facilities and the super-light element is made by a mixture of in-situ cast grouting mortar with extra water and sand added to improve the workability of the mixture, the other part of the boundary condition is made from mineral wool. The grouting mortar has compressive strength 30 MPa. The influence of the curing time of the grouting mortar on the boundary condition was unknown so both the airborne transmission loss and impact transmission was measured at three different curing times, namely 18 hours, 1 week and 3 weeks, in order to investigate any significant changes in the boundary condition.

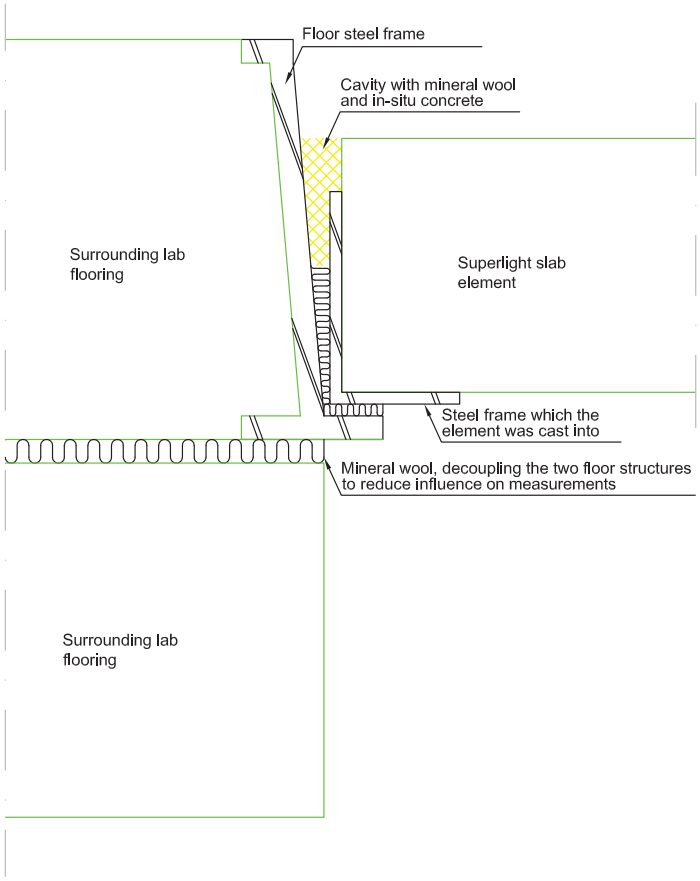

***Figure 3.6**: The boundary connection between the super-light element, the steel frame it is cast in and the laboratory flooring.*

The stiffness development is of greatest interest of the properties of the grouting mortar as it has the biggest influence on the boundary condition. It is giving by Eq. 3.2, (Eurocode 2-1-1 2004)

$$E_{cm}(t) = \beta_{cc}(t)E_{cm} = \exp\left(s\left(1 - \sqrt{\frac{28}{t}}\right)\right)^{0.3} E_{cm} \tag{3.2}$$

where s is a coefficient depending on the cement type, here $s = 0.25$ for class N cement is used and t is the curing time in days, t must be normalized to account for days at $20°C$, e.g. a day of curing at $5°C$ t is less than one, here the concrete was kept at $20°C$. For the three measurements this means that the stiffness had developed to 68%, 93% and 99% respectively. The measurements after 1 and 3 week were very alike, while some differences could be observed at the lower frequencies for the measurements after a day.

For the flanking transmission simulations it is the measurements of the element just described which is used as a basis. The analysis is made as a parametric study of 168 different configurations of the room. The elements used for the simulations fall in two distinctive main groups, a floor group and a partition and room setup group.

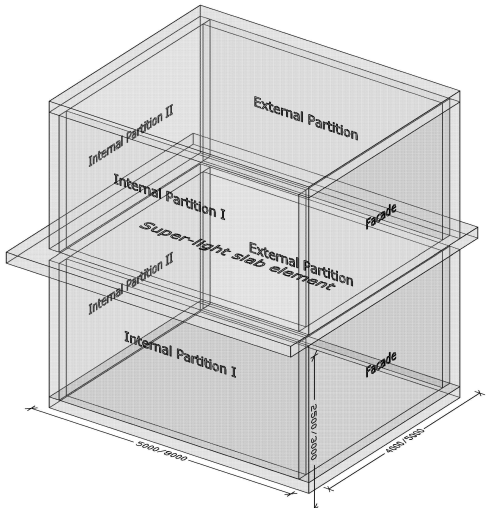

***Figure 3.7**: The model of the room and partitions for the flanking setup.*

The room setup for the analysis is shown in Fig. 3.7, it is a rectangular room consisting of four partitions, a facade, an external partition, which separate different apartments and two internal partitions separation rooms inside an apartment. The different floorings in use is summed up in Tab. 3.1 and partitions in Tab. 3.2. Elaboration on floorings, partitions and setups can be found in (Christensen et al. 2013b). In general the chosen partitions are based on current trends and methods in the pre-fabricated building industry in Denmark after the latest change of legislation to building acoustic as discussed in the introduction.

In addition two room sizes has been used a normal size room of $5 \times 4 \times 2.5$ m and $8 \times 5 \times 3$ m and resilient layers applied in joints with thickness $t = 12$: mm and stiffness $E = 3$ GPa specified as being common by (Osipov and Vermier 1996).

3.3 Theory

In this section the main ideas behind the improvement in acoustical performance compared in relation to surface mass and similar traditional pre-

***Table 3.1**: Overview of the parametric study and the choices of different partitions, ΔR and ΔL is the improvement of the flooring in a laboratory.*

Flooring			
No.	Description	ΔR,ΔL,[dB]	Ref.
1	Knudsen kilen with a layer of filt	3/24	(Hoffmeyer 2011b; Hoffmeyer 2011a)
2	Knudsen kilen without a layer of filt	-/21	(Hoffmeyer 2011c)
3	Harpun lydbrik	-/26	(Hoffmeyer 2005)
4	Swimming floor, 22 mm chipboard on 30 mm rockwool	9/23	(Metzen 2010)

fabricated concrete elements are explained along with a model used to give a statistical energy analysis (SEA) model of the element.

One of the most significant improvements compared to pre-fabricated concrete elements is that the super-light element with its blocks is designed in a way that makes it behave as an isotropic plate contrary to a hollow core slab. For the acoustic test element the bending stiffness has been calculated and is for each direction $B_1 = 1.282 \cdot 10^7$ Nm and $B_2 = 1.153 \cdot 10^7$ Nm, which leads to an effective torsional rigidity for an orthotropic plate, based on theory by (Szilard 2004), to $B_{12} = \sqrt{B_1 B_2} = 1.216 \cdot 10^7$ Nm, with the stiffness in each direction so close it is clear that the element can be thought of a isotropic; the calculations of each of the bending stiffness is given in App. A.

The critical frequency, (Cremer and Heckl 2005) page 486, describes the frequency where matching of bending waves between bending waves in the super-light deck element and in the ambient fluid, in this case air. Around the critical frequency this creates an amplified sound radiation, above the radiation is dominated by resonance waves with almost constant radiation efficiency, below it is a forced radiation, which is of limited interest for the super-light element. It is important for the critical frequency to be as low as possible and especially below the building acoustic frequency range of 100 Hz − 3150 Hz. The critical frequency is

$$f_c = \frac{c^2}{2\pi}\sqrt{\frac{m}{B}} = 96.4\,\text{Hz} \tag{3.3}$$

where c is the acoustic wave speed in air, m is the surface density and B is the bending stiffness, B_{12} will be substituted into the equation as an approximation for the bending stiffness of the element. Using B_1 and B_2 yields a

***Table 3.2**: Overview of the parametric study and the choices of different partitions.*

Facade walls			
No.	Description	ΔR_w, $[dB]$	Ref.
1	150 mm concrete wall with insulation and masonry 200 kg/m^2	54	(Metzen 2010)
2	150 mm concrete wall with insulation and masonry 200 kg/m^2 with gypsum cladding	54+20	(Metzen 2010)
3	13 mm gypsum - 145 mm rockwool - 9 mm gypsum - 28 mm air - 28 mm wooden panel	48	(Metzen 2010)
External partitions			
1	200 mm concrete wall	59	(Metzen 2010)
2	3 × 13 mm gypsum - 190 mm rockwool - 80 mm air - 3 × 13 mm gypsum	73	(Metzen 2010)
Internal partitions			
1	100 mm lightweight aggregate concrete wall 1350 kg/m^3	42	(Metzen 2010)
2	13 mm gypsum - 30 mm rockwool - 90 mm air - 13 mm gypsum	49	(Metzen 2010)

critical frequency of 93.9 Hz and 99.0 Hz which confirms the idea that the slab behaves as an isotropic slab. The critical frequency is below 100 Hz, this means that for most of the building acoustic frequency range the radiation efficiency σ_{res} is expected to be close to 1.

Due to the low critical frequency contribution to the sound transmission through the forced transmission can be neglected, and the resonant SEA model, which is given by (Vér and Holmer 1988), can be used to calculate the sound transmission loss of the slab, which can be compared with the measured sound transmission. It is based on a statistical description of energy transfer, caused by modes, between subsystems. Here, the source room, receiving room and the super-light element acts as subsystems.

$$R_{res} = 20\log_{10}\left(\frac{\pi f m}{\rho c}\right) - 10\log_{10}\left(\frac{c^2\sigma_{res}^2}{2\eta_{tot}Sf}\frac{\Delta N}{\Delta f}\right) \tag{3.4}$$

where f is the frequency, m is the surface mass, $\rho = 1.21\,\mathrm{kg/m^3}$ is the density of air and $c = 344\,\mathrm{m/s}$ is the speed of air, both at 20 °C. The first part of the

equation constitutes the common mass law. σ_{res} is the radiation efficiency, η_{tot} is the total loss factor, S is the surface area and $\Delta N/\Delta f$ is the modal density. All of these factors can be boiled down to be dependent on the stiffness, mass and damping as is common for dynamic problems.

The modal density is a measure for how many modes are present within a limited frequency range. For bending modes, which is most important in relation to single number rating, it is proportional to the critical frequency further enhancing the desire for a low critical frequency, which is done by a reduction of the mass and increase of the stiffness. The modal density used here is based on work by (Rindel 1994), both the modal density for thin plates and thick plates are used, the thin plate model is used when bending waves are present in the element at the lower frequencies, and the thick plate model is used when surface waves are present in the element. Half the cross over-frequency

$$f_s = \frac{c_s^2}{2\pi}\sqrt{\frac{m}{B}} \tag{3.5}$$

determines which model will be used, c_s is the speed of shear waves in the slab element and f_s is the cross-over frequency. The modal density is calculated as

$$\frac{\Delta N}{\Delta f} = \begin{cases} \frac{\pi}{c^2} S f_c & \text{if } f \leq \frac{f_s}{2}, \\ \frac{2\pi}{c_s^2} S f & \text{if } f > \frac{f_s}{2}. \end{cases} \tag{3.6}$$

The modal density for the bending waves has been calculated for an isotropic element by setting $B = B_{12} = 1.216 \cdot 10^7\,\mathrm{Nm}$. It is found as $\Delta N/\Delta f = 0.025$. The modal density for an orthotropic plate is based on calculating natural frequencies for the orthotropic plate based on (Szilard 2004) and Eq. 3.7 beneath.

$$f_{mn} = \frac{\omega_{mn}}{2\pi} = \frac{\pi^2 \sqrt{\frac{B_1}{M}\left(\frac{m^4}{L_1^4} + 2\frac{B_1}{B_{12}}\frac{m^2 n^2}{L_1^2 L_2^2} + \frac{B_1}{B_2}\frac{n^4}{L_2^4}\right)}}{2\pi} \tag{3.7}$$

When the modal density is calculated accordingly to the first part in Eq. 3.6 with the material parameters of the super-light slab the modal density was found as $\Delta N/\Delta f_{iso} = 0.025$. Calculated according to Eq. 3.7 with the material parameters of the super-light slab it averages $\Delta N/\Delta f_{ortho} = 0.024$. The small difference is due to the randomness of counting modes compared to the statistical value and is of no importance here.

Compared to a more normal concrete element it is expected that the loss factor is increased in the super-light slab element due to the presence of lightweight aggregate concrete. As reported by (Cremer and Heckl 1973), lightweight aggregate concrete has a higher loss factor, 0.01 than normal concrete $0.004-0.008$ meaning that the porous lightweight aggregate concrete

has a loss factor $1.25 - 2.5$ times the loss factor of normal concrete. But more importantly is that the blocks of lightweight aggregate concrete can be thought as damping layer as described by (Cremer and Heckl 1973) (page 243-247) further increasing the damping in the element.

As an rough estimate the formula provided by Cremer and Heckl is evaluated for the super-light slab element. The formula is developed with a simpler element in mind. The super-light slab is simplified in order to comply with the modal, all the material has been smeared into two layers with constant height and then this simplified model is used in order to estimate the additional damping of the bending waves when the lightweight aggregate blocks are considered as an attached layer

$$\eta_B = \eta_{lc} \frac{E_{lc} d_{lc} a^2}{B_{12}} = 0.1 \eta_{lc} \tag{3.8}$$

where $\eta_{lc} = 1 \cdot 10^{-2}$, $d_{lc} = 99\,\text{mm}$ is the average depth of the of lightweight aggregate concrete over the element, $a = 64\,\text{mm}$ is the distance between the centre of equilibrium of each of the two materials found from the values in Eq. A.1 and Eq. A.3. With $\eta_{lc} = 1 \cdot 10^{-2}$ it means that total loss factor of bending waves in Eq. 3.8 equals $\eta_B = 0.001$. The value of the loss factor η_B is lower than both the loss factor of both the normal concrete and lightweight aggregate concrete, implying that Eq. 3.8 can not be used to describe how the damping layer influences the super-light deck element, but the principle of an added damping layer should still be sound.

3.4 Input mobility

Fig. 3.8 shows the input mobility measured for the slab, from these measurements natural frequencies and loss factors have been determined as peaks and half power bandwidth respectively. The natural frequencies is used to identify the actual boundary condition in Fig. 3.6 and trends in peaks and anti-peaks for the sound transmission at the lower frequency range.

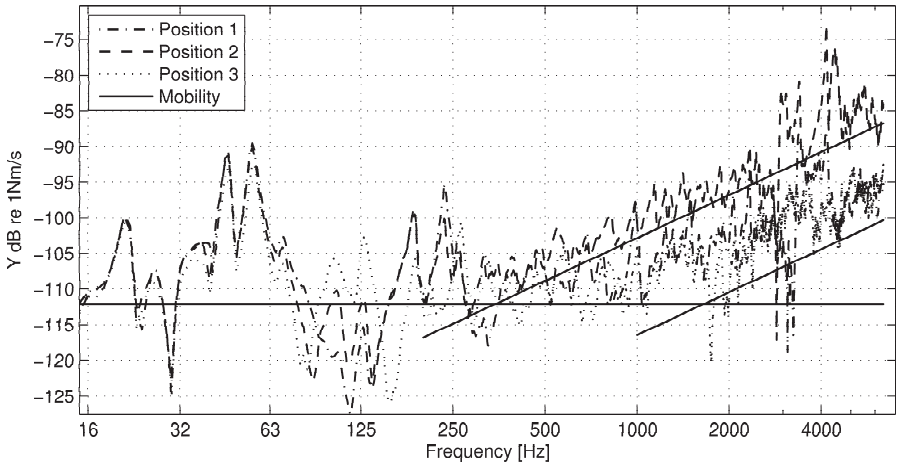

***Figure 3.8**: Input mobility measurements of the super-light element in frequency range* $1 - 6400$ *Hz*

The main results obtained from the input mobility measurements are summed up in Tab. 3.3. The blank entries are covering the modes which either was not possible to identify from the measurements or from the setup of the measurements. Noise from the surrounding floor structure on the input mobility of the super-light slab has been identified by measuring the surrounding floors input mobility with the super-light slab being driven by the driver. The influence from the floor on the input mobility of the super-light slab then has been removed, by identifying and comparing peaks in the input mobility of the two measurements.

Estimations to the results listed in Tab. 3.3 can be made due to the near isotropic bending stiffness distribution of the element and the table can be expanded. It is argued that (1,2) has a similar result to (2,1) and that (2,2) should be close four times $(1,1)\cdot 4 = 220\,\text{Hz}$ creating a limited frequency range ($188\,\text{Hz} - 262\,\text{Hz}$) with a large concentration of some of the lowest modes. Elaborations on the influence and significance of the input mobility is available in the enclosed paper (Christensen et al. 2013a).

3.5 Airborne sound insulation

The airborne sound transmission loss of the super-light slab element has been measured and in Fig. 3.9 it is shown after three weeks of curing for the concrete constituting the boundary. The SEA-model given by Eq. 3.4 and the mass law is also depicted.

***Table 3.3**: Input mobility results*

Mode	f_{mn} [Hz]	η [%]
(1,1)	55	4.9
(2,1)	188	5.4
(1,2)	-	-
(2,2)	-	-
(3,1)	262	5.1
(1,3)	235	4.1
(3,2)	-	-
(2,3)	-	-
(3,3)	-	-

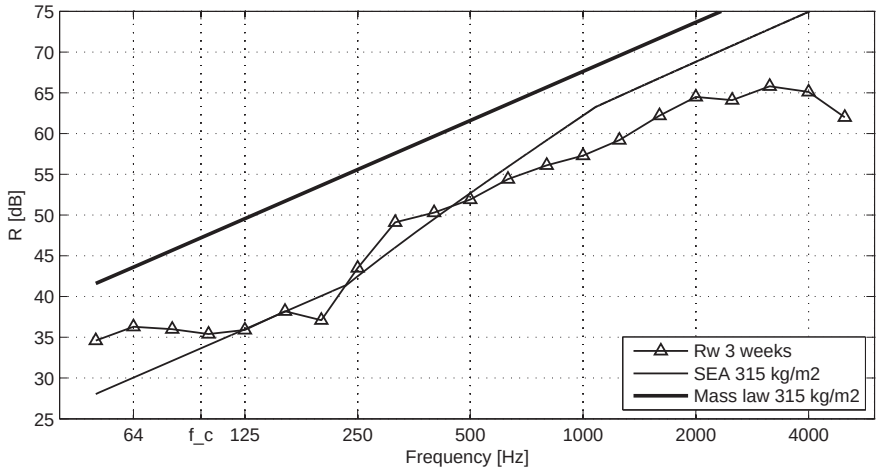

***Figure 3.9**: Airborne transmission loss of the super-light slab compared with SEA model Eq. 3.4*

The main results are the single number ratings of the measurement and SEA model transmission losses, they both are found to $R_w = 55$ dB according to the method supplied by (ISO 717-1 1996). For the spectral adaption term there is a difference between the two curves, $C_{50-5000,lab} = -3$ dB and $C_{50-5000,SEA} = -1$ dB. However the SEA-model cannot be expected to describe the transmission loss at low frequencies very well so there is uncertainty about $C_{50-5000,SEA} = -1$ dB. In general there is a good agreement between the theory and measurements above 315 Hz with an exception for very high

frequencies where the SEA model provides superior transmission loss, however, this decreased sound insulation do not affect the single number rating R_w and $C_{50-5000}$. Above 315 Hz the modal overlap factor is sufficient high so that the transmission can be described with statistic methods. Below this frequency there is a lot of variation on the measurement comparable to the distribution of natural frequencies in the element as discussed and presented in Tab. 3.3.

The mass law for a 315 kg/m^2 heavy element is included in Fig. 3.9, and it can be thought of as an upper value for what is possible to achieve in transmission loss given a certain mass. It has a single number rating of $R_w = 66$ dB, 11 dB higher than the measurements and SEA prediction implying that there is still room for improvement on the sound transmission loss of the super-light slab, by improving on the critical frequency, modal density or the loss factor.

3.6 Impact sound transmission

The impact sound transmission measured on the super-light element without any external flooring is shown on Fig. 3.10 along with a prediction as described by the SEA model and the mass law for an element with a surface density on 315 kg/m^2.

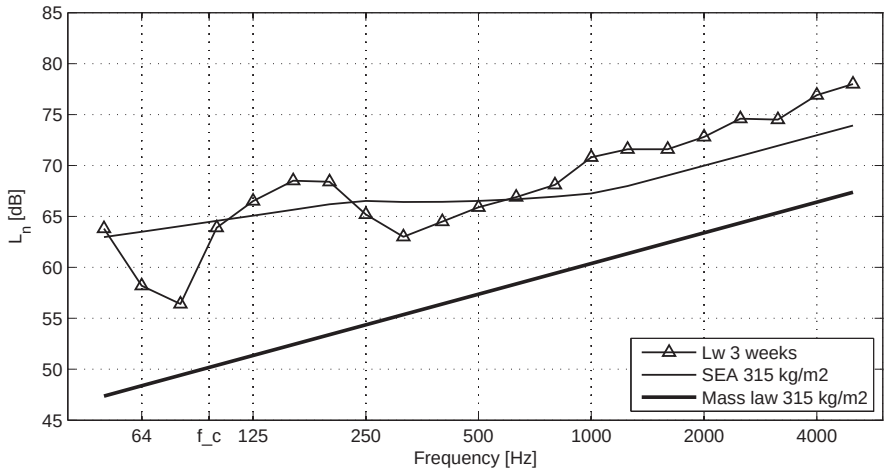

***Figure 3.10**: Impact transmission of the super-light slab compared with SEA model*

The main results from Fig. 3.10 of the impact transmission are the requirements of flooring in order to achieve acceptable acoustic ratings. The

single number rating of the element is of less interest due to the nature of how the single number rating is found. For the element without a floor it is solely the higher frequencies that determines the single number rating. If a floor is applied to the element it is solely the lower frequencies that will determine the single number rating.

For the impact sound transmission a difference in the single number rating was found $L_{n,w,\text{lab}} = 79\,\text{dB}$ and $L_{n,w,\text{sea}} = 76\,\text{dB}$ with spectral adaption terms $C_{I,\text{lab}} = -12\,\text{dB}$ and $C_{I,\text{sea}} = -9\,\text{dB}$. For impact the uncertainties regarding accuracy of the SEA model should be minimized as it is primary the high frequencies determining the results where the accuracy of the SEA model should be at its best. However a difference of 3 dB is observed caused by the fact that for high frequencies SEA predicts significant less transmitted sound compared to the measurements. At the lower frequencies the trends of mode distribution in the super-light slab, from Fig. 3.8, is clearly visible.

The mass law for a $315\,\text{kg/m}^2$ heavy element is included again and can be thought of an upper value. The single number rating for the mass law is $L_{n,w} = 70\,\text{dB}$. As expected the difference between the mass law and the SEA model and measurements is of the same magnitude, $\approx 10\,\text{dB}$, as it was for the airborne transmission loss, leading to the same conclusions for possible improvements of the super-light slab.

In the flanking transmission analysis several floorings was tested and compared to each other and a setup with no floor, the results is shown in Fig. 3.11 where it is standard room setup which has been used is described in Sec. 3.7 along with the four floors.

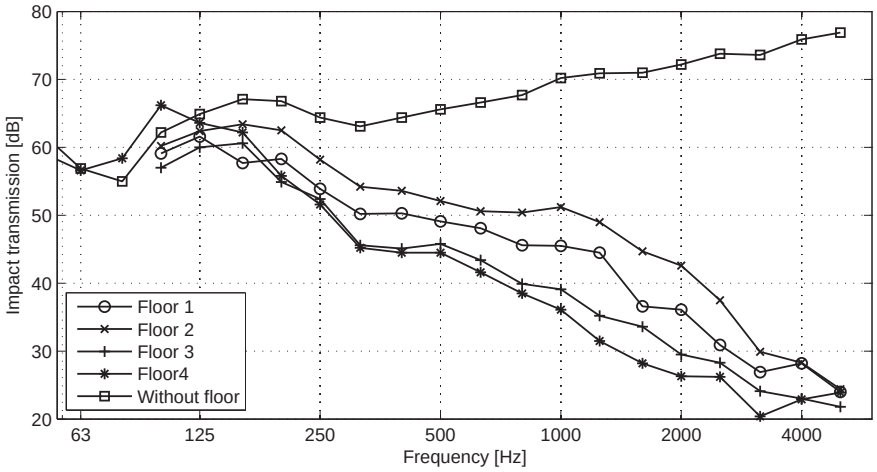

***Figure 3.11**:*

In relation to the single number ratings, the floors shift the determining

frequencies from the higher range to the lower range. All the simulated floors vastly improve the single number ratings and are 50 dB, 55 dB, 49 dB and 52 dB for floor 1, 2, 3 and 4 respectively giving a $\Delta L_{n,w} = 24 - 30$ dB. The first three floors, which are lay-up floors, work particular well with super-light slab, while the fourth floor, a floating floor expected to give the largest improvement, and has a poor performance in the important lower frequencies.

3.7 Flanking transmission

From Tab. 3.1 and Tab. 3.2 a standard room setup is created by using the first floor and partitions listed in a normal sized room without any resilient layers applied to the junctions. The standard room setup carries the main emphasis of the flanking transmission analysis and constitutes the first part; the standard room setup mimics the current pre-fabricated construction scheme. The second part of the flanking transmission analysis is a parametric study on all of the combinations of floorings, partitions, room sizes and junction detailing.

In Fig. 3.12 the airborne sound transmission loss is shown for the flanking analysis in the standard room setup. It is compared to the laboratory measurements available in Fig. 3.9

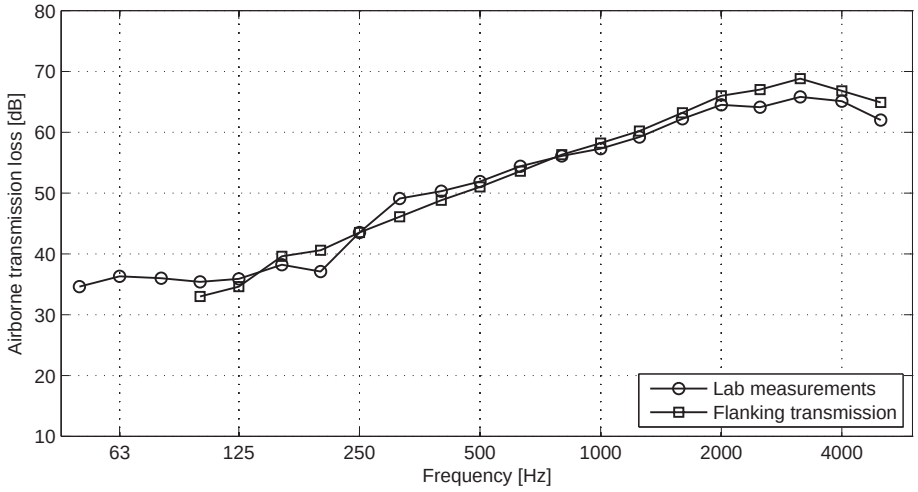

***Figure 3.12**: Flanking transmission of airborne sound insulation for the super-light deck element with the standard room setup*

The single number rating of the airborne flanking transmission loss is $R_w = 54$dB, one dB lower than the lab measurement. The initial expectations that the floor should compensate for the increased transmission caused by flanking did not hold true. (Christensen et al. 2013b) shows that the direct transmission accounts for 58 % of the transmitted sound, which is a little higher than the 50% implied by the rule-of-thumb that flanking transmission decrease the airborne sound transmission loss by 3 dB. This leads to the conclusion that the floor is not providing an increase of the airborne sound transmission loss of $\Delta R = 3$ dB as it has been measured on the standard 140 mm massive standard concrete slab.

In Fig. 3.13 the impact sound transmission is shown for the flanking analysis in the standard room setup with and without the floor. It is compared to the laboratory measurements from Fig. 3.10

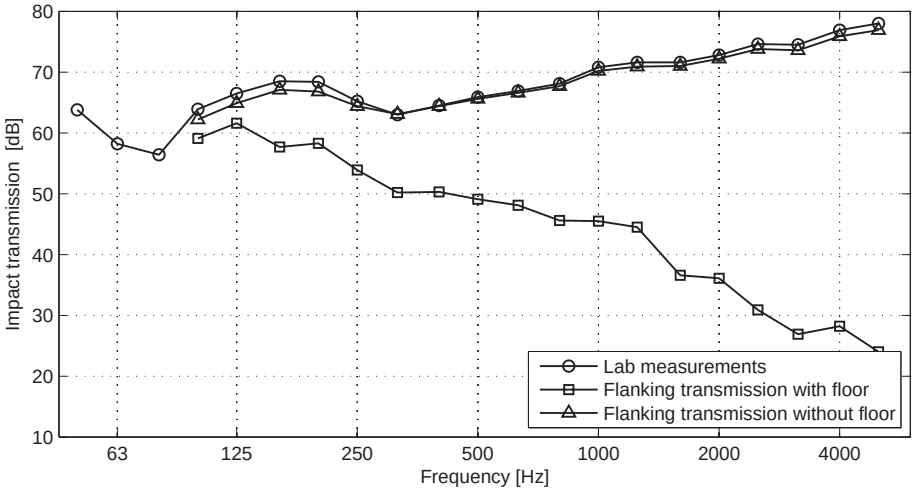

***Figure 3.13**: Flanking transmission of impact sound insulation for the super-light deck element with the standard room setup*

The single number rating of the impact flanking transmission is $L_{n,w} = 50$ dB and $L_{n,w} = 78$ dB with and without the floor respectively, meaning that $\Delta L = 28$ dB. If Fig. 3.10 is studied, it can be seen that at the higher frequencies there is a slight tendency, that the slope of the measurements is greater than the slope of the SEA model and mass law, accounting for some of the difference i ΔL compared to specification of floor 1 from Tab. 3.1.

In Fig. 3.14 show histograms of the distribution of single number ratings for the parametric study for both airborne and impact sound insulation.

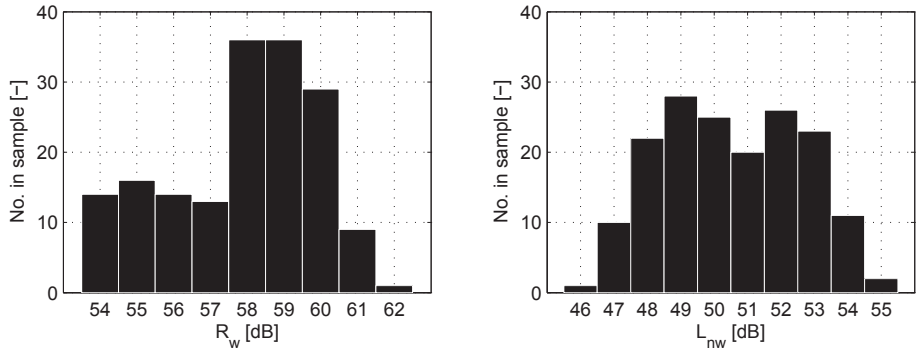

***Figure 3.14**: Histogram of the single number ratings of all simulations, on the left airborne sound transmission, on the right impact sound transmission.*

The statistics of Fig. 3.14 yields average single number ratings and standard deviations of $R_w(\mu, \sigma) = (58.3 \pm 0.45\,\text{dB}, 2.0 \pm 0.32\,\text{dB})$ and $L_{n,w}(\mu, \sigma) = (50.1 \pm 0.32\ \text{dB}, 2.1 \pm 0.23\ \text{dB})$, where the $\pm$ sign indicates the 95 % confidence intervals of the means and standard deviations. The single number rating of the standard setup ($R_w = 54$ dB) is in the lower bracket, implying that improving just one of the partitions would vastly improve the single number rating. For impact, the same cannot easily be identified as the floorings have a much larger influence of the results. The standard setup ($L_{n,w} = 50$ dB) is placed in one of the middle brackets. It is shown that groups of floorings can be decoupled from the rest of the flanking transmission (Christensen et al. 2013b), and that the within each floor group the distribution of single number ratings could be described as a normal distribution, except for floor 4, which is the swimming floor, for the airborne flanking transmission.

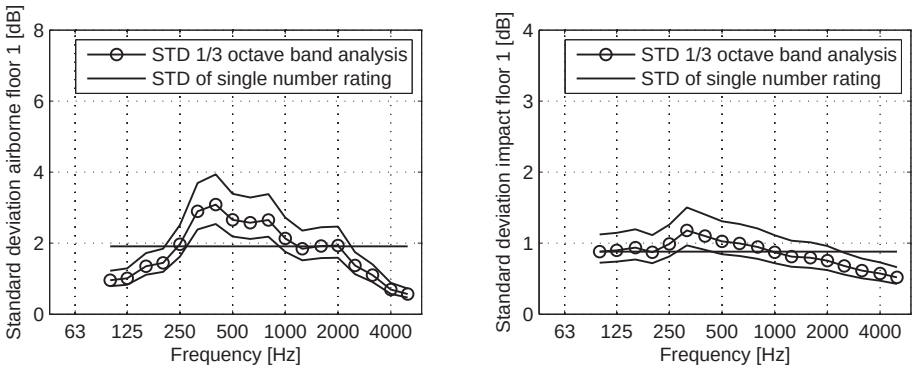

***Figure 3.15**: Standard deviation spectrums for the group consisting of floor 1 for airborne sound insulation of the left and impact sound insulation on the right.*

In Fig. 3.15 the spectrums of the standard deviations for the group of both airborne and impact flanking transmission based on floor 1 are shown along with their 95% confidence intervals. In (Christensen et al. 2013b) a model of how to incorporate these uncertainties in the model for calculating the single number ratings of the super-light element including assessments regarding uncertainties is available. A total standard deviation for the results of the parametric study regarding unknown partitions, including uncertainties of measurement reproducibility, workmanship and the model in EN 12354, were found for two different floors to be $\sigma_{Rw,1} = 2.79$ dB and $\sigma_{Rw,4} = 2.95$ dB for the airborne flanking transmission simulations and $\sigma_{Lnw} = 1.18$ dB for all floorings regarding the impact flanking transmission simulations based on the parametric study.

Chapter 4

Static design

Apart from fulfilling acoustic requirements, which was a main emphasis in the design of the element, the element must also fulfil static requirements, including both the ultimate limit state (ULS) and the serviceability limit state (SLS). For a super-light slab element it means that bending and shear have to be tested experimentally to verify that the element behaves as it can be expected from the already known theory. Also anchorage of the steel wires has been briefly addressed. Furthermore, deflection and dynamic properties such as vibration have been investigated. Finally, as another branch of test the elements resistance against fire have been investigated. Elaborations on some of the key findings are described by (Hertz et al. 2013).

For investigation of the statics the slab has been considered a simple supported beam eliminating plate-like behaviour. This is usual for prefabricated slabs. At first known beam theory is applied on the slab in order to estimate the expected performance. This is then later compared with experimental results to verify the applicability of the theory.

The normal concrete used for these test series have a characteristic compressive strength of 50 MPa, an elastic modulus of 37 GPa and density 2300kg/m^3. The lightweight aggregate concrete has a characteristic compressive strength of 3 MPa, an elastic modulus of 3 GPa and density 600 kg/m^3. The prestressed steel used has a characteristic tensile strength of 1860 MPa and an elastic modulus of 210 GPa, the strands have a diameter of 12.5 mm with a nominal steel area of 93 mm^2 and they have been prestressed to 75% of their tensile strength.

4.1 Test elements

A couple of elements have been designed for the different purposes of the static tests. For each type of the test in the ULS the element and test setup must be designed properly in order to provoke the correct type of failure.

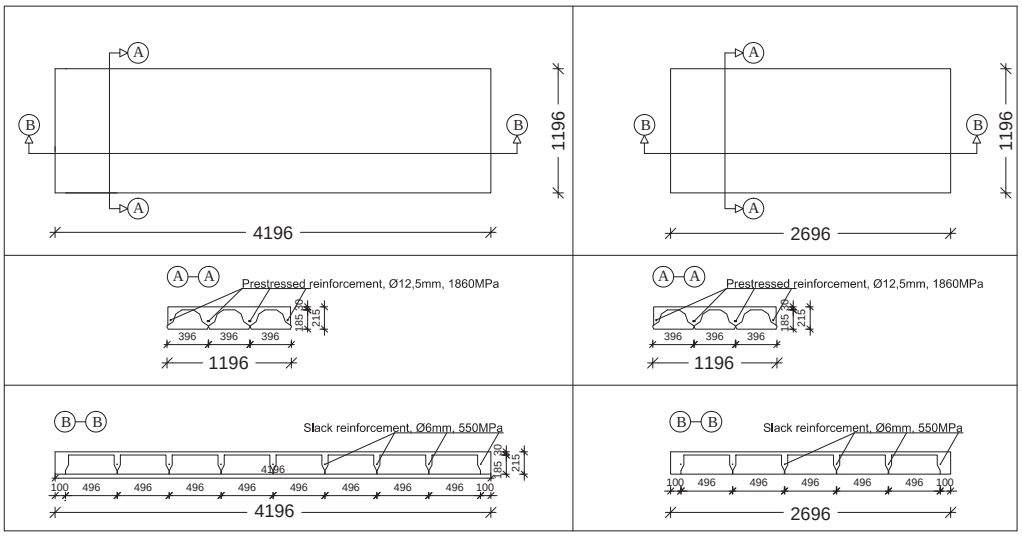

***Figure 4.1**: Two elements used where only the length is varying. The long one is for bending, deflection and vibration, while the short one is for shear and anchorage.*

In general two elements are designed for the ULS and SLS tests. A long one with length 4.2 m which is exposed to bending failure and a short one with length 2.7 m which will be more susceptible to shear failure. For all calculations of cross-section resistances the characteristic material properties have been used.

The expected failure loads are evaluated in the following for bending. It is the classic plastic calculation, where the internal lever arm between the tensile reinforcement and the centre of the compression zone in concrete is used, (Nielsen and Hoang 2010)

$$M_r = F_s z = 133\,\text{kNm} \tag{4.1}$$

where $F_s = A_s f_y$ is the yield force of the reinforcement and $z = d - 0.4x$ is the internal lever arm between the reinforcement and compression zone which have the depth of $0.8x$ in order to balance the yield force in the steel reinforcement.

An approach for shear of wide beams without shear reinforcement is used. This approach includes the improvement by an arch-like behaviour near the support, which will increase the shear resistance of the cross-section by up to five times near the supports. It is the same approach as the one available in the Eurocode for concrete structures (Eurocode 2-1-1 2004).

$$V_{R,c} = \beta \left(C_{R,c} k \left(100 \rho_l f_c\right)^{1/3} + k_1 \sigma_{cp} \right) A_{cn} = 217\,\text{kN} \tag{4.2}$$

where $\beta = 2.5d/x_f$ is the arch strengthening contribution near the support and x_f the distance from the cross-section to the support, $C_{R,c} = 0.18$, $k = 1 + \sqrt{200/d} \leq 2 = 2$ for this cross-section since $d = 137\,\text{mm} \leq 200$ and k is the scale effect, $\rho_l = A_{sl}/bd$ is the degree of tensile longitudinal reinforcement in the element, $f_c = 50\,\text{MPa}$ is the characteristic compression strength, $k_1 = 0.15$, $\sigma_{cp} = N_E/A_c = 6.67\,\text{MPa} < 0.2 f_c = 10\,\text{MPa}$ is the compression stress from the prestressed longitudinal reinforcement and A_{cn} is the concrete area between the longitudinal reinforcement and centre of the compression zone. For this calculation, the full cross-section including the lightweight aggregate blocks has been used determining the compression σ_{cp} from the prestressing. Here only the strong concrete is applied calculating the shear capacity. This is because the tensile strength of the lightweight aggregate concrete is very low compared to the tensile strength of the normal concrete, and it gives a slightly conservative evaluation of the expected shear resistance of the cross-section. Additionally it is very rare that it is the shear resistance of a slab element that ends up being decisive for the design.

The flexural bending stiffness has been calculated and is included in App. B only for the full cross-section, the calculation for the reduced cross-section follows the same principles. The main result is the total flexural stiffness of the test element and it is calculated to $EI = 12.76\,\text{MNm}^2$ for a full cross-section, $EI_{red} = 10.95\,\text{MNm}^2$ for a reduced cross-section, where the bottom 30 mm of the lightweight aggregate concrete blocks has been excluded, so the total height of the element is 185 mm. A small gap exists between the blocks at the bottom of the element. These gaps may open in deflection causing that some of the block will not deform fully as the rest of the element. The flexural stiffness of the element must therefore be expected to decrease. This principle is illustrated in Fig. 4.2. The two values are extremes and the actual flexural stiffness will be somewhere in between.

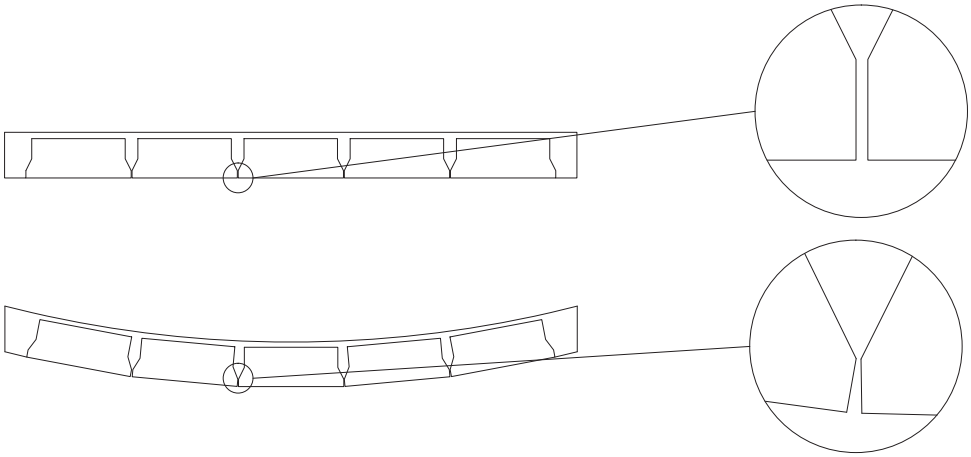

***Figure 4.2**: Flexural stiffness model, top part: un-deformed the gaps are constant as the element deforms and the blocks contribute 100% to the flexural stiffness, bottom part: the gap increases as the element deforms causing the bottom* 30 *mm of the block to not contribute to the flexural stiffness of the element.*

These results are used in the models for predicting the deflection, cracking moment and first natural frequency of the slab element. The deflection is assessed in the elastic range, and only short term conditions are included, which means the long term effects of shrinkage, creep and relaxation are excluded because the tests consider short term loads. The beam deflections formulas are then simple and can be found in a technical handbook, as e.g. (Teknisk Staabi 2004). The deflection model of the element applied includes the influence of camber due to prestressing in order to evaluate its size.

The camber is caused by a constant moment from the prestressing along the beam which gives the following maximum deflection at midspan

$$u_{camber,max} = \frac{1}{8}\frac{M_0 l^2}{EI} \quad \text{for} \quad x = \frac{1}{2}l \tag{4.3}$$

where $M_0 = N_0\,(d - e)$ is the moment from the prestressing, N_0 is the the prestressing force, d is the depth of the prestressing and e is the depth of the centroid Eq. B.39, EI is the bending stiffness and l is the length of the slab element.

The dead load of the beam is a constant line load with a maximum deflection at midspan

$$u_{dead,max} = \frac{5}{384}\frac{q l^4}{EI} \quad \text{for} \quad x = \frac{1}{2}l \tag{4.4}$$

where q is the line load.

The applied load for testing is a point load in the middle of the beam that should give an elastic maximum deflection at midspan of

$$u_{app,max} = \frac{1}{48}\frac{Ql^3}{EI} \quad \text{for} \quad x = \frac{1}{2}l \tag{4.5}$$

where Q is the point load, EI is the bending stiffness and l is the length of the slab element.

These different contributions yields a combined expected deflection of the element of as a function of the applied load Q

$$\begin{aligned} u_{max} &= u_{dead,max} + u_{app,max} - u_{camber,max} && (4.6)\\ &= 0.94\,\text{mm} + (0.104\,\text{mm/kN})\,Q - 8.1\,\text{mm} && (4.7)\\ &= (0.104\,\text{mm/kN})\,Q - 7.16\,\text{mm} && (4.8) \end{aligned}$$

where the contribution of the camber is negative as it works in the opposite direction of the load.

The expected cracking moment is calculated according to the methodology used by the Eurocode for concrete structures (Eurocode 2-1-1 2004) which is an elastic model based on cracking to occur when the stress in the element exceeds the flexural tensile strength of the concrete in use. The flexural tensile strength will be modified statistically according to the beam height.

$$f_{ctm,fl} = \max\begin{cases} \left(1.6 - \frac{h}{1000\,\text{mm}}\right) f_{ctm} \\ f_{ctm} \end{cases} = 5.80\,\text{MPa} \tag{4.9}$$

where $h = 185$ mm as it is the height of the slab element and $f_{ctm} = 4.1$ MPa which is the flexural tensile strength for a concrete with a compressive strength of 50 MPa. This modified strength is used as a criterion for how much moment is needed to apply to the slab element before cracks occur, meaning that the cracking moment can be calculated as

$$M_{crack} = M_0 + \left(f_{ctm,fl} + \frac{N_0}{A_t}\right)\frac{I_t}{h-e} = 84.5\,\text{kNm} \tag{4.10}$$

where M_0 is the moment caused by the prestressing, N_0 is the normal force caused by prestressing which is countered first, A_t is the transformed area, I_t is the transformed second moment of area and e is the distance from the centroid to the bottom of the element, where the cracking happens. All three cross-sectional constants are found according to the calculations in App. B for the reduced cross-section.

The natural frequency of the deck element is calculated as a one dimensional beam element being simple supported as this is how the element could

be tested. The first mode is considered as this is measured and the expected natural frequency is found by Eq. 4.11

$$f_1 = \frac{\omega_1}{2\pi} = \frac{\pi}{2L_b^2}\sqrt{\frac{EI}{\mu}} = 18.6\,\text{Hz} \tag{4.11}$$

where $L_b = 4\,\text{m}$ is the length of the beam $EI = 12.76\,\text{MNm}^2$ is the bending stiffness of the beam and $\mu = 355\,\text{kg/m}$ is the mass pr. length of the beam.

The moment capacity after 120 minutes of a standard fire is calculated for a hot condition, the cold condition after the fire exposure is not investigated in Sec. 4.6. The normal concrete in the section is insulated by the lightweight aggregate concrete and there will be no reduction to its strength or size during the hot condition in the compression zone of the concrete. The prestressed steel will have its strength reduced depending on how hot it gets. The coefficient for the strength reduction is found with the program ConFire (Confire user guide 2012) with the thermal conductivity for the lightweight aggregate concrete $\lambda = 0.3\,\text{W/mK}$. The strength reduction coefficient for the steel is found to be

$$\xi_{side} = 0.7959 \tag{4.12}$$

$$\xi_{middle} = 0.7253 \tag{4.13}$$

$$\xi_{120} = \frac{1}{6} = (2\xi_{side} + 4\xi_{middle}) = 0.7488 \tag{4.14}$$

since there are two prestressing wires in the side of the element and four in the middle of the element. These reductions correspond to a temperature of 191° in the cold drawn prestressed wires.

With this knowledge the moment resistance is calculated by the same method as the pre-fire moment resistance was calculated in Eq. 4.1 with the difference that the yield force of the steel wires is lower and therefore the internal lever arm is slightly larger as the concrete compression zone is slightly smaller.

$$M_{r,fire120} = F_{s,fire120} z = 101\,\text{kNm} \tag{4.15}$$

The characteristic capacity is reduced from 133 kNm to 101 kNm after two hours of standard fire.

4.2 Bending

An element spanning $L_b = 4\,\text{m}$ is exposed to three-point bending with a point load at the middle of the element as shown on Fig. 4.3, where a small

steel I-profile is placed across the width of the element in order to distribute the point force

***Figure 4.3**: Test setup for bending test of super-light element, the steel profile along the element is for deflection measurements.*

The element is being loaded with a constant increasing rate of pressure. Fig. 4.4 shows the deflection-force diagram of the two test carried out on identical test elements along with prediction models of the deflection

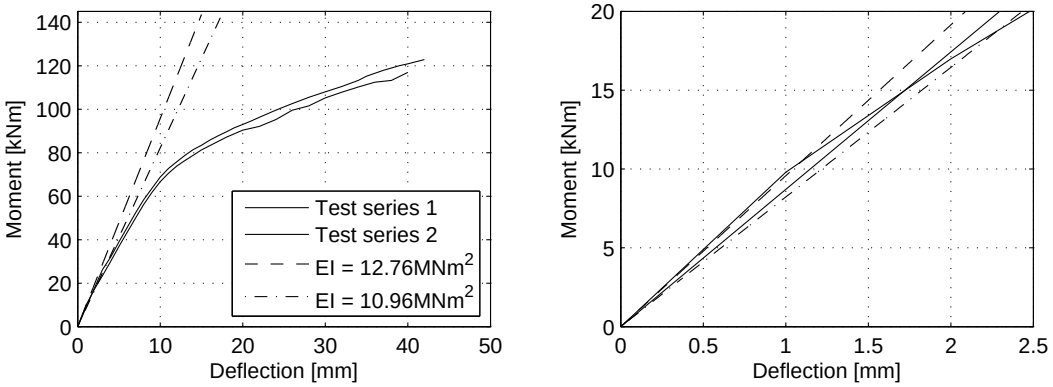

***Figure 4.4**: Deflection-force diagram of the bending tests, with theoretical elastic deflection models. At the right a detailed view of the first part of the deflection.*

The contribution from the dead load of the beam is not included in Fig. 4.4. The size of the moment from the dead load at midspan is calculated by

$1/8qL^2 = 7.0\,\text{kNm}$ with $q = \mu g = 355\,\text{kg/m} \cdot 9.81\,\text{m/s}^2 = 3.48\,\text{kN/m}$ and $L = 4\,\text{m}$.

The first test yielded a failure moment of 146 kNm and the second test a failure moment of 148 kNm, whereto 7 kNm should be added considering the dead load. This is a little larger than the expected moment resistance of the slab element of $M_r = 133\,\text{kNm}$ which show that the calculated moment resistance is on the safe side. It is worth noting that both elements failed at approximately the same load and by exactly the same mechanism. Fig. 4.5 shows the development of cracking in one of the tests at failure.

***Figure 4.5**: Cracking development in the super-light slab element tested in bending, the wet area is leaked oil from the oil press.*

The pattern of cracks in the element is a little disturbed by the fact that the layer of normal concrete is rather shallow in the lower part of the element at the edge towards the lightweight aggregate block which also is indicated by the drawings in Fig. 4.1. Nevertheless several vertical tensile cracking lines can be identified on the element. Late in the test, just before failure, a long longitudinal crack between the two different concretes appeared at the side surface as it can be seen in Fig. 4.5. This happened due to the combination of a very large deflection of the element and that cracks are more likely to follow paths in the lightweight aggregate concrete close to the border to the strong concrete than in the strong concrete, under normal structural loads these cracks will not occur and it has have no influence of the performance of the slab element.

On Fig. 4.4 the first part of the rate of deflection is very linear corresponding to the linear elastic deformation of the element. When the moment

reach between approx. $65 - 80$ kNm the slope of the deflection rate decreases which indicates the beginning of cracking and an accelerated deflection rate. This is in pretty good agreement with the estimate from Eq. 4.10 which predicted a cracking moment of $M_{crack} = 84.5$ kNm when the moment of the dead load is included which means that cracks are predicted to start when the moment reach 77.5 kNm in Fig. 4.4. Due to limitations of the capacity of the automated deflection measurement equipment only deflections till 40 mm have been measured. This means that the influence of steel yielding is not visible on the deflection-force diagram, the deflection at failure was manually measured to approximately 200 mm.

4.3 Shear

The shear test was made with the short element in Fig. 4.1. The test setup is shown in Fig. 4.6, where it can be seen that the point force is applied near one of the supports so that the shear force in the element is increased compared to the moment and shear can be the failure mechanism. At the same time the force must be applied at least in a distance $2.5d = 373$ mm away from the support in order to avoid increasing the shear resistance of the cross-section to due to the arch effect. This is the reason that the force is placed in a distance to the support of 485 mm. Since the model is empirical, the extra 100 mm makes it on the safe side. Furthermore, it can be seen that the anchorage length is sufficient long in order to avoid any mechanisms due to failure of the anchorage of the prestressed wires.

***Figure 4.6**: Test setup for shear test of super-light element.*

At failure the shear force applied to the element was 265kN well above the prediction model from the Eurocode regarding shear resistance in elements without shear reinforcements which was found in Eq. 4.2 to $V_{R,c} = 217$ kN. The rather large difference can partly be ascribed to the fact that the contribution from the lightweight aggregate concrete is omitted in the prediction model and that the model is empirical and some statistic, based on a scattering of test results, has been applied in order to make it safe to use.

On Fig. 4.7 the element is shown just after failure where several tensile cracks caused by a moment was developed before the element failed in shear.

***Figure 4.7**: Shear test at failure, cracking occurred from tensile stresses with a sudden shear failure.*

The actual moment in the element at failure had a magnitude of 113kNm which explains why the tensile cracks occurred, and as the previous bending test showed the moment was not large enough to cause failure for the element.

A similar test was made with a much shorter anchoragelength of the reinforcement at the support. The ultimate load was measured with a shear force of 149 kN, well below the previous result and the prediction model, indicating that here it was an anchorage failure namely in the bond between the prestressing wires and the concrete causing the failure. This is further confirmed as it was observed that the prestressed reinforcement was withdrawn approximately 20 mm into the end of the element. The mechanics behind this failure is further explored in depth in the accompanying paper (Hertz et al. 2013) and by (Hertz 1982).

4.4 Deflections

The deflection setup is visible in Fig. 4.3, the measurement equipment is mounted on top of the element which means it is calibrated to be zero after the effects of prestressing and dead load have been applied to the slab, meaning that it is only the deformation caused by the external applied load which is measured. On Fig. 4.4 the theoretical deflection is included as a function of the moment for both models of the bending stiffness. At the start of loading the rate of deflection follows the elastic model quite well as it is in between each of the limits specified by the two bending stiffness, but after a few millimetres of deflection inelastic behaviour starts to occur as the tangential E-modulus is reduced as the load increases.

4.5 Dynamic

The natural frequency of the element was measured by hanging a mass from the element in a string. By burning the string the element was set into a free harmonic vibration. The oscillation was measured by an accelerometer placed at the middle of the super-light element above the point where the mass was hanging. Here it translated the measurement of the acceleration of the vibration into the natural frequency of the element in its accompanying software. The measurement gave a natural frequency of the slab element of 14.8 Hz, which is considerable lower than the one of 18.6 Hz estimated by Eq. 4.11. The general accuracy of the test setup and measurement equipment is estimated to be ± 1 Hz. From Eq. 4.11 it is clear that the boundary condition, the length, the stiffness and the mass are factors which have influence on the natural frequency. For the test, the element was resting on wooden blocks having a rather short anchorage length, which means that the restraining moment is negligible small and the slab is very close to be perfectly simple supported. The span of the element was measured and is accurate. The same goes for the mass of the element which was weighted. Taking a closer look at Fig. 4.4 reveals that at very low deflections the slope of the deflection curve of the element is parallel with the theoretical value which means that the stiffness used for the vibration test should be quite accurate.

4.6 Fire

The element has been tested for fire safety. The test was a two hour standard fire with a load corresponding to Danish domestic live load $q_{imposed} = 1.5\,\mathrm{kN/m^2}$ and an estimated supplementary permanent load $q_{supp} = 1\,\mathrm{kN/m^2}$

(Eurocode 1-1-1 2002). After two hours of standard fire the load was increased until failure. The slab was tested with four point bending and the pistons delivering the load was placed at the quarter-points, meaning that a constant moment of $1/4QL$ was present between the pistons with Q being the force applied by one piston. The test setup was made by installing two 1.2 m wide super-light elements with a length of 6.4 m in a durable frame which was placed on top of an oven providing the standard fire. The total free span of the super-light elements was 6.0 m, the setup is shown in Fig. 4.8 where equipment for measuring temperature and deflection is present.

***Figure 4.8**: Test setup for fire test of super-light element.*

The moment from domestic load including the dead load (15.68kNm) and additional permanent load had a total magnitude of 29.2 kNm corresponding to each of the pistons acting with a force $1/2qL = 9$ kN. The moment from the domestic load was significant smaller than the moment resistance and no indication of failure could be observed, a deflection at midspan of 25 mm was measured after 120 min of standard fire exposure. Then the load was increased. Each of the pistons was increased to their maximum capacity applying a total force of 61.25 kN corresponding to a moment on the slab element of 110.1 kNm without any failure in the element, approximately 10% more than the capacity estimated by calculation. At this time, a steel temperature of $150°C$ was measured well below the calculated temperature of $191°C$ from ConFire, thus increasing the moment resistance of the element. At the maximum load the deflection was measured to 200 mm. After unloading the element the deflection was 35 mm. A relative small permanent

damage from the fire and load. As it is seen from Fig. 4.9 showing the element from below, the element is unharmed after the two hour standard fire test.

***Figure 4.9**: View of the element used for the fire test from below after the test.*

Chapter 5

Design with super-light elements

Besides the super-light elements that have been designed as a part of the experimental production series for full-scale testing of acoustics, statics and fire, another project has been carried out, in which super-light deck elements have been applied in a building.

5.1 Indoor pedestrian footbridge

In this project an indoor pedestrian footbridges are hung down in two levels from the ceiling. They are made with super-light deck elements. It is a two storey building, has a plan area of 2000 m^2 and consists of eight individual towers. The super-light pedestrian bridges provide access between these towers and have a total area pr. storey of 200 m^2, which means a total area of 400 m^2. The plan of the building including the placement of the super-light deck elements can be seen on Fig. 5.1.

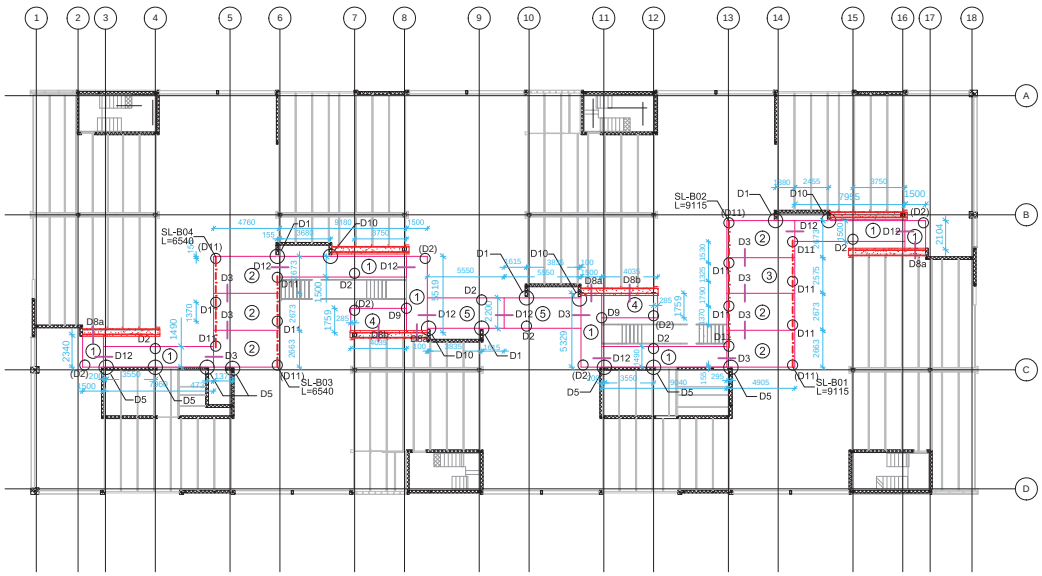

***Figure 5.1**: Plan of the building with the super-light indoor pedestrian bridge connecting the eight towers with each other.*

There is a requirement that a footbridge should have a width of at least 1500 mm in order to provide accessibility to disabled persons, which in combination with additional architectural features of the bridge meant that it was not possible to use the standard widths of either 1200 mm or 2400 mm. The elements were instead custom made in special moulds and prestressing them was therefore not a possibility.

The non-existing possibility of prestressing was the cause for introducing short spans to eliminate the risk of cracking and thus very large deflections and vibration amplitudes. This meant that a maximum span of 5.5 m was used in the design. The supports consist of three different kinds of point supports and one continuous support. In total there was a superior amount of point supports compared to continuous supports. There was also a need to prepare the super-light elements for a large amount point forces, not something the lightweight aggregate concrete blocks are especially suited to handle.

The lightweight aggregate concrete block had the geometry as depicted earlier in Fig. 2.3. Therefore it was a necessity to enhance the existing design of the super-light slab element so that it could accommodate all the requirements to geometry, supports and constructability.

In Fig. 5.2 a section of the finished pedestrian bridges are shown, including parts of the support system in form of hangers.

***Figure 5.2**: View of some of the finished super-light bridge elements.*

Edge-, end-, cross-beams

The concept of edge-, end-, and cross-beams in the super-light deck elements was developed in this project as special solutions. They consist of concrete beams integrated into the elements and include stirrups and longitudinal reinforcement as shown in Fig. 5.3 where the reinforcement arrangement can be seen before the normal concrete is cast and how the internal beams looks like in the element.

***Figure 5.3**: Internal beams in the super-light element, on the left before normal concrete is cast on the right how the beams are visible in the final product. The steel parts are interim supports and the nut plate support a hanger carrying the element.*

The internal beams are advantageous in relation to the varying width of the pedestrian bridge, as the size of lightweight aggregate concrete blocks lack flexibility. This is instead supplied by the internal beams which support widths between $75 - 150$ mm. The minimum is in order to have room for stirrups and the maximum is limited by the fact that if they were any wider, an extra line or row of lightweight aggregate blocks could have been placed instead. In the internal beams there are room for more longitudinal reinforcement and without lightweight aggregate concrete blocks at the bottom these can have a larger depth. This increased reinforcement and stiffness reduces the penalty caused by not pre-stressing the elements. Finally, the beams are ideal for establishing the point supports, as it is possible to have nests of reinforcement around the support details in both directions.

Design of support solutions

In total four kinds of supports were used in the building, three point supports and one line support. The line support is common and there has been no special preparation of the super-light element for it other than edge or end beams are placed at the support. The point supports consist of a hanger suspended from steel beams in the ceiling. A support based on inserts to exchange forces with adjacent walls, a console connection attached to a wall and finally elements connected with a blade connection solution rather than applying bedding materials to connect the elements. All of these connections is described more in-depth in the accompanying paper (Christensen and Hertz 2013).

The hanger support is completed by supplying the element with a hole in an intersection between an edge-beam and a cross-beam. Here, beam reinforcement surrounds the hole in both directions absorbing the concentrated point force and eliminating any risk of punching shear. The point force is further distributed by a $200 \times 200 \times 16$ mm thick steel plate beneath the element.

The insert connection is made by casting four inserts into the concrete edge beams in the element. Here they are connected via steel parts, over a gap of 100 mm, to the wall on which the steel parts are bolted. The inserts are supported in the internal cross-beam where longitudinal and stirrup reinforcement has been placed to anchor the tension forces from the inserts over a larger concrete area.

The console connection is completed by bolting steel parts on a wall and placing the super-light deck element to rest there. The only preparation of the element is that cross- or end-beams are present at this kind of support in order to absorb the concentrated point forces.

The final detail mentioned here in the indoor pedestrian super-light bridge

is the connection between two super-light deck elements. Here a blade connection has been designed so that through-out the construction of the building the elements are overlapping each other and are bolted together to create a solid transfer of forces between the elements.

***Figure 5.4**: Left: detailed drawing of the connection, middle: example on how connection and reinforcement is established in a super-light element, right: example of the detail.*

Chapter 6

Discussion

6.1 Acoustic design

The single number ratings of the airborne and impact sound insulation laboratory measurements was found as $R_w = 55\,\text{dB}$ and $L_{n,w} = 79\,\text{dB}$. Recently measured hollow-core airborne and impact sound insulation are not publicly available, (NM and BR 1974a) and (NM and BR 1974b) supplies results for a 185 mm hollow-core element with a surface mass of 300 kg/m^2 for airborne and impact sound insulation. The results of the measurements are $R_w = 53\,\text{dB}$ and $L_{nw} = 80\,\text{dB}$ for the case without any additional flooring.

With the statistics obtained for the flanking results, quantiles of thresholds of the super-light slab element is obtained, see (Christensen et al. 2013b) for an elaboration of which models and statistics are used to obtain the results discussed in the following. For the standard room the uncertainties is addresses using the work by (Mahn and Pearse 2009), (Craik and Steel 1989) and (Craik and Evans 1989) as lack of accuracy of the flanking transmission model, workmanship and measurements errors. The results are expressed in terms of the probabilities $P(R'_w \geq x = F_x(\mu_{R'w}, \sigma_{R'w})$ and $P(L'_{nw} \geq x = F_x(\mu_{L'nw}, \sigma_{L'nw})$ with F being the cumulative distribution function of a normal distribution.

$$\begin{aligned} P\left(R'_{w,1} \geq 55\,\text{dB}\right) &= 42.0\,\% \\ P\left(L'_{nw,1} \leq 53\,\text{dB}\right) &= 94.0 : \% \\ P\left(R'_{w,1} + x_1 \geq 55\,\text{dB}\right) &\geq 95.0\,\% \quad , \quad x_1 > 3.7\,\text{dB} \\ P\left(L'_{nw,1} - x_2 \leq 53\,\text{dB}\right) &\geq 95.0\,\% \quad , \quad x_2 > 0.2\,\text{dB} \end{aligned} \tag{6.1}$$

In regards to legislation requirements, as they were discussed in the introduction, the single number rating of the airborne flanking transmission for the super-light slab element was just below the requirement. When including uncertainties, this gives a probability of achieving the requirement of the

legislation on less than 50 %, from Eq. 6.1 it is also evident that a large improvement of the single number rating of the super-light element is needed to achieve 95 % probability of satisfying the legislation. The results are more optimistic regarding the impact flanking transmission, where a probability of 95 % satisfying legislation is almost obtained. In Sec. 6.3 it is discussed how improvements to the slab can be made in order to achieve a better quantile for the standard room when considering airborne sound insulation.

For the parametric study the partitions are unknown, this gives rise to another uncertainty, which together with the uncertainties of the accuracy of the flanking transmission model, workmanship and measurements errors, can be described by probabilities. Here, the quantiles is addressed in groups dependent on the floor. Results regard the airborne flanking transmission are listed in Eq. 6.2 and in Eq. 6.3 for the impact flanking transmission simulations.

$$\begin{aligned}
P\left(R'_{w,1} \geq 55\,\mathrm{dB}\right) &= 86.7\,\% \\
P\left(R'_{w,4} \geq 55\,\mathrm{dB}\right) &= 91.2\,\% \\
P\left(R'_{w,1} + x_{R'w,1} \geq 55\,\mathrm{dB}\right) &\geq 95.0\,\% \quad \Rightarrow \quad x_{R'w,1} > 1.5\,\mathrm{dB} \\
P\left(R'_{w,4} + x_{R'w,4} \geq 55\,\mathrm{dB}\right) &\geq 95.0\,\% \quad \Rightarrow \quad x_{R'w,4} > 0.9\,\mathrm{dB}
\end{aligned} \tag{6.2}$$

The probability that the super-light element in the unknown room will pass legislation requirements are overall high and only a small amount of improvement is needed to obtain probability of 95 %. As the standard room was placed in the lowest bracket of the full simulation see, e.g., Fig. 3.14, it is clear from the results of the parametric study that improvement of the flanking partitions is a strong alternative to improving the airborne sound insulation of the standard room compared to increasing the surface density of the super-light element. Only a small difference between the floor groups exist, this is unexpected as the laboratory measurement of the two floors were very different $\Delta R_1 = 3\,\mathrm{dB}$ and $\Delta R_4 = 9\,\mathrm{dB}$.

$$\begin{aligned}
P\left(L'_{nw,1} \leq 53\,\mathrm{dB}\right) &= 92.3\,\% \\
P\left(L'_{nw,2} \leq 53\,\mathrm{dB}\right) &= 57.3\,\% \\
P\left(L'_{nw,3} \leq 53\,\mathrm{dB}\right) &= 99.3\,\% \\
P\left(L'_{nw,4} \leq 53\,\mathrm{dB}\right) &= 79.6\,\% \\
P\left(L'_{nw,1} - x_{L'nw,1} \leq 53\,\mathrm{dB}\right) &\geq 95.0\,\% \quad \Rightarrow \quad x_{L'nw,1} > 0.5\,\mathrm{dB} \\
P\left(L'_{nw,2} - x_{L'nw,2} \leq 53\,\mathrm{dB}\right) &\geq 95.0\,\% \quad \Rightarrow \quad x_{L'nw,2} > 3.2\,\mathrm{dB} \\
P\left(L'_{nw,3} - x_{L'nw,3} \leq 53\,\mathrm{dB}\right) &\geq 95.0\,\% \quad \Rightarrow \quad x_{L'nw,3} > -1.7\,\mathrm{dB} \\
P\left(L'_{nw,4} - x_{L'nw,4} \leq 53\,\mathrm{dB}\right) &\geq 95.0\,\% \quad \Rightarrow \quad x_{L'nw,4} > 1.8\,\mathrm{dB}
\end{aligned} \tag{6.3}$$

The results of the parametric study for the impact flanking transmission analysis show a much higher degree of dependency on each of the floor groups compared to the airborne flanking transmission analysis. As the standard deviation is equal for all of the floor groups, since all flanking transmission paths originate from the floor, the difference of $x_{L'nw}$ is also a difference of the mean of single number rating in each of the floor groups. Combining the super-light element with floor 1 yields very good results with little need for improvement of the super-light slab element, while floor 3 requires no improvement at all.

The flanking transmission analysis for the standard room can be directly compared to a flanking transmission analysis made with similar concrete elements in form of hollow-core slabs (Christensen 2012). These simulations are made for a room setup equal to the standard room. Here an element with surface density 316 kg/m^2 has been simulated for both airborne and impact flanking transmission. The results are for airborne sound insulation $R'_{w,316} = 53$ dB and for impact sound transmission $L'_{nw,316} = 54$ dB. It is also shown that the mass needed to achieve an airborne sound insulation of $R'_w \geq 55$ dB is 367 kg/m^2 and to achieve an impact sound insulation $L'_{nw} \leq 53$ dB is 323 kg/m^2 for a hollow-core slab. In Sec. 6.3 it is argued by means of Eq. 6.4 that an airborne sound insulation of $R'_w \geq 55$ dB would be achieved for a super-light slab element with surface mass 328 kg/m^2, while the requirement of impact sound insulation $L'_{nw} \leq 53$ dB is obeyed be a margin of 3 dB for a super-light element with surface mass 315 kg/m^2. With the limited amount of data sets available it cannot be proven that there is a statistical difference of the two results, as the results listed are subject to the earlier discussed uncertainties regarding building acoustic performance evaluation for flanking transmission. But the difference obtained here of 40 kg/m^2 indicate that the super-light slab element design is an improvement compared to the similar hollow-core concrete element.

Traditionally when constructing multi-storey housing with pre-fabricated concrete elements, the load-bearing elements are installed first. This means at the time internal partitions, typically 100 mm wide lightweight concrete elements with a density of 1350 kg/m^3, are installed, the floor slab above it already has been installed. Due to the tolerance associated with pre-fabricated elements the height of the internal partition will be less than the height of the storey it is to be installed in. The bottom of the internal partition is grouted with a mortar in order to seal it, this mortar typically has a compressional strength of $f_c = 30$ MPa, and will not influence the attenuation of structure-borne sound in the junction. However, at the top of the internal partition it will be sealed to the floor slab by soft expanding foam, creating a resilient layer to the junction between the internal partition and the

floor slab Fig. 6.1. From the parametric study of the flanking transmission, where resilient layers were included as a parameter, it is known that those resilient layers improve the performance of the super-light slab element in flanking transmission. For the standard room the airborne sound insulation R'_w is increased by 3.2 dB from 54.6 dB to 57.8 dB, while the influence of the resilient layers are less pronounced for the impact sound insulation $L_{n,w}$, here, the performance is increased by 0.6 dB from 49.9 dB to 49.3 dB. In the simulated situation the resilient layers are applied in eight places in the room for all four junctions, while for the situation in-situ just described, it would be applied in just two places in the room, so the influence is not to be expected to be as large as the simulation show. However, (Christensen et al. 2013b) showed that the internal partitions contributed the largest amount of flanking transmission so this condition of how internal partitions are installed could improve the airborne flanking transmission performance of the super-light slab element.

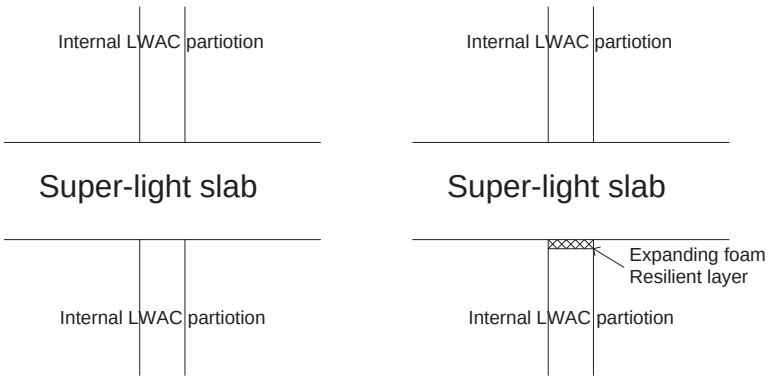

***Figure 6.1**: On the left the junction model used in simulation, on the right junction model with implementation of an expanded foam seal between the partitions.*

6.2 Static design

The results obtained in Chap. 4, where the static performance of the super-light element was evaluated, is based on test procedures and calculations according to the design codes for concrete structures (Eurocode 2-1-1 2004) and (Eurocode 2-1-2 2004). These are often based on simplifications and/or empirical models, this means that models have been used despite it will be

less accurate and return a lower load-bearing capacity than what the situation for the super-light slab actually is.

In general secondary effects from the pre-stressing and long-term loading of the element have been ignored. The experiments conducted here along with verifications of the ultimate limit state in live buildings are done according to short term loading. The long-term effects of loading regarding, relaxation of the pre-stressing wires, shrinkage of the concrete and creep are relevant regarding the serviceability limit state. The long-term effects for normal concrete are well documented both by the daily application of pre-stressed concrete and in literature by, e.g., (Collins and Mitchel 2001, chapter 3). The long-term effects of the lightweight aggregate concrete in combination with prestressing and in combination with normal concrete is unknown and subject for further research. It is mentioned that the effect of creep has been included in the design of the pedestrian bridges in relation to the verification of the SLS requirements.

The shear has been calculated according to an empirical method based on experiments available in the structural concrete code for concrete beams without stirrup reinforcement. Shear failure and the mechanics behind has been subject to a lot of research and some of the most important findings are given by (Nielsen and Hoang 2010, chapter 5), where the crack sliding theory is presented for beams without shear reinforcement. Here, it is argued that the shear capacity of a cracked concrete section compared to an uncracking concrete section will be lower, as indicated by Fig. 6.2.

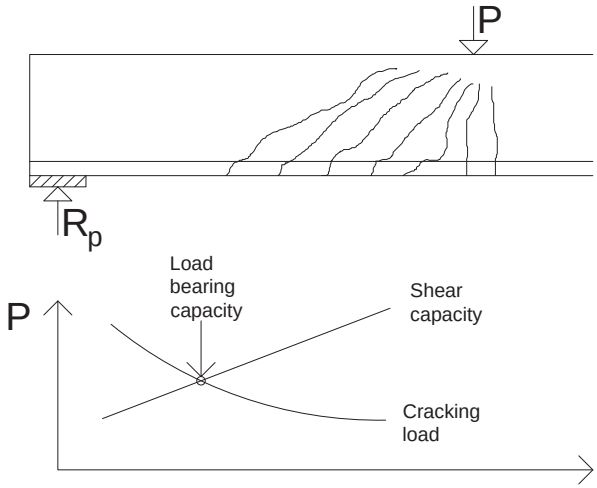

Figure 6.2*: Crack formation and shear capacity of concrete beams without shear reinforcement.*

The theory is based on a homogenous beam of plain concrete and can

therefore not be directly applied to the super-light element. It is proposed that some sort of weighting, of either the normal concrete area or the compression and tensile strength of the concrete depending on ratio of normal concrete to lightweight aggregate concrete, needs to be done to use the theory with the super-light slab element. This is further complicated by the lower bound solution of the shear capacity which is derived based on a diagonal region of concrete in uniaxial compression from the a point force to the support, this region has a height of half the beam. Depending on where a cut in the section of the super-light slab is taken, the ratio of normal concrete and lightweight aggregate concrete is changing. It is not possible to make any assessments to this idea as only data from one experiment is available.

6.3 Future changes to design of super-light slab

Since the testing series of the super-light slab element has been carried out for acoustics, statics and fire, several iterations of the super-light slab design has optimized the performance. The tests are all based on comparing the element with regulations; verify known theory and calculation methods. For the static test series this was all fulfilled. However, a rather large difference of the dynamic measurements of the vibration of the slab compared to the expected was observed. In the fire test, the super-light slab element behaved as expected and the results of the two hours test can be extrapolated to a four hour standard fire. For the acoustic measurements and simulations the super-light slab was 0.4 dB lower than the requirement of the regulations for the airborne sound transmission loss rating when the setup was the standard partitions and floor, this result is something that requires an improvement of the element, also in relation to the general uncertainties for the measurements and simulations as discussed in Sec. 3 and by (Christensen et al. 2013b).

Apart from completing the holistic design of the super-light slab covering all requirements and regulations other heavy weighing factors is influencing the design of the element, most notable cost, which can relate to many things, but also the production setup should be compatible with the design of the element.

The most important change for the element is that the density of the lightweight aggregate concrete increases from 600kg/m^3 to 800kg/m^3. This is made for two reasons, to improve the acoustics and to improve the production speed of the element. The lightweight aggregate will be cast continuous and when the density is increased the stiffness and strength likewise will be

increased this will allow that the normal concrete can be cast earlier without compromising the integrity of the lightweight aggregate concrete shape. This allows that the elements can be cast within a day cycle. For a 2.4 m wide element this means an increase in surface mass from $328\,\mathrm{kg/m^2}$ to $349\,\mathrm{kg/m^2}$ and for the acoustical test element it would mean an increase from $315\,\mathrm{kg/m^2}$ to $335\,\mathrm{kg/m^2}$ corresponding to increases of the surface mass of 6.4% and 6.3% respectively for the general element design and the element designed for the acoustic test. For the acoustic element used in the measurements compared to the final surface mass of $349\,\mathrm{kg/m^2}$ this is an increase of 10.1% in the surface mass. In terms of the mass law this can directly be estimated to increase the airborne sound transmission loss by

$$\Delta R_w = 20\log_{10}(1.063) = 0.54\,\mathrm{dB} \tag{6.4}$$

$$\Delta R_w = 20\log_{10}(1.108) = 0.89\,\mathrm{dB} \tag{6.5}$$

which should accommodate the requirements for the most common room and partition setup.

Another major change is the width of the element, going from the former standard width of 1200 mm to 2400 mm. The slack cross reinforcement of the super-light slab element makes it possible to double the width of the element. The main motivation behind this change is to reduce the number of element lift at the construction site which should constitute significant economical and time benefits, which is further enhanced by the fact that the fewer elements also requires less details to complete the construction. The doubling of the width is done by mirroring the 1.2 m wide element implying that the experimental work carried out on the 1.2 m wide element can be applied for this wider element as well, as it is a mirror.

A smaller redesign is new geometries to the blocks which will be narrower and longer. From having a box dimension of $400 \times 500 \times 185$ mm to having a box dimension of $375 \times 600 \times 185$ mm. The blocks have been made less wide in order to make room for a solid block of concrete in the centre of the element, if needed; a duct can be placed here in order to prepare the element for posttensioning. The redesign of the block shape create a new stiffness distribution in the element, in order to see the influence of the redesign the bending stiffness is calculated for the element used in bending test, Fig. 4.1, but remade with a total width of 2400 mm and the new block design. The influence of the redesign of the blocks on the surface mass of the element has been included in the calculations in relation to Eq. 6.4. For the old design this gives an array of 6×8 blocks while for the new design it is an array of 6×6 blocks. The second moment of area is calculated by the same method

applied in App. A, and are as following

$$\begin{aligned} B_{1,o} &= 10.85 \cdot 10^6 \qquad B_{2,o} = 9.61 \cdot 10^6 \qquad B_{12,o} = \sqrt{B_{1,o}B_{2,o}} = 10.20 \cdot 10^6 \\ B_{1,n} &= 13.00 \cdot 10^6 \qquad B_{2,n} = 9.78 \cdot 10^6 \qquad B_{12,n} = \sqrt{B_{1,n}B_{2,n}} = 11.24 \cdot 10^6 \end{aligned} \tag{6.6}$$

where the subscript $_o$ indicates old design and the subscript $_n$ indicates new design. The new block design makes the slab 9.6 % more stiff improving on vibration, deflection and the critical frequency. However it is also more orthotropic, with the old design there was a difference of 11% in the bending stiffness in the two principal directions, now there is 25% difference, this corresponds to critical frequencies for each the principal directions on $f_{c,1} = 97$ Hz and $f_{c,2} = 112$ Hz, but still almost within the same one-third octave band.

Another option is to cover the bottom of the element with a plaster. The design with super-light structures for the pedestrian bridge and the super-light element used for the experimental tests showed that the bottom of the element did not always look good. Uneven distributions of moisture could be observed on the blocks and the block array was not always straight which disturbed the pattern and in some places concrete would leak through the small cavities between the blocks. And overall the pattern of blocks may not always be satisfying all architectural desires. Some of these issues are indicated on Fig. 4.9 and Fig. 5.3 where the bottom of the element is visible. The method of casting the lightweight aggregate concrete has changed so it is a continuous big block only interrupted by sections of full concrete for anchorage at supports. As the whole element is cast in one sequence, uneven moisture patterns should be eliminated and there is no disturbance of the pattern or no places where the normal concrete can leak. The opportunity to cover the lightweight aggregate in plaster will cause the element to lose the sound absorbing qualities, coming from the porosity, in regards to room acoustics.

Chapter 7

Conclusions

A super-light floor element has been holistically designed. Not all disciplines of a holistic designed is treated in this thesis, but they may have affected choices made for the disciplines treated. Statics, dynamics, structural fire safety and building acoustics have been addressed with a main emphasis on the building acoustic part. In addition, it has been shown that combination of lightweight aggregate concrete and normal concrete gives the super-light element the properties wanted in relation to production, through casting of prototypes to the test series of the element and casting of elements used for the super-light pedestrian bridges. In the conclusions the main findings for each of the chapters in the thesis are reviewed.

The first design of a super-light element has been carried out. By means of a production of prototypes it has been shown that the design of a super-light slab element is producible. The lightweight aggregate blocks are produced by means of moulds according to the geometry in Fig. 2.3. The blocks are placed by hand in a desired array on a plane surface and normal concrete is cast on top of the lightweight aggregate blocks. From Fig. 2.5 it is shown that the plastic normal concrete completes the section without leaving any voids in the section or causing other complications. This is further confirmed by Fig. 2.6, where the penetration of normal concrete in the porous lightweight aggregate concrete is shown to be equal through a line along the connection of the two concrete materials.

It is shown that the single number ratings of the airborne and impact sound insulation of the super-light element are $R_w = 55\,\mathrm{dB}$ and $L_{nw} = 79\,\mathrm{dB}$. This is for an investigation of the super-light slab element in a controlled environment in a laboratory; these ratings are without an additional floor covering. By means of the flanking transmission model based on calculation standard EN 12354 and the results of the laboratory measurements, the performance in-situ of the super-light element is found. The flanking

transmission analysis is split into two parts. The first one shows that the sound insulation of the super-light slab element in a standard room based on the current construction scheme, in terms of single number ratings, is $R'_w = 54$ dB and $L'_{nw} = 50$ dB for airborne and impact flanking transmission respectively. The analysis include a second part, where the element was investigated for unknown flanking partitions, this was done by means of a large parametric study. It was found that each of the floorings applied to the super-light element could be decoupled from the full analysis and it was shown that within such floor group the distribution of single number ratings was normal, allowing each floor group to be described by a mean and a standard distribution in order to predict the general performance of the super-light element depending on the additional floor covering. The results of this analysis are shown and summarized by Eq. 6.2 and Eq. 6.3, and from that it is concluded that improvement of the flanking partitions is a more feasible design solution than just adding mass to the super-light slab element in order to obtain 95 % quantile of obeying legislation.

It is verified by means of tests of the load-bearing capacity in the ultimate and serviceability limit state, that the super-light element behaves as expected and the test results can be described and calculated by known theory. A simple plastic moment calculation provided a moment resistance of the cross-section of 133 kNm Eq. 4.1, which is on the safe side compared to the bending test results of 148 kNm and 146 kNm. The shear capacity of the element, verified by a simplified model without including the contribution of the lightweight aggregate by Eq. 4.2, is on the safe side compared to the experiments, 217 kN compared to 265 kN, this method is equivalent to how the element will be designed in relation to design codes. By means of the bending tests, elastic behaviour regarding deflections and vibrations have been observed with a tendency that the super-light element is not as stiff as first expected. A two hour standard fire test confirmed, that the high thermal insulation of the lightweight aggregate blocks protect the reinforcement and normal concrete so that excellent results of fire safety are achieved for the element.

It is shown that a variation of the super-light element successfully has been designed and introduced in a live construction as indoor pedestrian bridges. In order to construct the bridges, it is shown that a wide array of known technologies is applicable to use with the super-light element including edge-, end- and cross-beams, applications of connection details such as inserts, holes for hangers and blade connections. This design shows the versatility of the super-light slab element and expands the array of design solutions it is possible to apply with the element.

Bibliography

Bagger and Hertz 2010. A. Bagger, K.D. Hertz Structural behaviour of super-light structures, Proceedings Internatonal Symposium of the International Association of Shell and Spatial Structures (IASS) Shanghai 2010, 2697-2708, 2010

Betonelement 2010. http://www.betonelement.dk/ Marts 2010

Bullock 2002. N. Bullock, Building the Post-War World: Modern Architecture and Reconstruction in Britain, first ed., Routledge, 2002

Bygningsreglementet 2008. Anon., Generel building code 2008 Denmark(Bygningsreglementet 2008 in Danish), Energi styrelsen, 2008

Castberg and Hertz 2012a. Folded shapes with Super-Light Structures. Proceedings of the International Association for Shell and Spatial Structures (IABSE-IASS) Symposium 2011 "Taller, Longer Lighter", London 2011

Castberg and Hertz 2012b. "The Battery" designed with Super-Light (concrete) Decks. Proceedings of the International Association for Shell and Spatial Structures Symposium 2012, Seoul 2012

Christensen 2012. B. Christensen, BEF Bulletin No 1 - July 2012 Lydisolation for tungt byggeri af beton- og letbetonelementer - eksempelsamling (Sound insulation for heavy construction of concrete and lightweigth concrete elements - collection of examples), Betonelementforeningen, 2012 http://www.bef.dk/files/DanskBeton/%C3%98vrige%20publikationer/Bulletin%20no%201%20-%20med%20beregningsbilag.pdf

Christensen and Hertz 2013. J.E. Christensen, K.D. Hertz, Super-light prefabricated deck elements integrated in traditional concrete prefabricated elements construction. Unpublished, Department of Civil Engineering at the Technical University of Denmark, Kgs Lyngby, Denmark, Paper IV in this thesis

Christensen et al. 2013a. J.E. Christensen, K.D. Hertz, J. Brunskog, Airborne and impact sound transmission loss in super-light structures, Unpublished, Department of Civil Engineering at the Technical University of Denmark, Kgs Lyngby, Denmark, Paper I in this thesis

Christensen et al. 2013b. J.E. Christensen, K.D. Hertz, J. Brunskog, Simulation of flanking transmission in super-light structures, Unpublished, Department of Civil Engineering at the Technical University of Denmark, Kgs Lyngby, Denmark, Paper II in this thesis

Collins and Mitchel 2001. M.P. Collins, D. Mitchell, Prestressed concrete structures, Prentice Hall, 2001

Confire user guide 2012. K.D. Hertz, Confire user guide 2. edition and confire freeware program, Depertment of Civil Engineering Technical University of Denmark, 2012

Craik and Evans 1989. R.J.M Craik, D.I. Evans The effect of workmanship on sound transmission through buildings: Part 2 - structure-borne sound, App Acoust, 27, 137-145, 1989

Craik and Steel 1989. R.J.M Craik, J.A. Steel The effect of workmanship on sound transmission through buildings: Part 1 - airborne sound, App Acoust, 27, 57-63, 1989

Cremer and Heckl 1973. L. Cremer, M. Heckl, E.E. Unger, Structure-Borne Sound, second ed., Springer-Verlag, 1973

Cremer and Heckl 2005. L. Cremer, M. Heckl, B.A.T. Petersson, Structure-Borne Sound, third ed., Springer-verlag, 2005

Cunliffe 2005. B. Cunliffe, Iron Age Communities in Britain: An Account of England, Scotland and Wales from the Seventh Century BC until the Roman Conquest, fourt ed., Thomas Telford Publishing, 2005

DS490 2007. Anon., DS 490 Lydklassifikation af boliger (sound classification of dwellings), DS, 2007

EN12354-1 2000. Anon., EN 12354-1:2000 Estimations of acoustics performance of building from the performance of elements - Part 1: Airborne sound insulation between rooms, CEN, 2000

EN12354-2 2000. Anon., EN 12354-2:2000 Estimations of acoustics performance of building from the performance of elements - Part 2: Impact sound insulation between rooms, CEN, 2000

Eurocode 1-1-1 2002. Anon., Eurocode 2: Actions on structures - Part 1-1: General actions - Densities, self-weight, imposed loads for buildings, CEN, 2002

Eurocode 1-1-2 2002. Anon., Eurocode 1: Actions on structures - Part 1-2: General actions - Actions on structures exposed to fire, CEN, 2002

Eurocode 2-1-1 2004. Anon., Eurocode 2: Design of concrete structures - Part 1-1: General rules and rules for buildings, CEN, 2004

Eurocode 2-1-2 2004. Anon., Eurocode 2: Design of concrete structures - Part 1-2: General rules - Structural fire design, CEN, 2004

Gerretsen 1979. E. Gerretsen, Calculation of the sound transmission between dweillings by partitions and flanking structures, App Acoust, 12, 413-433, 1979

Gerretsen 1994. E. Gerretsen, European developments in prediction models for building acoustics, Acta Acoust, 2, 205-214, 1994

Hertz 1982. K.D. Hertz, The anchorage capacity of reinforcing bars at normal and high 2 temperatures, Mag Concrete Res, Vol.34, No. 121, 213-220, 1982

Hertz 2009. K.D. Hertz, Super-light concrete with pearl-chains, Mag Concrete Res 61, No.8. 655-663, 2009

Hertz 2010. K.D. Hertz, Light-weight load-bearing structures. Application no. EP 07388085.8. European Patent Office, Munich. November 2007. Application no. 61/004278 US Patent and Trademark Office. November 2007. PCT (Patent Cooperation Treaty) Application PCT/EP2008/066013, 21. November 2008. Pcr Patent January 2010.

Hertz 2011. K.D. Hertz Light-weight load-bearing structures reinforced by core elements made of segments and a method of casting such structures. Application no. EP 08160304.5 European Patent Office, Munich, July 2008. Application no. 61/080445 US Patent and Trademark Office, July 2008. PCT (Patent Cooperation Treaty) Application no. PXCT/EP2009/052984, 13. March 2009. Pcr Patent January 2011.

Hertz and Bagger 2011. K.D. Hertz, A. Bagger, CO2 emissions from Superlight Structures, Proceedings of the International Association for Shell and Spatial Structures (IABSE-IASS) Symposium 2011 "Taller, Longer Lighter", London 2011

Hertz et al. 2013. K.D. Hertz, J.E. Christensen, N.A. Castberg, Super-light concrete decks, Unpublished, Department of Civil Engineering at the Technical University of Denmark, Kgs Lyngby, Denmark, Paper III in this thesis

Hoffmeyer 2005. D. Hoffmeyer, Orienterende målinger af trinlyddæmpning for strøegulvkonstruktion på harpun grøn opklodsning, Techincal report AV 1264/25, Delta, Hørsholm, Denmark, 2005

Hoffmeyer 2011a. D. Hoffmeyer, Orienterende måling af forbedring af luftlydisolation for et trægulv på strøer på kombi max kiler med lydbrik udlagt på et 140 mm betondæk, Techincal report AV 1223/11, Delta, Hørsholm, Denmark, 2011

Hoffmeyer 2011b. D. Hoffmeyer, Måling af trinlyddæmpning for et trægulv på strœer på kombi max kiler med lydbrik udlagt på et 140mm betondæk, Techincal report AV 1165/11, Delta, Hørsholm, Denmark, 2011

Hoffmeyer 2011c. D. Hoffmeyer, Måling af trinlyddæmpning for et trægulv på strøer på kombi max kiler udlagt på et 140 mm betondæk, Techincal report AV 1166/11, Delta, Hørsholm, Denmark, 2011

Hopkins 2005. C. Hopkins, Statistical energy analysis of coupled plate systems with low modal density and low modal overlap, J Sound Vib, 251, 193-214, 2002

Hopkins 2007. C. Hopkins, Sound Insulation, first edition, Butterworth-Heinemann, 2007

ISO 140-2 1992. DS/ISO 140-2:1992 Acoustics – Measurement of sound insulation in buildings and of building elements – Part 2: Determination, verification and application of precision data, ISO, 1992

ISO 717-1 1996. Anon., ISO 717 Acoustics – Rating of sound insulation in buildings and of building elements – Part 1: Airborne sound insulation, ISO, 1996

ISO 717-2 1996. Anon., ISO 717 Acoustics – Rating of sound insulation in buildings and of building elements – Part 2: Impact sound insulation, ISO, 1996

ISO 10140-2 2010. Anon., ISO 10140-2:2010 Acoustics – Laboratory measurement of sound insulation of building elements – Part 2: Measurement of airborne sound insulation, ISO, 2010

ISO 10140-3 2010. Anon., ISO 10140-3:2010 Acoustics – Laboratory measurement of sound insulation of building elements – Part 3: Measurement of impact sound insulation, ISO, 2010

Jensen 1991. J.F. Jensen, Betonelementer, Håndbog i 4 bind, Betonelementforeningen, 1991

Kristensen and Rindel 1989. J. Kristensen, J.H. Rindel, SBI anvisning 237 Bygningsakustik teori og praksis (Building acoustic teory and pracksis), 1st edition, Statens Byggeforskningsinstitut, 1989

Mahn and Pearse 2009. J. Mahn, J. Pearse, On the uncertainty of the EN12354-1 estimate of the flanking sound reduction index due to the uncertainty of the input data, Building Acoustics, 16, 199-231, 2009

McElroy 1990. D.L. McElroy, Insulation Materials, Testing, and Applications (Astm Special Technical Publication// Stp), first ed., American Society for Testing & Materials, 1990

Metzen 2010. H.A. Metzen, Bastian Manual, Datakustik GmbH, Greifenberg, Germany, 2010

Nielsen and Hoang 2010. M.P. Nielsen, L.C. Hoang, Limit analysis and concrete plasticy, third edition, CRC Press Taylor & Francis group, 2010

Nightingale and Bosmans 2003. T.R.T. Nightingale, I. Bosmans, Expression for first-order flanking paths in homogeneous isotropic and lightly damped buildings, Acustica united with Acta Acoust, 89, 110-122, 2003

NM and BR 1974a. NM, BR, Techincal Report 709/74, Lydteknisk Laboratorium, Lyngby, Denmark,1974

NM and BR 1974b. NM , BR, Techincal Report 710/74, Lydteknisk Laboratorium, Lyngby, Denmark,1974

Osipov and Vermier 1996. E. Gerretsen, Sound transmission in building with elastic layers at joints, App Acoust, 49, 141-162, 1996

Rasmussen 2010. B. Rasmussen, Sound insulation between dwellings - Requirements in building regulations in Europe, Appl Acoust, 71, 373-385, 2010

Rasmussen and Rindel 2010. B. Rasmussen, J.H. Rindel, Sound insulation between dwellings - Descriptors applied in building regulations in Europe, Appl Acoust, 71, 171-180, 2010

Rasmussen et al. 2011. B. Rasmussen, C.M. Møller, D. Hoffmeyer, SBI anvisning 166 Lydisolering mellem boliger - nybyggeri (Sound insulation between dwellings - new constructions), 1st edition, Statens Byggeforskningsinstitut, Aalborg Universitet, 2011

Rindel 1994. J.H. Rindel, Dispersion and absorption of structure-borne sound in acoustically thick plates, App Acoust, 41, 97-111, 1994

Simmons 2004. C. Simmons, Ljudisolering i bostadshus byggda 1880-2000 Praktiska erfarenheter och indata fö r berä kningar, Techincal report 0405, FoU-Vä st, Gothenborg, Sweden, 2004

Simmons 2005. C. Simmons, Reproducibility of measurements with ISO 140 and calculations with EN 12354, NT technical report 603, Nordic innovation centre, 2005

Spæncom 2010. http://www.spaencom.dk/betonelementer.aspx Marts 2010

Sutherland et al. 2001. R.J.M. Sutherland, D. Humm, M. Chrimes, Historic Concrete: The Background to Appraisal, first ed., Routledge, 2001

Szilard 2004. R. Szilard, Theories and applications of plate analysis, 1st edition, John Wiley and Sons, 2004

Teknisk Staabi 2004. Anon., Teknisk Ståbi 18. udgave, Nyt Teknisk Forlag, 2004

Vér and Holmer 1988. I.L. V'er, C. I. Holmer, Interaction of sound waveswith solid structures, in: L.L. Beranek, Noise and vibration control, INCE, 1988, pp. 270-357

Öqvist et al. 2012. R. Öqvist, F. Ljunggren, A. Ågren, App Acoust, 73, 904-912, 2012

Part II

Appendix

Appendix A

Stiffness calculation for acoustic test element

This appendix contains the stiffness calculation for the acoustic element used in the experiments regarding sound transmission, and calculations of flanking transmission. It is based on the element shown in Fig. 3.5 and the block geometry in Fig. 2.3.

The bending stiffness of the element is calculated from the area, centre of equilibrium (measured form the top of the element) and second moment of area, which all has been taken directly from the CAD-model of the element and are both directions. The normal concrete is denoted by the subscript nc and one block of lightweight aggregate concrete is denoted with the subscript lc and multiplied according to the total number in each direction.

$$A_{nc,1} = 28.43 \cdot 10^4 \text{ mm}^2 \qquad e_{nc,1} = 69.23 \text{ mm} \qquad I_{nc,1} = 7.91 \cdot 10^4 \text{ mm} \tag{A.1}$$

$$A_{lc,1} = 5.12 \cdot 10^4 \text{ mm}^2 \qquad e_{lc,1} = 137.31 \text{ mm} \qquad I_{lc,1} = 1.34 \cdot 10^4 \text{ mm} \tag{A.2}$$

For the other direction the same geometrical constants are found to

$$A_{nc,2} = 20.60 \cdot 10^4 \text{ mm}^2 \qquad e_{nc,2} = 64.38 \text{ mm} \qquad I_{nc,2} = 7.37 \cdot 10^4 \text{ mm} \tag{A.3}$$

$$A_{lc,2} = 8.79 \cdot 10^4 \text{ mm}^2 \qquad e_{lc,2} = 125.19 \text{ mm} \qquad I_{lc,2} = 2.45 \cdot 10^4 \text{ mm} \tag{A.4}$$

With a stiffness ratio of $\alpha = E_{lc}/E_{nc} = 3 \text{ GPa}/37 \text{ GPa} = 0.081$ the transformed areas is found

$$A_{t,1} = A_{nc,1} + \alpha \cdot (7A_{lc,1}) = 3.13 \cdot 10^5 \text{ mm}^2 \tag{A.5}$$

$$A_{t,2} = A_{nc,2} + \alpha \cdot (6A_{lc,2}) = 2.49 \cdot 10^5 \text{ mm}^2 \tag{A.6}$$

and the first moment of area from the top of the element can also be calculated

$$S_{t,1} = S_{nc,1} + S_{lc,1} = A_{nc,1}e_{nc,1} + 7\alpha(A_{lc,1}e_{lc,1}) = 2.37 \cdot 10^7 \text{mm}^3 \quad \text{(A.7)}$$
$$S_{t,2} = S_{nc,2} + S_{lc,2} = A_{nc,2}e_{nc,2} + 6\alpha(A_{lc,2}e_{lc,2}) = 1.86 \cdot 10^7 \text{mm}^3 \quad \text{(A.8)}$$

and with this the can the centre of equilibrium for the whole element be found as

$$e_{t,1} = \frac{S_{t,1}}{A_{t,1}} = 75.55\,\text{mm} \quad \text{(A.9)}$$
$$e_{t,2} = \frac{S_{t,2}}{A_{t,2}} = 74.83\,\text{mm} \quad \text{(A.10)}$$

with this can the second moment of area be calculated

$$\begin{aligned} I_{t,1} &= I_{nc,1} + A_{nc,1}(e_{nc,1} - e_{t,1})^2 + 7\alpha(I_{lc,1} + A_{lc,1}(e_{lc,1} - e_{t,1})^2) \\ &= 9.89 \cdot 10^8\ \text{mm}^4 \quad \text{(A.11)} \\ I_{t,2} &= I_{nc,2} + A_{nc,2}(e_{nc,2} - e_{t,2})^2 + 6\alpha(I_{lc,2} + A_{lc,2}(e_{lc,2} - e_{t,2})^2) \\ &= 9.88 \cdot 10^8\ \text{mm}^4 \quad \text{(A.12)} \\ & \quad \text{(A.13)} \end{aligned}$$

and this leads to the bending stiffness being able to be calculated as

$$B_1 = \frac{E_{nc}I_{t,1}}{L_1(1-\mu^2)} = 1.282 \cdot 10^7\ \text{Nm} \quad \text{(A.14)}$$
$$B_2 = \frac{E_{nc}I_{t,2}}{L_2(1-\mu^2)} = 1.153 \cdot 10^7\ \text{Nm} \quad \text{(A.15)}$$

where $L_1 = 3\,\text{m}$ and $L_2 = 3.3\,\text{m}$ is the size of the slab element and poisons ratio is $\mu = 0.2$. The stiffness in each direction gives the effective torsional rigidity for an orthotropic plate $B_{12} = \sqrt{B_1 B_2} = 1.216 \cdot 10^7$ Nm as shown earlier.

Appendix B

Stiffness calculation for beam element

This appendix contains the stiffness calculation for the beam element used in the experiments regarding deflection, cracking moment and natural frequency. It is based on the element shown in Fig. 4.1 and the block geometry in Fig. 2.3. The stiffness calculation is based on calculation one block with a width of 400 mm and then upscale it to the full width which is three three blocks 1200 mm. For the strong normal concrete it is split up into six parts, rectangles and triangles as shown on Fig. B.1

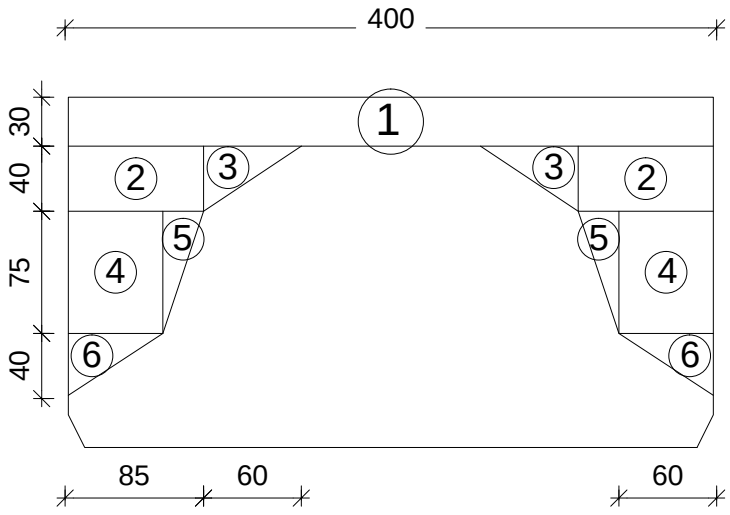

***Figure B.1**: The six parts the normal concrete is divided into*

At first the cross-sectional constants is calculated, the influence of the different concretes stiffness is added in the end when the modulus of elasticity

is considered in order to get the bending stiffness.
The area of each of the six considered parts is calculated, for all parts it is the total area of it which is considered

$$A_{c,1} = 400 \cdot 30 = 12000\,\text{mm}^2 \tag{B.1}$$
$$A_{c,2} = 2 \cdot 85 \cdot 40 = 6800\,\text{mm}^2 \tag{B.2}$$
$$A_{c,3} = 2 \cdot \frac{1}{2} 60 \cdot 40 = 2400\,\text{mm}^2 \tag{B.3}$$
$$A_{c,4} = 2 \cdot 60 \cdot 75 = 9000\,\text{mm}^2 \tag{B.4}$$
$$A_{c,5} = 2 \cdot \frac{1}{2} 25 \cdot 75 = 1875\,\text{mm}^2 \tag{B.5}$$
$$A_{c,6} = 2 \cdot \frac{1}{2} 60 \cdot 40 = 2400\,\text{mm}^2 \tag{B.6}$$
$$A_c = \sum_{i=1}^{6} A_{c,i} = 34475\,\text{mm}^2 \tag{B.7}$$

And their corresponding depths to their centroid in regards to the top surface of the element, the centroid of a triangle is found at one third of the height from its base.

$$e_{c,1} = \frac{30}{2} = 15\,\text{mm} \tag{B.8}$$
$$e_{c,2} = 30 + \frac{1}{2} 40 = 50\,\text{mm} \tag{B.9}$$
$$e_{c,3} = 30 + \frac{1}{3} 40 = 43.3\,\text{mm} \tag{B.10}$$
$$e_{c,4} = 30 + 40 + \frac{1}{2} 75 = 107.5\,\text{mm} \tag{B.11}$$
$$e_{c,5} = 30 + 40 + \frac{1}{3} 75 = 95\,\text{mm} \tag{B.12}$$
$$e_{c,6} = 30 + 40 + 75 + \frac{1}{3} 40 = 158.3\,\text{mm} \tag{B.13}$$

The first moment of area is then simply found for each of the parts in regards

to the top surface of the element

$$S_{c,1} = e_{c,1}A_{c,1} = 1.80 \cdot 10^5 \text{ mm}^3 \tag{B.14}$$
$$S_{c,2} = e_{c,2}A_{c,2} = 3.40 \cdot 10^5 \text{ mm}^3 \tag{B.15}$$
$$S_{c,3} = e_{c,3}A_{c,3} = 1.04 \cdot 10^5 \text{ mm}^3 \tag{B.16}$$
$$S_{c,4} = e_{c,4}A_{c,4} = 0.97 \cdot 10^5 \text{ mm}^3 \tag{B.17}$$
$$S_{c,5} = e_{c,5}A_{c,5} = 1.78 \cdot 10^5 \text{ mm}^3 \tag{B.18}$$
$$S_{c,6} = e_{c,6}A_{c,6} = 3.80 \cdot 10^5 \text{ mm}^3 \tag{B.19}$$
$$S_c = \sum_{i=1}^{6} S_{c,i} = 21.50 \cdot 10^5 \text{ mm}^3 \tag{B.20}$$

The centroid of the combined normal concrete is found, again with respect to the top of the element

$$e_c = \frac{S_c}{A_c} = 62.4 \text{ mm} \tag{B.21}$$

The second moment of area of the normal concrete is calculated with regards to the combined centroid e_c

$$I_{c,1} = \frac{1}{12}400 \cdot 30^3 + A_{c,1}\left(e_c - e_{c,1}\right)^2 = 27.81 \cdot 10^6 \text{ mm}^4 \tag{B.22}$$
$$I_{c,2} = 2\frac{1}{12}85 \cdot 40^3 + A_{c,2}\left(e_c - e_{c,2}\right)^2 = 1.94 \cdot 10^6 \text{ mm}^4 \tag{B.23}$$
$$I_{c,3} = 2\frac{1}{36}60 \cdot 40^3 + A_{c,3}\left(e_c - e_{c,3}\right)^2 = 1.08 \cdot 10^6 \text{ mm}^4 \tag{B.24}$$
$$I_{c,4} = 2\frac{1}{12}60 \cdot 75^3 + A_{c,4}\left(e_c - e_{c,4}\right)^2 = 22.56 \cdot 10^6 \text{ mm}^4 \tag{B.25}$$
$$I_{c,5} = 2\frac{1}{36}25 \cdot 75^3 + A_{c,5}\left(e_c - e_{c,5}\right)^2 = 2.58 \cdot 10^6 \text{ mm}^4 \tag{B.26}$$
$$I_{c,6} = 2\frac{1}{36}60 \cdot 40^3 + A_{c,6}\left(e_c - e_{c,6}\right)^2 = 22.32 \cdot 10^6 \text{ mm}^4 \tag{B.27}$$
$$I_c = \sum_{i=1}^{6} I_{c,i} = 21.50 \cdot 10^5 \text{ mm}^4 \tag{B.28}$$

The cross-sectional constant contribution from the lightweight aggregate concrete is derived from the fact that the total cross-section is rectangular and the cross-sectional constants are known for the normal concrete this means the area of a lightweight aggregate concrete block is

$$A_{lc} = 215 \cdot 400 - A_c = 51525 \text{ mm}^2 \tag{B.29}$$

And the first moment of area is found in the same fashion

$$S_{lc} = \frac{1}{2}400 \cdot 215^2 - S_c = 70.95 \cdot 10^5 \text{ mm}^3 \tag{B.30}$$

And the depth to the centroid of the lightweight aggregate block

$$e_{lc} = \frac{S_c}{A_c} = 137.7 \text{ mm} \tag{B.31}$$

This again gives the second moment of area around this centroid for the lightweight aggregate block as

$$I_{lc} = \frac{1}{12}400 \cdot 215^3 - I_c - A_{lc}\left(\frac{215}{2} - e_{lc}\right)^2 = 13569 \cdot 10^6 \text{ mm}^4 \tag{B.32}$$

The axial stiffness for the different parts are than

$$AE_c = A_c E_c = 1275.6 \cdot 10^6 \text{ N} \tag{B.33}$$
$$AE_{lc} = A_{lc} E_{lc} = 157.6 \cdot 10^6 \text{ N} \tag{B.34}$$
$$AE_p = A_p E_p = 39.1 \cdot 10^6 \text{ N} \tag{B.35}$$

where the pre-stressed rebars are included by AE_p and they consist of the six strands with a diameter of 12.5 mm with a nominal area each of 93 mm^2 and modulus of elasticity for steel of 210 GPa.
The first moments of area are calculated with their stiffness weight

$$SE_c = S_c E_c = 79.5 \cdot 10^6 \text{ Nm} \tag{B.36}$$
$$SE_{lc} = S_{lc} E_{lc} = 21.3 \cdot 10^6 \text{ Nm} \tag{B.37}$$
$$SE_p = A_p e_p = 5.3 \cdot 10^6 \text{ Nm} \tag{B.38}$$

This allows for the total centroid of the full cross-section to be calculated

$$e = \frac{SE_c + SE_{lc} + SE_p}{A_c + A_{lc} + A_p} = 72.3 \text{ mm} \tag{B.39}$$

The flexural stiffness for each of the materials including the steel rebar in regards to the total centroid of the full cross-section

$$EI_c = I_c E_c + AE_c (e - e_c)^2 = 3.02 \cdot 10^6 \text{ Nm}^2 \tag{B.40}$$
$$EI_{lc} = I_{lc} E_c + AE_{lc} (e - e_{lc})^2 = 1.07 \cdot 10^6 \text{ Nm}^2 \tag{B.41}$$
$$EI_p = AE_p (e - e_p)^2 = 0.16 \cdot 10^6 \text{ Nm}^2 \tag{B.42}$$
$$EI = EI_c + EI_{lc} + EI_p = 4.25 \cdot 10^6 \text{ Nm}^2 \tag{B.43}$$

This means that $3EI = 12.76 \cdot 10^6$ Nm^2 is the flexural bending stiffness of the element.

Part III

Appended Papers

Paper I

"Airborne and impact sound transmission loss in super-light structures"

J.E. Christensen, K.D. Hertz & J. Brunskog

Submitted to: *Applied Acoustics, 2012*

Airborne and impact sound transmission loss in super-light structures.

Jacob E. Christensen[a,*], Kristian D. Hertz[a], Jonas Brunskog[b]

[a] *Building Design, Department of Civil Engineering, Technical University of Denmark, DK-2800, Kongens Lyngby, Denmark*
[b] *Acoustic Technology, Department of Electrical Engineering, Technical University of Denmark, DK-2800, Kongens Lyngby, Denmark*

Abstract

Super-light structures is a newly invented concept for creating concrete construction and concrete building elements. In this study the super-light deck element will be investigated for its acoustic performance, namely in airborne and impact sound transmission.
The super-light deck element is being developed to be lighter than comparable pre-fabricated concrete elements by utilizing arches to improve the static performance. In spite of it being a lighter element it should still achieve an acoustical performance on the same level or better as compared with common concrete elements. It is the airborne sound transmission loss which then carries the main emphasis in the design of the slab as external flooring for improving performance in impact is not considered here.
Through calculated estimates it is expected that the mass of the super-light deck element can be reduced by 10-15% compared to similar concrete elements and still achieve the same acoustical performance in airborne sound transmission loss. These expectations are being verified experimentally.

Keywords: Lightweight concrete structures, Airborne sound transmission, Impact sound transmission, Super-light structures

*Corresponding author
Email addresses: jacoc@byg.dtu.dk (Jacob E. Christensen), khz@byg.dtu.dk (Kristian D. Hertz), jbr@elektro.dtu.dk (Jonas Brunskog)

1. Introduction

Traditionally good properties of building acoustics for a floor element is associated with a high mass or adding of mass, due to the mass law. During recent years a higher emphasis on lightweight structures and environmental friendly building elements have emerged. In order to accommodate these new desirable properties research have been carried out in e.g. wood structures [1] and [2] and other materials [3] and [4]. Super-light structures explore another branch of possibilities by optimizing on a monolithic concrete structure by introducing a composite concrete element consisting of two different concretes.

Super-light structures were invented in 2007 [5] and the accompanying pearl-chain theory was later developed in 2008 [6]. The overall principle of super-light structures is to combine a high-strength concrete with a lightweight aggregate concrete in order to optimize the utilization of the favorable properties of the different concretes. Most important are the high compression strength of concrete utilized by arches in compression in the elements and the high thermal insulation of the lightweight aggregate concrete in order to increase fire safety, these principles are further elaborated in Ref. [7].

The super-light deck element considered here started development in 2009, the development is holistic and demands from both ultimate and serviceability limit state closely have been considered during the development. This includes statics, stability, fire safety, deflections, thermal performance, vibrations, room and building acoustics which all have influenced the design. Testings have been carried out on the statics and fire safety and are due to be published at a later date.

The super-light element is made from blocks of lightweight aggregate concrete, they are shaped in order to establish arches within the element across its width as exemplified on Fig. 1. Six blocks are placed in the width of the element and thus six arches are established, considerations of the production of the blocks also influenced their design.

The element and blocks are designed so that the compression zone depth is sufficient in the complete width of the element to ensure the structural integrity of the element while keeping the span to height ratio of the arches as low as possible. Prestressed reinforcement to accommodate tension forces and prevent cracking is placed in the grooves between the lightweight aggregate blocks. Slack reinforcement is placed in the secondary direction at a

spacing corresponding to the block length. If necessary, the element can be prepared for post-tensioning in both directions. The combination of normal concrete, lightweight aggregate concrete and steel reinforcement yields an element surface density of 314 $\mathrm{kg/m^2}$. The lightweight aggregate blocks have a very open porous structure which means that the plasticity of the normal concrete ensures that it penetrates the pores of the lightweight aggregate concrete by $5 - 10$ mm creating a strong and stable connection of the two concretes.

The acoustical performance of the super-light slab is enhanced by combin-

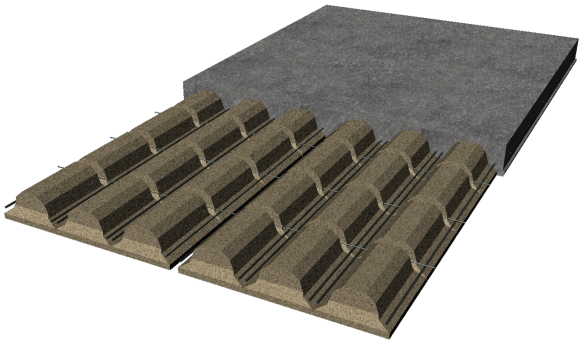

Figure 1: Super-light slab element

ing pre-made blocks of lightweight aggregate concrete and normal concrete in a vaulted form to enhance the geometrical stiffness of the element. This causes the critical frequency to be lowered as compared to a homogenous concrete plate, which is further enhanced by the deck elements lower weight. Furthermore, the introduction of lightweight aggregate concrete increases the damping in the deck element which is further enhanced by the connection between the two different concretes.

2. Method and Theory

2.1. Super-light Element

The dimensions of the super-light deck element used for this investigation of acoustic properties is fitted to accommodate the geometry of the hole which separates the source and receiver room at the testing facilities. The test element is designed to mimic the actual super-light element as much as possible.

The cross-sectional views of the tested element is shown on Fig. 2. The dimensions of the element is $3.330 \times 3.000 \times 0.185$ m. This leaves room for six times seven lightweight aggregate concrete blocks in the element leaving an excess space of 200 mm and 330 mm that the lightweight aggregate blocks cannot cover compared to the overall geometrical demands of the element and testing facilities. These spaces has been filled with full sections of concrete at the edges of the element to reduce the influence the increased weight will have on the measurements. The element is reinforced with six slack Y16 rebars in the principal direction and seven slack Y6 rebars in the secondary direction. The element is reinforced to such a degree that no cracking occurs in the concrete so that the full sections of concrete is contributing to the stiffness of the element.

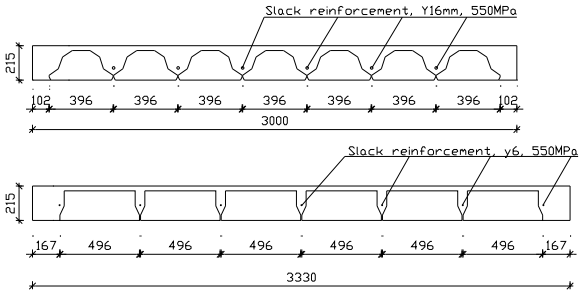

Figure 2: Cross-sectional views of the super-light element.

2.2. Experimental Method

The measurements were carried out in the reverberation chamber at the Technical University of Denmark. Two loudspeakers were present in the source room and were used for the airborne sound transmission measurements. Five different microphone locations were used in both the source and receiver room, according to the requirements specified in ISO 10140 [8]. The impact measurements were carried out by the standard tapping machine at five different locations on the slab varied in placement on the ribs of solid concrete, lightweight aggregate blocks and angled differently compared to the ribs and lightweight aggregate blocks. Four different microphone positions in the receiver room were applied according to requirements [9], no floor coverings were included in the tests. Reverberation time and background noise were measured at three different positions in the receiver room. Craik and Steel discusses [10] the accuracy of the method used to test an element

for airborne and impact sound transmission and it is shown that the standard deviation of such measurements can be expected to be around 1 dB in laboratory conditions.

The super-light deck element was cast into an L-shaped steel frame formed to fit the opening between the source and receiver room. The steel L-frame was placed on another steel frame in the separation hole with a layer of mineral wool in between the two steelframes. The bottom third of the cavity between the steel frames was filled with more mineral wool while the top two thirds was filled with in situ cast grouting mortar with a characteristic compression strength of 30 MPa. The mortar was mixed with extra water and sand to improve its workability; it was expected that this connection will be close to a clamped boundary condition. The boundary condition was created in order to compare measurements results with previous measurements of hollow-core concrete slabs, in addition the boundary condition closely resembles those used in-situ with pre-fabricated elements. Measurements were made after 18 hours, 1 week and 3 weeks at an average curing temperature of 20°C in order to assess the influence of the different curing time.

A sound level meter B&K 2250 was used for the measurement and the built-in microphone was recording the signals.

Input mobility measurements were carried out on the element in order to investigate the boundary conditions and to help explain the nature of transmission through the super-light element at lower frequencies. The input mobility measurements were made with the same installations as the airborne and impact sound transmission measurements, but only once after 3 weeks. The element was put in motion by a shaker suspended from the ceiling through a force transducer. An accelerometer were placed next to the contact point to record the vibration. Measurements of the input mobility were made in various frequency ranges from $1\,\mathrm{Hz} - 12.8\,\mathrm{kHz}$ with various resolutions from $0.0625\,\mathrm{Hz} - 2\,\mathrm{Hz}$ corresponding to 6400 discrete measurements in each frequency range investigated. The input mobility was measured at three points along a line in the middle of the super-light element and at the floor structure at the measurements facilities. The placements of the measurements on the elements were in the middle above a rib, denoted placement 1, on the middle of an adjacent lightweight aggregate concrete block, denoted placement 2 and on the next concrete rib, denoted placement 3, these placements are shown on Fig. 3 along with nodal lines. The nodal lines describe a line where the element for a given mode will have no oscillation and therefore they have a potential to influence the identification of modes if measured on

a nodal line.

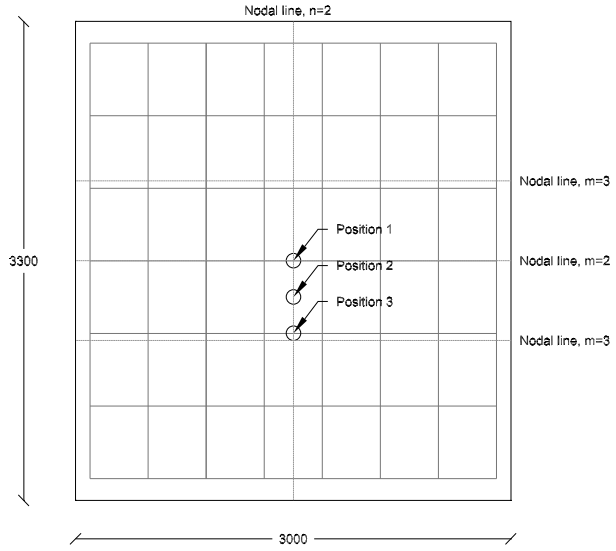

Figure 3: Placements on the super-light slab element where the input mobility has been measured.

2.3. Theory

In this section it is discussed which mechanics causes the expectation that the super-light deck element can achieve the same building acoustic properties with less mass than comparable concrete elements.

The vaults created by the lightweight aggregate concrete blocks geometrically stiffens the element while at the same time the lightweight aggregate concrete reduces the total surface mass of the element. Increased stiffness and lower surface density both contributes to decreasing the critical frequency [11]

$$f_c = \frac{c^2}{2\pi}\sqrt{\frac{m}{B}} \tag{1}$$

which is dependent on the factor $\sqrt{m/B}$, where m is the surface density and B is the bending stiffness. The surface mass of the element is $316\,\mathrm{kg/m^2}$. Due to the geometry and orientation of the lightweight aggregate concrete blocks the super-light element is orthogonal; therefore the bending stiffness for the two different directions have been calculated and are $B_1 = 1.282 \cdot 10^7\,\mathrm{Nm}$ and

$B_2 = 1.153 \cdot 10^7$ Nm respectively, leading to the effective torsional rigidity of an orthotropic plate $B_{12} = \sqrt{B_1 B_2} = 1.216 \cdot 10^7$ Nm, which is a valid approximation when poisson's ratio is the same in each of the directions, Ref. [12]. It has been shown that orthogonality weaken the acoustic properties of plates, Ref. [13]. However the difference of the bending stiffness in the two principal directions of the super-light slab element is 5%, which can be considered small and in general the plate can be expected to behave as an isotropic plate.

These results of the surface mass and the bending stiffness of the super-light element leads to an expected critical frequency of $f_c = 95.4\,\text{Hz}$. This is below the common building acoustic frequency range of $100 - 3150\,\text{Hz}$ used to address metrics in regards to legislation [14]. This means that for the entire building acoustic frequency range the radiation efficiency σ_{res} can be expected to be close to or equal to 1 and the contribution from the forced transmission can be neglected, here for the super-light element it will be calculated according to Vèr and Holmer [15]. Additionally this also means that the increase in transmitted sound due to resonance around the critical frequency is less influential on the single number rating compared to elements with a higher critical frequency.

$$R_r = 20 \log\left(\frac{\pi f m}{\rho c}\right) - 10 \log\left(\frac{c^2 \sigma_{res}^2}{2\eta_{tot} S f} \frac{\Delta N}{\Delta f}\right) \tag{2}$$

where f is the frequency, m is the surface density, $\rho = 1.21\,\text{kg/m}^3$ is the density of air, $c = 344\,\text{m/s}$ is the speed of sound in air, σ_{res} is the radiation efficiency, η_{tot} is the total loss factor, S is the surface area and $\Delta N/\Delta f$ is the modal density which is based on both thin and thick plate theory as described by Rindel [16]. Below half the cross-over frequency from bending waves to shear waves, Eq. (3), it is based on bending waves and thin plate theory, above it is based on shear waves and thick plate theory.

$$f_s = \frac{c_s^2}{2\pi} \sqrt{\frac{m}{B}} \tag{3}$$

The modal density can then be calculated as

$$\frac{\Delta N}{\Delta f} = \begin{cases} \frac{\pi}{c^2} S f_c & \text{if } f \leq \frac{f_s}{2}, \\ \frac{2\pi}{c_s^2} S f & \text{if } f > \frac{f_s}{2}. \end{cases} \tag{4}$$

The porous lightweight aggregate concrete has an internal loss factor which is 2-3 times higher than the internal loss factor of normal concrete [11].

Furthermore, with regard to the damping, it is expected that the lightweight aggregate concrete further increases the damping as its is acting as a damping layer as described by Cremer and Heckl [11] (page 243-247).

3. Results and Discussion

3.1. Input mobility

Input mobility has been measured to identify modes and boundary conditions in the super-light slab element.

Fig. 4 shows the input mobility of the super-light slab element. At lower fre-

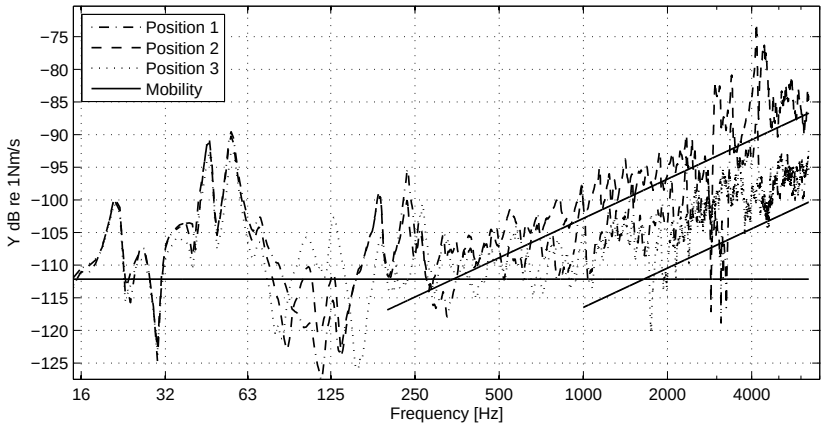

Figure 4: Input mobility of the super-light slab element in the frequency range 15 Hz – 6.4 kHz.

quencies the mobility oscillates around the theoretical value for the mobility of an infinite plate,

$$Y_\infty = \frac{1}{8\sqrt{mB}} \tag{5}$$

at higher frequencies the mobility is increased as it is governed by the local stiffness. This explains the difference that the mobility is measured higher at position 2 than position 1 and 3 at the higher frequencies. Position 2 is placed at the middle of a lightweight aggregate concrete block which have a stiffness based on the geometric average of the slab element: $(h_c E_c + h_{lc} E_{lc})/h = 7.7$ GPa where the subscript c denotes concrete and the subscript lc denotes lightweight aggregate concrete, $E_c = 37$ GPa and

$E_{lc} = 3$ GPa. The theoretical value of the mobility when controlled by the local stiffness Eq. (6), Ref. [17]

$$Y_{ls} = \frac{f}{2.4RG(1+i\eta)} \tag{6}$$

The local stiffness is based on the diameter of the contact point on the concrete R and the shear stiffness of the concrete in the element G. The agreement between the theoretical value of the mobility and the measured results at position 2 is good while the agreement between the measured value at position 1 and 3 is not quite that good compared to the expected mobility. If the stiffness is decreased to 18.5 GPa the agreement is better. The reason is that the rib of normal concrete is quite narrow, especially in the bottom of the element, causing the lightweight aggregate concrete to have influence on the stiffness and will thereby increase the mobility of the element.

The frequency resolution on Fig. 4 is rather low with a spacing of 1 Hz. On Fig. 5 a narrower frequency spacing of 0.0625 Hz for the lower frequencies range of 15 Hz $-$ 400 Hz is used. By comparing the mobility of the lab floor with the mobility of the super-light slab element the deceiving peaks coming from the vibration of the floor in the lab can be eliminated when identifying the natural frequencies of the super-light slab element. Half the mode-shapes will have a nodal line in the points where the mobility was measured (this was unavoidable due to the mounting of the setup for measuring the mobility, parts of the equipment was suspended in a crane in the ceiling which were only allowed movement in one direction along the nodal line), thus eliminating half the natural frequencies that could be identified.

The four lowest natural frequencies are found at 55 Hz for mode $(1,1)$, 188 Hz for mode $(2,1)$, 235 Hz for mode $(1,3)$ and 262 Hz for mode $(3,1)$. It is expected that mode $(1,2)$ have a frequency comparable to $(2,1)$ since the stiffness in each direction are very similar and the plate dimension of 3.3×3m is close to being quadratic. The same arguments can be used to approximate the natural frequency of mode $(2,2)$ to four times the one of mode $(1,1)$ as $\simeq 220$ Hz. As a result it is noted that a lot of the dominating mode-shapes and their natural frequencies are present within a rather narrow frequency range of $\simeq 188$ Hz $-$ 262 Hz.

By means of the half power bandwidth the loss factor η have been calculated for the four lowest identified modes, they are 4.9%, 5.4%, 4.1% and 5.1 %.

Fig. 6 shows the input mobility after the grouting mortar constituting the

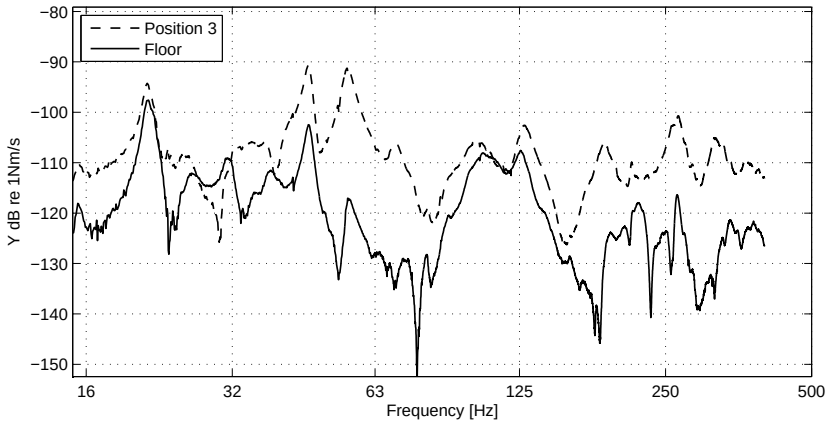

Figure 5: Input mobility of the super-light slab element and lab floor structure in the frequency range 15 Hz − 400 Hz.

boundary condition has been removed so that the super-light slab element is simple supported.

The lowest natural frequency for the simple supported plate is 36Hz which is significantly lower than the one measured when the grouting mortar was in place. As an approximation it can be shown that by using the Rayleigh's Quotient, Ref. [12], the ratio of the natural frequency between a clamped and a simple supported isotropic plate is $\simeq 1.89$ for quadratic plates to $\simeq 2.3$ for oblong plates. This imply that if the boundary condition had been fully clamped for the super-light slab it could be expected to be $\simeq 70$ Hz. The measured value of 55 Hz implicated that some restraining moment has been present due to the grouting mortar so that the actual boundary condition is undefined.

3.2. Airborne transmission

Fig. 7(a) shows the difference in the three measurements made at different curing times of the concrete in the cavity. The theoretical transmission loss for the element based of the resonant SEA formulation Eq. 2 is also depicted. The influence of the curing time is shown in the development of the stiffness of the grouting mortar which after 28 days at a curing temperature of 20°C will have achieved 100% of its characteristic stiffness value. According to the model in the concrete Eurocode [18] for stiffness development over time in concrete, the grouting mortar can be expected to have developed into 68%, 93% and 99% of the characteristic stiffness at 18 hours, 1 week and 3

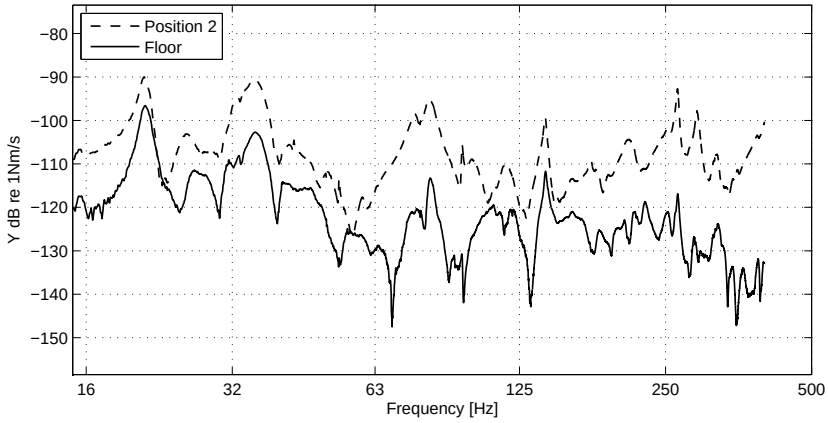

Figure 6: Input mobility of the super-light slab element on pinned supports and lab floor structure in the frequency range 15 Hz − 400 Hz.

weeks respectively, yielding a significant difference in the stiffness development between 18 hours and 1 and 3 weeks. This assessment of the stiffness can be identified on the measurement where they for the higher frequency range, where the modal overlap factor is high, are very alike. For the lower frequencies a clear difference in the 18 hours measurements compared to the measurements after 1 week and 3 weeks can be observed since the difference in stiffness of the grouting mortar constituting the boundary condition gives different restraining moments and thereby changes the natural frequencies of the super-light slab element.

The cluster of natural frequencies identified at the frequency range $\sim$ 188 Hz − 262 Hz can be observed by a drop in performance of the transmission loss at the one-third octave band at 200 Hz.

In the middle range of frequencies from 315 Hz − 2 kHz the measurements are constant with an increase in the airborne sound transmission loss of approximately 7 dB pr. octave. The measurement is also comparable to the SEA model for resonant radiation, Eq. (2). This range where the element perform as described is the most important for the improvement of sound insulation comparing to other concrete elements of similar mass. The tested element had a rather small surface area of 10 m^2 with an increasement in the area it can be expected that the natural frequencies will be lowered and this range will be extended to lower frequencies, thus increasing this important frequency range.

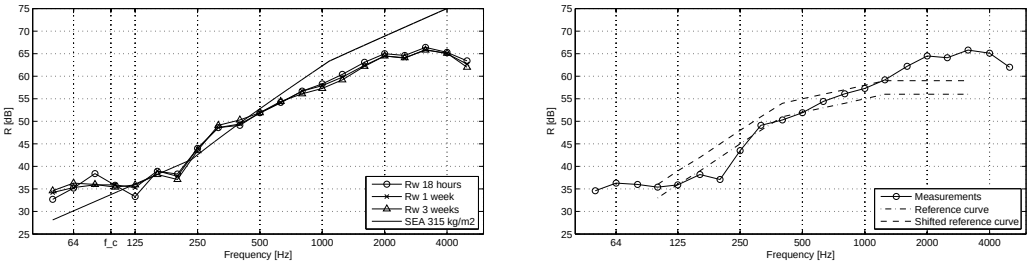

(a) The three different measurements of the airborne sound transmission loss at different times with the transmission loss determined by the SEA modal Eq. (2) for the super-light element with a surface density of 314 kg/m^2.

(b) Single number rating of the airborne transmission loss measured after three weeks.

Figure 7: Airborne measurements

Fig. 7(b) shows the single number calculations of the measurements of the super-light slab element after 3 weeks here it was calculated $R_w = 55\,\mathrm{dB}$ and the spectral adaption term $C_{50-5000} = -3\,\mathrm{dB}$. It is worth noting that the allowed unfavorable deviation from the reference curve is spread out in a large frequency range from $100\,\mathrm{Hz} - 1\,\mathrm{kHz}$ where as it was earlier discussed also partly covers the frequency range which is expected to have the best increase in airborne sound insulation. The single number rating for the resonant SEA calculations are $R_w = 55\mathrm{dB}$ and the spectral adaption term $C_{50-5000} = -1\mathrm{dB}$

3.3. Impact transmission

On Fig. 8(a) the variation of the impact transmission at different times is shown. Contrary to the airborne measurements there exist no significant difference of the measurement at the lower frequencies for measurements made at different times. The high concentration of natural frequencies earlier identified at $\sim 188\,\mathrm{Hz} - 262\,\mathrm{Hz}$ can be identified in the impact transmission loss measurements centered around the one-third octave bands with center frequencies 160 Hz and 200 Hz.

For the frequencies from 315 Hz and up to 5 kHz the slope is rather constant with an increase of approximately 6 dB pr. octave. There is a tendency that a slight difference between the measurements after 3 weeks and the other measurements exists. Between 315 Hz and 1 kHz the measurements after 3 weeks are a couple of dB worse while at the higher frequencies they are a couple of dB better. On Fig. 8(b) the calculation of the single number

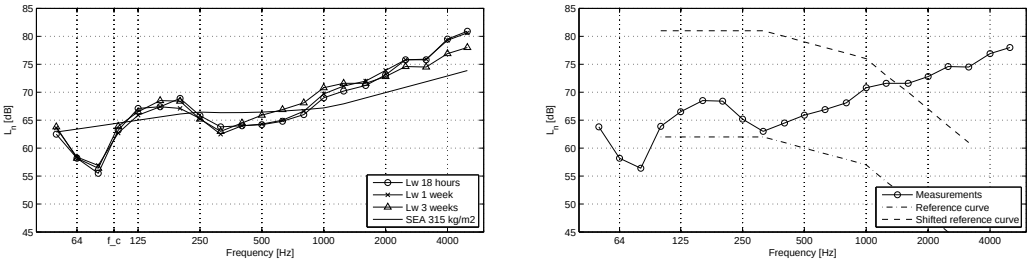

(a) The three different measurements of the impact sound transmission at different times with the impact transmission determined by the resonant SEA modal for the super-light element with a surface density of 314 kg/m^2.

(b) Single number rating of the impact transmission measured after three weeks.

Figure 8: Impact measurements

rating for the impact sound transmission of the super-light element is shown. A rating of $L_{n,w} = 79$ dB is achieved, the unfavorable deviation is located at the highest frequencies, the spectral adaption term is calculated at $C_I = -12$dB. The single number ratings have also been calculated for the resonant SEA calculations and is $L_{n,w} = 76$ dB with the spectral adaption term as $C_I = -9$ dB.

3.4. Discussion

Recently the building acoustic legislation for vertical sound transmission between dwellings have been changed in Denmark. The new requirements are rated by the apparent weighted sound reduction index R'_w from a single number rating of 53 dB to 55 dB in vertical airborne sound transmission and by the apparent weighted normalized impact sound pressure level $L'_{n,w}$ from a single number rating of 58 dB to 53 dB in impact [19]. This has created an opportunity to develop an element optimized for these new requirements, in the current state of development the emphasis is on the airborne sound transmission as the impact sound is dealt with at a later state through external means.

The super-light element used in the testing is different than the general design of the super-light element. From the time the experiments were carried out further iterations have been applied in the design of the super-light slab element. The changes are due to difficulties in the production process of the element. Most noteworthy is a slight increase of the density of the lightweight

aggregate blocks from 600kg/m^2 to 800kg/m^2, a new standard width of 2.4 metres rather than 1.2 metres, and slight altering of the lightweight aggregate blocks dimensions which will be less wide so that the outer box dimension is $375 \times 500 \times 185$ mm compared to $400 \times 500 \times 185$ mm. There alterations is based on other reasons than acoustics, most noteworthy an optimization of the production time. The element was first designed with a surface density 290 kg/m^2, with the discussed changes the element will have a slight increase in its weight comparable to the surface density of the measured element of 316 kg/m^2.

4. Conclusion

Measurements of the airborne and impact sound insulation have been carried out for a newly developed prefabricated composite concrete slab element. The element was mounted in the testing facilities partly with an in-situ grouting mortal and therefore measured at different times to eliminate the influence of the strength and stiffness development in the grouting mortal.

The super-light element achieved an airborne sound transmission loss single number rating of 55 dB and an impact sound transmission single number rating of 79 dB. The acoustic performance seems to be improved compared to similar pre-fabricated concrete elements through an increased damping in the elements and that the orthogonality is small so that the element can be considered as an isotropic plate.

5. Acknowledgements

The acoustic technology group at the department of electrical engineering at the Technical University of Denmark is thanked for having their staff, facilities and equipment at disposal for the measurements of the super-light slab.
The Danish Agency for Science and Technology and Innovation is also appreciated for their support to the research carried out in the above.

References

[1] F. Ljunggren, A. Ågren, Potential solutions to improved sound peformance of volume based lightweight multi-storey timber buildings, Appl Acsoustics 72, 231-240, 2011

[2] J. Forssèn, W. Kropp, J. Brunskog, S. Ljunggren, D. Bard, G. Sandberg, F. Ljunggren, A. Ågren, O. Hallström, H. Dybro, K. Larsson, K. Tillberg, K. Jarnerö, L. Sjökvist, B.Östman, K. Hagberg, Å. Bolmsvik, A. Olsson, C. Ekstrand, M. Johansson, Acoustics in wooden buildings state of the art 2008 Vinnova project 2007-01653, SP Sveriges Tekniska Forskningsinstitut, 2008

[3] R. Maderuelo-Sanz, M. Martìn-Castizo, R. Vìlchez-Gòmez, The performance of resilient layers made from recycled rubber fluff for impact noise reduction, Appl Acoustics 72, 823-828, 2011

[4] Z. Yang, H.M. Dai, N.H. Chan, G.C. Ma, P. Sheng, Acoustic metamaterial panels for sound attenuation in the 50-1000 Hz regime, Appl Phys Lett, 96, 041906, 2010

[5] K.D. Hertz, Light-weight load-bearing structures. Application no. EP 07388085.8. European Patent Office, Munich. November 2007. Application no. 61/004278 US Patent and Trademark Office. November 2007. PCT (Patent Cooperation Treaty) Application PCT/EP2008/066013, 21. November 2008. Patent January 2010.

[6] K.D. Hertz Light-weight load-bearing structures reinforced by core elements made of segments and a method of casting such structures. Application no. EP 08160304.5 European Patent Office, Munich, July 2008. Application no. 61/080445 US Patent and Trademark Office, July 2008. PCT (Patent Cooperation Treaty) Application no. PXCT/EP2009/052984, 13. March 2009. Patent January 2011.

[7] K.D. Hertz, Super-light concrete with pearl-chains, Mag Concrete Res 61, No.8. 655-663, 2009

[8] ISO 10140-2:2010 Acoustics – Laboratory measurement of sound insulation of building elements – Part 2: Measurement of airborne sound insulation, ISO, 2010

[9] ISO 10140-3:2010 Acoustics – Laboratory measurement of sound insulation of building elements – Part 3: Measurement of impact sound insulation, ISO, 2010

[10] R.J.M. Craik, J.A. Steel, The effect of workmanship on sound transmission through buildings: Part 1-Airborne sound, Appl Acoust, 27, 57-63, 1989

[11] L. Cremer, M. Heckl, E.E. Unger, Structure-Borne Sound, second ed., Springer-Verlag, 1973

[12] R. Szilard, Theories and applications of plate analysis, 1st edition, John Wiley and Sons, 2004

[13] M. Heckl, The Tenth Sir Richard Fairey Memorial Lecture: Sound Transmission In Buildings, J Sound Vib, 77, 165-189, 1980

[14] ISO 717 Acoustics – Rating of sound insulation in buildings and of building elements, ISO 1996

[15] I.L. Vèr, C. I. Holmer, Interaction of sound waveswith solid structures, in: L.L. Beranek, Noise and vibration control, INCE, 1988, pp. 270-357

[16] J.H. Rindel, Dispersion and absorption of structure-borne sound in acoustically thick plates, App Acoust, 41, 97-111, 1994

[17] B.A.T. Petersson, M. Heckl, Concentrated excitation of structures. J Sound Vib 196, 295-321, 1996

[18] Eurocode 2: Design of concrete structures - Part 1-1: General rules and rules for buildings, CEN, 2004

[19] Bygningsreglementet Danmark 2008, Energi stryrelsen, 2008

Paper II

"Simulation of flanking transmission in super-light structures"

J.E. Christensen, K.D. Hertz & J. Brunskog

Submitted to: *Applied Acoustics, 2013*

Simulation of flanking transmission in super-light structures

Jacob E. Christensen[a,*], Kristian D. Hertz[a], Jonas Brunskog[b]

[a] *Building Design, Department of Civil Engineering, Technical University of Denmark, DK-2800, Kongens Lyngby, Denmark*
[b] *Acoustic Technology, Department of Electrical Engineering, Technical University of Denmark, DK-2800, Kongens Lyngby, Denmark*

Abstract

Super-light structures is a new invention, which is developed to optimize concrete structures. Super-light structures combine a strong load-bearing concrete with a protective lightweight aggregate concrete in order to save material. A newly developed pre-fabricated super-light deck element is being investigated regarding flanking transmission in the present study.

The airborne sound insulation and the impact sound insulation of the super-light element has been measured in a laboratory. These results are applied in the acoustic software program Bastian to investigate the performance of the element by means of a parametric study of the flanking behavior combined with commonly used building elements and several external floorings.

The analysis is split up into two parts. The first part gives assessments of the performance of the super-light slab element for flanking transmission in a common construction based on current methods and trends in the pre-fabricated industry. The second part gives assessments on a more general level of the flanking transmission performance of the super-light slab element when the partitions are unknown. This is done by a parametric study on typically used partitions. By means of statistic tools the expected performance of the super-light element for flanking transmission is addressed.

Keywords: Lightweight concrete structures, Flanking transmission, Airborne sound transmission, Impact sound transmission, Super-light

*Corresponding author

Email addresses: jacoc@byg.dtu.dk (Jacob E. Christensen), khz@byg.dtu.dk (Kristian D. Hertz), jbr@elektro.dtu.dk (Jonas Brunskog)

1. Introduction

The concept of super-light structures was first invented in 2007 [1, 2] and the accompanying pearl-chain theory was developed in 2008 [3] . The super-light deck element is a pre-fabricated concrete deck element and is developed as a holistic design, a design method, which integrates and fulfil all functional requirements with respect to load-bearing capacity, energy consumption, material consumption, acoustics, indoor climate, fire safety, economy, applicability, and aesthetics. The super-light slab element is designed to be lighter than comparable concrete elements, in addition, the super-light deck element will be able to span longer, have better fire protection and decent building acoustic properties. The main feature is the combination of the strong concrete and lightweight aggregate concrete, which are shaped so that arches are created within the element in order to improve it static behavior, see Fig. 1. With this method the high compression strength of concrete is being utilized by using the strong concrete in the parts of the cross-section in compression.

The super-light deck element is designed in order to have at least as good acoustic measures as comparable concrete elements in terms of surface density and single number ratings of sound insulation [4, 5]. The combination of the two concrete materials increase the performance of the element in building acoustics as the lightweight aggregate concrete can be thought of as an added damping layer, furthermore the element is developed with a geometry which causes the elements to be close to equally stiff in each of its directions and act as an isotropic plate, which is not the case for e.g. a concrete hollow core slab.

The lightweight aggregate parts are made up by precast blocks which have a shape that can accommodate the establishment of internal arches of strong concrete. The prestressed reinforcement is placed in the grooves between the blocks in the main direction of the element to improve the performance in the serviceability limit state by preventing cracking, which reduces the stiffness. An example of a super-light element is shown in Fig. 1

The aim of the present work is to elaborate on the acoustic performance of the super-light deck element, which have had its airborne and impact transmission loss measured and documented earlier [6]. The flanking transmission evaluation of the super-light element is split up into two analysis. The first

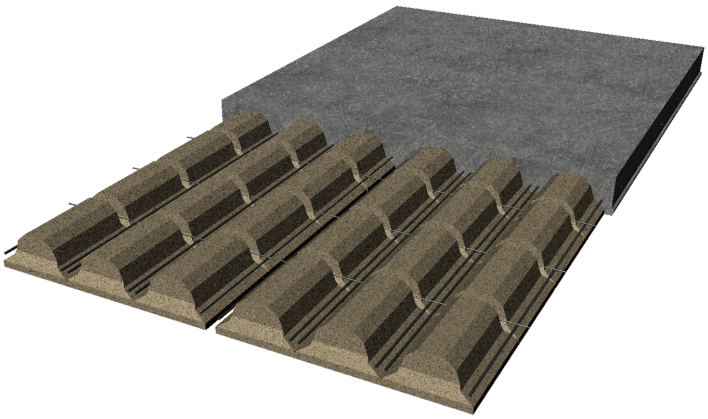

Figure 1: A super-light slab element

part is an analysis, where the partitions are known and are based on a common method applied for pre-fabricated concrete element constructions when multi-storey residential buildings are considered. For the second analysis the partitions are unknown and the performance is addressed by a parametric study in regards to flanking transmission. In total 168 combinations have been used in order to assess the flanking transmission performance of the super-light slab element, the array of different partitions are based on common and proposed solutions and cover both heavy and lightweight partitions. The super-light slab element is evaluated by means of a statistical analysis of the results, where uncertainty caused by variations in measurement methods, workmanship and accuracy of the model used to simulate the flanking transmission, are included.

2. Method and Theory

2.1. The super-light element

The super-light element constitutes the base of the investigation and it is described in [6]. Here, airborne sound insulation and impact sound insulation was measured for the element and its single number rating along with spectral adaption terms for included lower frequencies was determined as $R_w = 55\,\mathrm{dB}$ and $C_{50-5000} = -3\,\mathrm{dB}$ for airborne sound insulation. For impact sound insulation the results were $L_{n,w} = 79\,\mathrm{dB}$ and $C_I = -12\,\mathrm{dB}$.

The element was cast to accommodate the test facilities while mimicking the original design as it is shown in Fig. 1. The cross-sections of the test element is shown in Fig. 2, the element has a surface density of 315 kg/m^2.

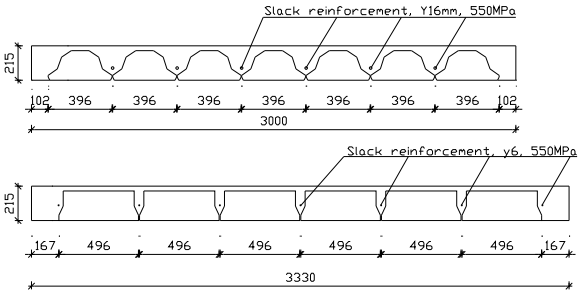

Figure 2: Cross-sectional views of the super-light element.

The difference of the bending stiffness in each of the principal directions of the slab is very low with this design, allowing the element to be thought of as isotropic. The strong direction, which is the top section in Fig. 2 has bending stiffness of $B_1 = 1.282 \cdot 10^7$ Nm, while the less stiff bottom section has bending stiffness of $B_2 = 1.153 \cdot 10^7$ Nm.

2.2. Flanking transmission predictions

Bastian is the acoustical software [7] used for the flanking transmission predictions. Bastian is based on EN 12354 [8, 9] for airborne and impact transmission respectively. The calculation standard EN 12354 is based on Gerretsen's work [10, 11], and is equivalent to a one way SEA [12]. A key point made by Gerretsen's and the EN 12354 models are an averaging between transmission and reciprocal transmission in opposite directions combined with measured data for direct sound transmission. The model does not work well with lightweight structures, but the super-light concrete element used here is not to be considered lightweight in that sense. The model is based on resonant sound radiation, meaning that the model is more accurate when the amount of modes in a one-third octave band is higher than five and the modal overlap factor is at least 1 [13]. In [6] it is revealed that these requirements are first met in the one-third octave band with a center frequency of 200 Hz, decreasing the accuracy of the model in the one-third octave bands below 200 Hz.

It is not possible to enter the orthotropic data for the super-light element in Bastian, the stiffness, and thereby critical frequency [14], has been entered

using the effective torsional rigidity for an orthotropic plate $B_{12} = \sqrt{B_1 B_2}$ [15] as the bending stiffness. The difference in bending stiffness in each of the directions however is low. This means that the orientation, and thereby change of stiffness ratio between the super-light element and the partitions, will have little influence on the results.

2.3. The parametric study

A large array of different configurations of flanking partitions have been applied in the parametric study, which consist of 168 different rooms. The varying factors that have been investigated includes different floorings, facades, internal partitions, external partitions, room sizes and connection details, a summery of these is available in Tab. 1. The considered room and partitions are shown in Fig. 3. In addition to an external floor it consist of one facade, two internal and one external partitions. This means that for the flanking transmission analysis one T-junction and three X-junctions are present. Windows and doors have been omitted from the analysis.

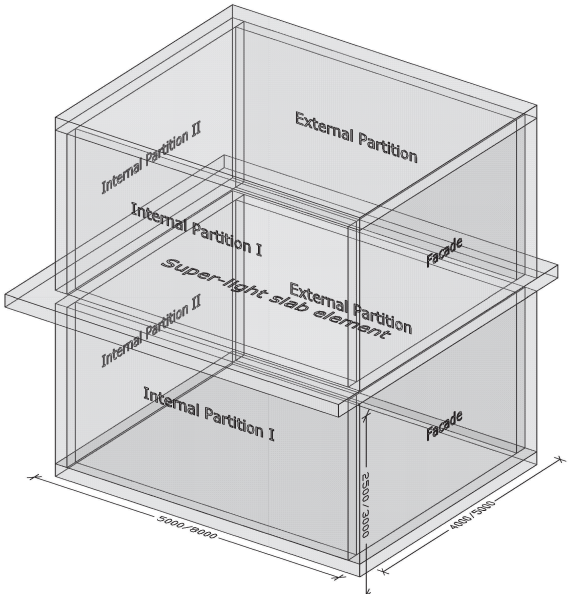

Figure 3: The room and partitions used for the flanking transmission analysis.

Four different floorings have been used in combination with the super-light slab element for the parametric study in order to improve the impact sound insulation. They are three recently developed lay up floors and a

floating floor. Of the lay-up floors two are of the local Danish brand Knudsen kilen (The Knudsen wedge) [16], the two floors are equally based on a wedge called Kombi Max. The only difference between them is a thin layer of filt that has been added to one of the systems beneath the wedge. The third floor is of the brand Harpun and is also based on a wedge [17]. The lay up floors have been measured in a laboratory on a standard 140 mm reinforced massive concrete plate. Only for one of them is its influence in the airborne sound insulation single number rating been measured, $\Delta R = 3$ dB [18], this is for the lay-up floor based on the Knudsen wedge and a layer of filt. For the improvement for impact sound insualtion the floors measured improvement of 24 dB [19], 21 dB [20] and 26 dB [21] for Knudsen kilen with the layer of filt, Knudsen kilen without the layer of filt and the Harpun wedge system respectively. The fourth floor is a floating floor with a 22 mm chipboard placed on 30 mm rockwool, it has been measured to have an increase of the airborne transmission loss of $\Delta R = 9$ dB and impact transmission loss of $\Delta L = 23$ dB [7]. The floors performance for the frequency domain is shown in Fig. 4, here it is also evident that the lay-up floors has only been measured in the reduced frequency range $100 - 5000$ dB, which is why there will be no calculations of the spectral adaption terms for the flanking transmission simulations.

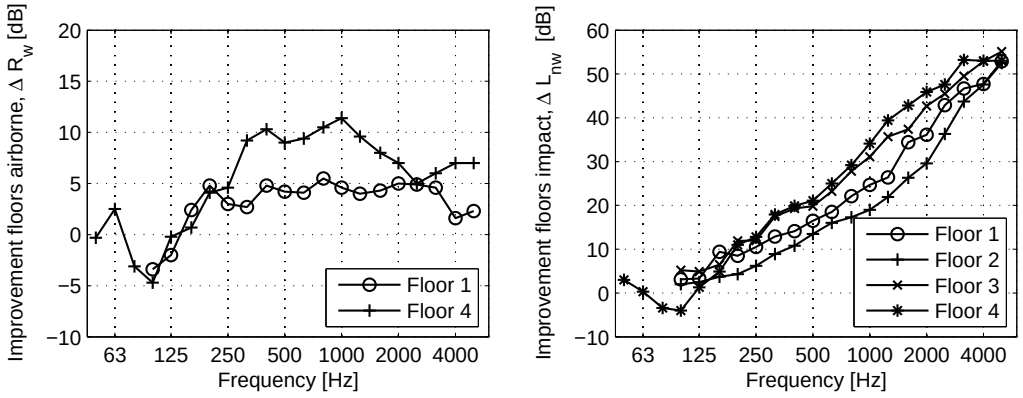

Figure 4: The floors in use measurements on a 140 mm reinforced homogenous concrete slab.

There are three different categories of flanking walls being used in the study: facade walls, external partitions between dwellings and internal partitions between rooms within the same dwelling. Three facade walls have

been used, a heavy double wall made of 150 mm concrete, insulation and masonry with a surface density of 200 kg/m^2. A variation of this double wall is included in the study, where the concrete is clad with gypsum boards in order to increase the acoustic performance of the facade walls. Finally a lightweight wooden triple wall: 13 mm gypsum-145 mm rockwool-9 mm gypsum-28 mm air-28 mm wooden panel is included. Two external walls have been used, a monolithic concrete wall with width 200 mm and a lightweight double gypsum wall consisting of three 12.5 mm gypsum boards separated by a cavity of 270 mm filled with 190 mm rockwool. Two internal partitions have been used for the study, a monolithic lightweight aggregate concrete wall with a density of 1350 kg/m^3 and a width of 100 mm, also a lightweight double gypsum wall have been tested which is built-up by two 12.5 mm gypsum boards separated by a cavity with width 120 mm filled with 30 mm rockwool.

Variation in room size, and thereby partition and floor size, has been addressed by investigation the flanking in a normal sized room $5 \times 4 \times 2.5$ m and a large sized room $8 \times 5 \times 3$ m.

Finally influence of the connection details have been simulated in terms of applying resilient layers at joints. Two different cases have been investigated, one without any resilient layers and one with resilient layers when they are compatible with the applied flanking walls and joint used in Bastian, which means that the resilient layers have not been used in combination with double walls. If resilient layers are applied to the simulation they are placed at all compatible joints. Fig. 3 shows the type of junction for each of the partitions, which is X-junctions for the internal and external partitions and T-junctions for the facade element. The resilient layer has the physical properties of thickness of 12 mm and an elastic modulus of 3 GPa discussed as common by Osipov and Vermier [22].

The choices of the different partitions that have been used is based on the pre-fabricated concrete element building industry in Denmark 2012 along with a sample of gypsum based double walls with good acoustical properties, which have been proposed to be used in order to decrease the flanking transmission. A standard set of flanking walls and the additional configurations of the room is created and used as a basis and reference throughout the study. The standard room configuration is created by the combination of the Knudsen kilen floor with filt, the heavy double facade wall without gypsum cladding, monolithic concrete partitions both external and internal, the normal (small of the two sizes investigated) sized room and no use of resilient layers at connection details.

2.4. Model of single number rating of the flanking transmission

An analysis of the variation of the parametric study has been carried of out in relation to estimate the uncertainties in the single number ratings for both airborne and impact sound insulation. The analysis is made for groups of each of the floors, which are floor 1 and 4 for airborne sound insulation and all four floors for impact sound insulation. The analysis of the variation is based on the null hypothesis that the single number ratings of the flanking transmission, for each of the floors, is a normal distribution. This will be investigated by a χ^2 goodness of fit test, p. 311-313 [23] at a 95 % level of significance, the χ^2 is calculated as,

$$\chi^2 = \sum_{i=1}^{k} \frac{(o_i - e_i)^2}{e_i} \tag{1}$$

with k being the number of observations, o_i is the observed value and e_i is the expected value according to a normal distribution based on the mean and standard deviation of the considered population.

The single number rating model is described by multiple factors

$$\begin{aligned} R'_w &= R_{w,0} + \Delta R_{w,i} + \Delta R_{w,f} + \varepsilon_{Rf,i} \\ L'_{nw} &= L_{nw,0} + \Delta L_{nw,i} + \Delta L_{nw,f} + \varepsilon_{Lf,i} \end{aligned} \tag{2}$$

with $R_{w,0}$ and $L_{nw,0}$ as the sound transmission measured in laboratory without the influence of any floorings, $\Delta R_{w,i}$ and $\Delta L_{nw,i}$ is the improvement from the floor, $\Delta R_{w,f}$ and $\Delta L_{nw,f}$ is the means of the influence of flanking transmission and $\varepsilon_{Rf,i}$ and $\varepsilon_{Lf,i}$ is errors, here as stochastic variables with zero mean and a variance estimated from the parametric simulations. The variance is used to describe uncertainties in the single number ratings of the super-light element and can also be used to find the probability that the single number rating is better than certain thresholds, e.g. demands from legislation, based on the cumulative normal distribution function.

The accuracy of the models can be increased by including errors from workmanship ε_w, the measurement procedure ε_m and uncertainty of the flanking transmission model in EN 12354 ε_{mo}.

$$\begin{aligned} R'_{w,i} &= R_{w,0} + \Delta R_{w,i} + \Delta R_{w,f} + \varepsilon_{Rf,i} + \varepsilon_w + \varepsilon_m + \varepsilon_{mo} \\ L'_{nw,i} &= L_{nw,0} + \Delta L_{nw,i} + \Delta L_{nw,f} + \varepsilon_{Lf,i} + \varepsilon_w + \varepsilon_m + \varepsilon_{mo} \end{aligned} \tag{3}$$

In [24] and [25] several identical floor elements were measured in-situ to identify the uncertainty caused by workmanship. Here, it was concluded

that the standard deviation from measurements on the single number rating was 0.8dB and that the standard deviation of the workmanship was 1.3dB on the single number rating of the tested floors and that these two values were statistical independent. Mahn and Pearse [26] provides an estimate of the uncertainties of the model in EN12354 regarding input data. The uncertainty of EN 12354 has a standard deviation ranging from 0.9 dB to 2.4 dB with most uncertainty at the lower frequencies.

The total error coming from the four different sources of error is estimated by adding the four standard deviations as,

$$\begin{aligned} \sigma_{Rw} &= \sqrt{\sigma_{Rf}^2 + \sigma_w^2 + \sigma_m^2 + \sigma_{mo}^2} \\ \sigma_{Lnw} &= \sqrt{\sigma_{Lf}^2 + \sigma_w^2 + \sigma_m^2 + \sigma_{mo}^2} \end{aligned} \tag{4}$$

which is valid when the covariance is zero and the stochastic variables describing the different errors are independent for the assessment of the parametric study. For the assessment of the accuracy of the standard room $\sigma_{Rf} = 0$ and $\sigma_{Lf} = 0$ will be used. The final model can be described by a single combined error

$$\begin{aligned} R'_{w,i} &= R_{w,0} + \Delta R_{w,i} + \Delta R_{w,f} + \varepsilon_{Rw,i} \\ L'_{nw,i} &= L_{nw,0} + \Delta L_{nw,i} + \Delta L_{nw,f} + \varepsilon_{Lnw,i} \end{aligned} \tag{5}$$

Here $R_{w,0} + \Delta R_{w,i} + \Delta R_{w,f}$ is the mean for a floor group and $\varepsilon_{Rw,i}$ the error with $\mu = 0$ and $\sigma = \sigma_{Rw}$. If the distribution is normal the probability that the airborne or impact sound insulation exceeds certain thresholds for the single number rating is

$$\begin{aligned} P(R'_{w,i} \geq x) &= 1 - F_x(\mu_{R'_{w,i}}, \sigma_{R'_{w,i}}) \\ P(L'_{nw,i} \leq x) &= F_x(\mu_{L'_{nw,i}}, \sigma_{L'_{nw,i}}) \end{aligned} \tag{6}$$

where $F_x(\mu, \sigma)$ is the cumulative distribution function for a normal distribution with mean μ and standard deviation σ.

3. Results

A total of 168 combinations of different rooms for the flanking transmission have been tested with Bastian, but due to limited information available on floor 2 and 3; only 84 combinations of rooms have been made for airborne sound insulation.

3.1. Influence of Flanking Transmission on Super-light Deck

The stand-alone effects of flanking transmission on the super-light deck is first investigated. In Fig. 5 the laboratory measurements and flanking transmission simulations for the standard room without the floor is shown in order to evaluate the influence of flanking transmission on the floor-less super-light slab element. For the airborne sound transmission loss almost no differences can be seen for frequencies below 200 Hz and frequencies above 2.5 kHz. Between these limits the flanking simulation provides less transmission loss with a maximum difference of 4 dB at the one-third octave band with center frequency 315 Hz. The total single number rating of the laboratory measurement was $R_w = 55$ dB, the flanking simulation had reduced this rating to 53 dB, 2 dB less, but still a slightly better performance than the expected rule-of-thumb of 3 dB for heavy-heavy constructions, which is the case for the standard room. For impact transmission the flanking transmission simulation transmits approximately 2 dB lower impact noise over most of the frequency range. The super-light element without a floor it is only the higher frequencies above 1.6 kHz that influence the single number rating due to the shape of the reference curve for impact noise transmission. For the laboratory measurements of the slab it was found to be $L_{n,w} = 79$ dB while the simulation with Bastian also is $L'_{n,w} = 79$ dB. The reason that no reduction in the single number rating can be observed may be caused by difference in floor size, which is 10 m^2 for the laboratory measurements and 20 m^2 in the simulations increasing the total length of the joints from 12.6 m to 18 m.

3.2. Standard Room Setup

The results in Fig. 5 was simulated for the standard room without a floor. The standard room setup includes a lay-up floor and this simulation is shown in Fig. 6. The floor is expected to increase the performance of the super-light slab for both airborne sound insulation, and in particular for impact sound insulation.

In Fig. 6 all the flanking transmission paths are shown: the total, the direct and each of the four flanking paths. For airborne sound transmission the results are more or less as they could be expected, the direct path is dominating the amount of transmitted sound with a contribution on 58 %, which is not far of the rule-of-thumb on 50 %. The heavy facade (7 %) and external partition (2 %) have the least flanking transmission. For the facade this is despite it is the weaker T-junction compared to a X-junction in

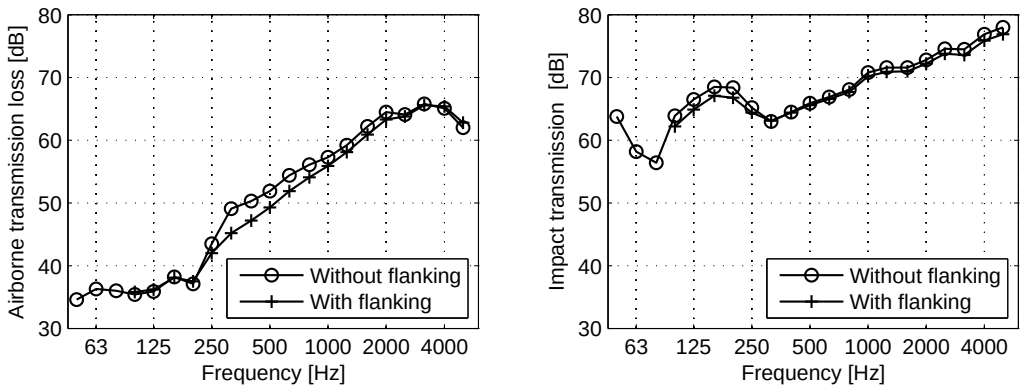

Figure 5: On the left airborne sound insulation of the super-light element measured in laboratory and simulated with flanking transmission, on the right impact sound insulation of the super-light element measured in laboratory and simulated with flanking transmission without flooring.

relation to flanking transmission. The two lightweight internal partitions are somewhere in between and contribute (14 % ,I) and (19 %, II). The difference is caused by the different sizes of the internal partitions as it is shown in Fig. 3. The single number rating of this airborne flanking transmission analysis yields $R'_w = 54$dB which is 1dB lower than the measurement in the laboratory and 1 dB higher than the flanking simulation without a floor. This means that the floor increases the airborne sound transmission loss with 1 dB rather than 3 dB, which was measured on a standard massive concrete floor in a laboratory. For the flanking transmission for impact sound insulation some of the same observations are applicable. The direct path contributes by far the most transmission (74 %), while the internal partitions have the second and third most (9 %, I) and (11 %, II), the facade has little contribution (4 %) as do the external partition (2 %). The single number rating for the impact transmission is 50 dB increasing the impact transmission performance with 28 dB compared with the floor-less flanking simulations, which is 4 dB higher than the measured $\Delta L_{n,w} = 24$ dB improvement of the floor measured in a laboratory.

3.3. Parametric Study

The full array of simulations in the parametric study gives a broad range of results. Fig. 7 shows a histogram of all of the single number ratings in the parametric study for both airborne and impact sound insulation. The mean

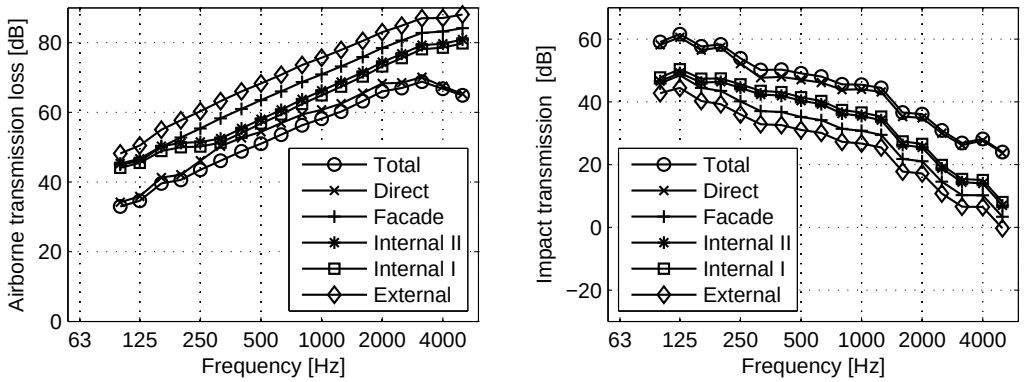

Figure 6: On the left airborne flanking transmission loss of the super-light element for standard room setup, on the right impact flanking transmission of the super-light element for standard room setup. The legend refers to Fig. 3

and standard deviation are $\mu_{R'w} = 58.6$dB, with a 95% confidence interval of $58.1-59.0$dB, $\sigma_{R'w} = 2.08$dB, with a 95% confidence interval of $1.81-2.46$dB for the airborne simulations. For the impact sound insulation, the statistic measures are $\mu_{L'nw} = 50.1$dB, with a 95% confidence interval of $49.8-50.4$dB, $\sigma_{L'nw} = 2.11$ dB, with a 95 % confidence interval of $1.90 - 2.37$ dB. These results, amongst others, are summed up in Tab. 2, where it is also evident that the null hypothesis, that the distribution of single number ratings is a normal distribution, are rejected.

The single number ratings of the airborne sound transmission loss varies from 54 dB to 62 dB. The standard room setup is placed in the lower bracket, but as it is also evident from Tab. 1 that most of the room variations compared to the standard room should be building acoustical better solutions, whether it is double wall solutions, cladding, heavier solutions or incorporation of resilient layers. At single number ratings of 59 dB, 60 dB and partly 58 dB there is a peek of simulation results. This is corresponding to when two of the acoustical better solutions have been substituted into the standard configuration, this situation is the most common room for all of the 84 different room for the flanking transmission analysis.

The single number ratings of the impact sound transmission varies from 46 dB to 55 dB. The different floors in use have a lot of influence on the direct transmission which makes it hard to identify any of the same, or any other trends in the room configuration as it was possible for the airborne single

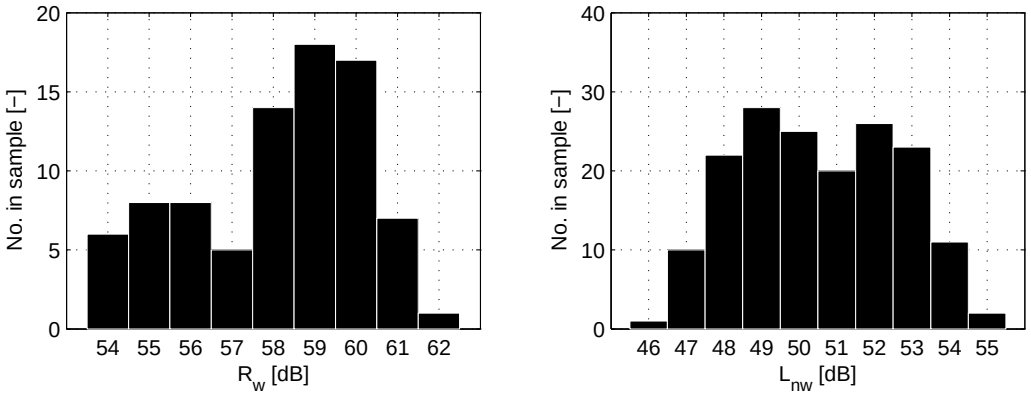

Figure 7: Histogram of the single number ratings of all simulations in the parametric study, on the left for airborne sound insulation and on the right for impact. The single number rating for the airborne sound insulation is 54 dB and for the impact transmission it is 50 dB for the standard room setup.

number ratings, e.g., the standard room setup were identified as having a rather poor performance in relation to flanking transmission. The floor used here is decent in impact flanking transmission, and therefore the standard room is placed in one of the middle brackets with a single number rating $L_{n,w} = 50$ dB.

In Fig. 8 and Fig. 9 the standard deviation spectrums are shown for both the airborne and impact flanking transmission. Each spectrum is based on a floor group, this means that each of standard deviation spectrums are calculated for a sample size of 42 simulations.

Both spectrums of the two floor regarding airborne sound insulation have the same shape overall. The standard deviation is small at the low and high frequencies, while there is a peak of the magnitude of the standard deviation in the middle frequencies from 250 Hz to 1000 Hz.

The standard deviation spectrums for the four floors for the impact flanking transmission are all identical. This is due to the model and the fact that all flanking paths originate from the floor, contrary to the airborne case where flanking paths exists outside of the floor. The improvement of the floor in impact sound insulation is for all cases applied before any junction attenuation, which means the variance for all rooms will be the same. The same argument is used to claim that the standard deviation regarding the single number rating should be equal despite that they vary a little, see Tab.

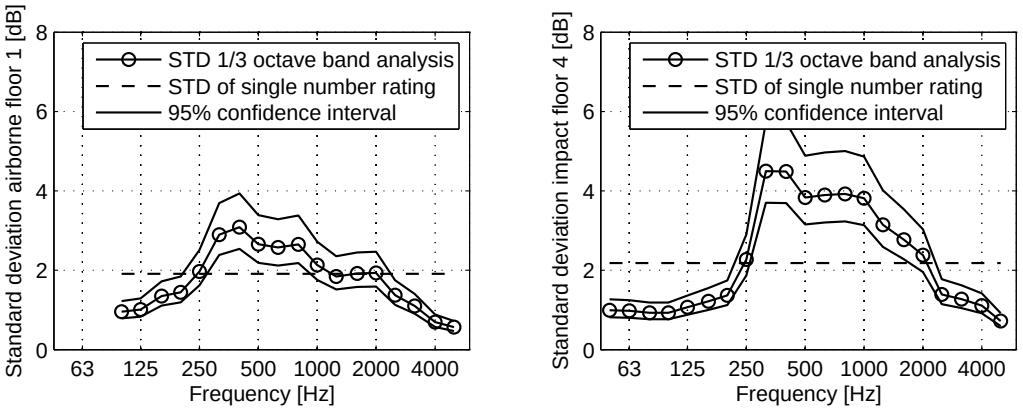

Figure 8: Standard deviation spectrum based on airborne flanking transmission for floor 1 (left) and 4 (right), including standard deviation on the single number rating and 95 % confidence intervals of the standard deviation.

2. This is caused since the single number ratings is calculated in increments in steps of one dB regarding the unfavorable deviation. The four standard deviations is averaged, which gives $\sigma_{floor} = \sqrt{\left(\sum_{i=1}^{4} \sigma_i^2\right)/4} = 0.89\,\text{dB}$.

The standard deviation for the impact flanking transmission is small compared to the standard deviation for the airborne flanking transmission. It is constant for the lower frequencies until 250 Hz. Here, a small peak exists, just like for the airborne spectrums.

Fig. 10 show the histograms of the distribution of single number ratings of the airborne flanking transmission, grouped for each of the floors. Floor 1 has a mean of 58.1 dB and a standard deviation of 1.91 dB and floor 4 has a mean of 59.0 dB and a standard deviation of 2.18 dB .

The distribution mirrors the one in Fig. 7 with peaks for the same values of single number ratings. A χ^2 goodness of fit reveal that the null hypothesis, that it is a normal distribution, is accepted for floor 1 while it is rejected for floor 4. The plots also reveal that the difference, which is 0.9 dB between the lay-up floor and the swimming floor is small compared to their laboratory measurements, which yielded an improvement of the airborne sound insolation of $\Delta R = 3\,\text{dB}$ for floor 1 and $\Delta R = 9\,\text{dB}$ for floor 4.

In Fig. 11, histograms of the distribution of single number ratings for impact flanking transmission shown. The means are 49.9 dB, 52.6 dB, 47.7 dB and 51.2 dB for the four floors and the standard deviation 0.88 dB, 0.86 dB, 0.91 dB and 0.90 dB.

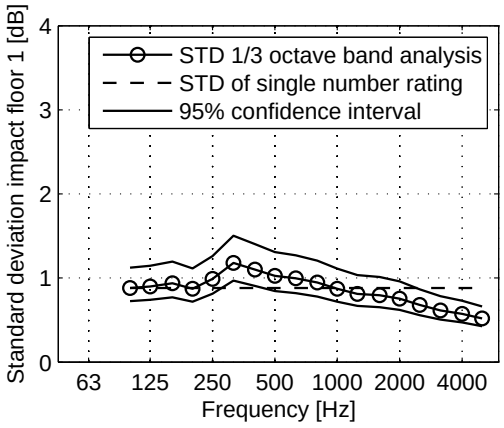

Figure 9: Standard deviation spectrum based on impact flanking transmission for floor 1, including standard deviation on the single number rating and 95 % confidence intervals of the standard deviation.

The null hypothesis for all the distributions have been accepted, implying that they can be described by a normal distribution. Contrary to the airborne flanking transmission, the difference in the measured improvement for the four floors is in agreement with the means of the impact flanking transmission. The standard room is placed in the 50 dB-bracket, 55 dB-bracket, 49 dB-bracket and 52 dB-bracket respectively for the four floors.

The results of the means and standard deviation along with the results of the χ^2 goodness of fit test against normal distributions are summed up for the groups investigated in Tab. 2.

4. Discussion

The results regarding which samples of the population that can be described by a normal distribution are listed in Tab. 2. For the two groups with all the measurements of single number ratings the normal distribution is not a good approximation to describe the spread of the results. If the variation of the floor is removed, by looking at samples based on floor groups, it is clear the distribution of results can be described by a normal distribution. These results support the idea to decouple the floors from the flanking transmission.

The accuracy of the parametric simulations are evaluated with Eq. 5, where variations from workmanship, measurement procedure and the flank-

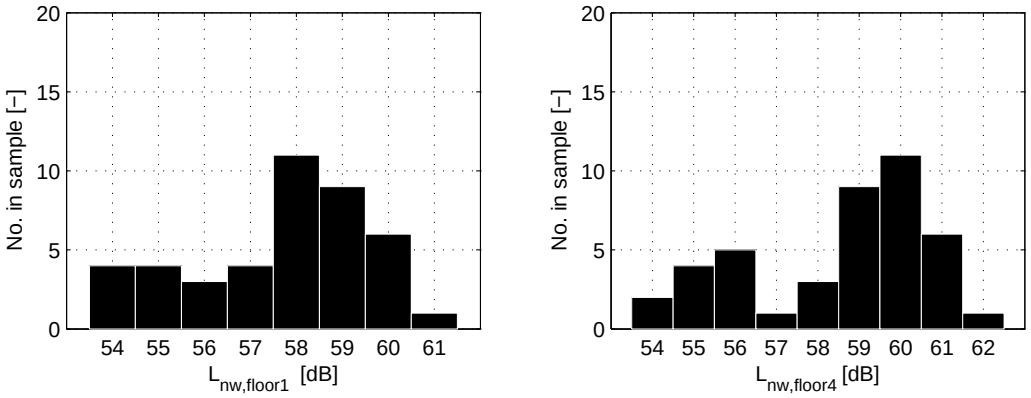

Figure 10: Histogram of the single number ratings grouped by floors for airborne sound insulation. On the left for floor 1, on the right for floor 4.

ing transmission model are included as a standard deviation.

By means of Eq. 4 the total error, expressed by a standard deviation, is determined for each of the floor groups. As argued all floors for impact sound insulation will have the same standard deviation. The total errors is determined for each of the two investigated cases regarding known and unknown room. The standard deviation of the standard room with the common partitions are determined by the uncertainties regarding workmanship, measurement procedure and inaccuracy of the flanking transmission model in EN 12354, it is given by Eq. 7,

$$\sigma_{R'w} = \sigma_{L'nw} = 1.99\,\text{dB} \tag{7}$$

while the standard deviations for the more general case where the partitions is unknown is given Eq. 8 and calculated with the standard deviations obtained from Fig. 8 and Fig. 9 along with uncertainties regarding workmanship, measurement procedure and inaccuracy of the flanking transmission model in EN 12354.

$$\begin{aligned} \sigma_{R'w,1} &= 2.79\,\text{dB} \\ \sigma_{R'w,4} &= 2.95\,\text{dB} \\ \sigma_{L'nw} &= 2.18\,\text{dB} \end{aligned} \tag{8}$$

In comparison EN12354-1 estimates a standard deviation of $1.5 - 2.5\,\text{dB}$ for airborne sound insulation and EN12354-2 estimates a standard deviation of 2 dB for impact sound insulation.

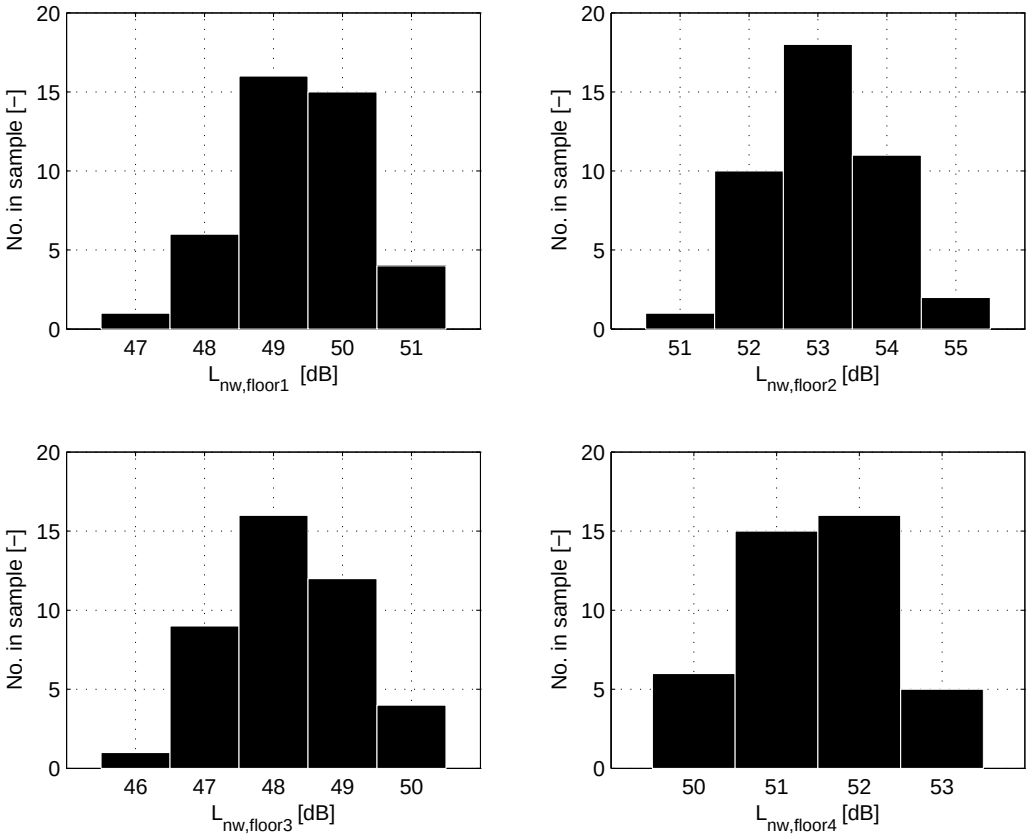

Figure 11: Histogram of the single number ratings grouped by floors for impact sound insulation. On the top left for floor 1, on the top right for floor 2, on the bottom left for floor 3 and on the bottom right for floor 4.

The investigation of the flanking properties was partly made with the new Danish legislation for building acoustics in mind [28]. The requirements of vertical sound insulation for the apparent weighted sound reduction index R'_w have increased from 53 dB to 55 dB and for the apparent weighted normalize impact sound pressure level $L'_{n,w}$ from 58 dB to 53 dB; on an European scale these are amongst the strictest acoustical legislation [29].

One of main result of the study regarding the Danish legislation is the flanking transmission of the standard room. The single number ratings are obtained as the mean of Eq. 5, they are found as 54.6 dB for airborne sound insulation and as 49.9 dB for impact sound insulation. By means of Eq. 6 probabilities based on the cumulative distribution function for the

normal distribution can be found, in relation to the Danish building code and the standard room setup with common partitions, $P\left(R'_w \geq 55\,\mathrm{dB}\right) = 42.0\,\%$ and $P\left(L'_{nw} \leq 53\,\mathrm{dB}\right) = 94.0\,\%$ is obtained. As the airborne flanking transmission simulation of the standard room was below 55 dB it is clear that the probability for it to above must be less than 50%, as the errors are based on normal distributions. For the flanking simulation of impact sound insulation the result of the single number rating is higher than the legislation requirement by a margin of 3 dB yielding a high probability to obey the legislation when uncertainties are considered. The requirement of the of R'_w and L'_{nw} in order to obtain a probability of 95 % that they will obey the building code, is found by solving the equations $P\left(R'_w + x_{R'w} \geq 55\,\mathrm{dB}\right) \geq 95.0\,\%$ and $P\left(L'_{nw} - x_{L'nw} \leq 53\,\mathrm{dB}\right) \geq 95.0\,\%$, which give $x_{R'w} > 3.7\,\mathrm{dB}$ and $x_{L'nw} > 0.2\,\mathrm{dB}$ respectively. This implies that it is needed to improve R'_w by 3.7 dB and L'_{nw} by 0.2 dB, equivalent to single number ratings of the airborne flanking transmission of $R'_w \geq 58.3\,\mathrm{dB}$ and impact flanking transmission of $L'_{nw} \leq 49.7\mathrm{dB}$, in order to obtain a probability of 95% that the standard room setup will pass the legislation requirements when including uncertainties.

The other main results are for the more general case when estimating the super-light slab element's performance with unknown partitions. The probabilities are calculated by Eq. 6, when the partitions are unknown for all floor groups and uncertainties, in addition to the unknown partitions, including workmanship, measurement errors and the error of the model in EN 12354. The single number ratings for airborne and impact sound insulation is listed in Tab. 2 for each of the floor groups.

$$\begin{aligned} P\left(R'_{w,1} \geq 55\,\mathrm{dB}\right) &= 86.7\,\% \\ P\left(R'_{w,4} \geq 55\,\mathrm{dB}\right) &= 91.2\,\% \end{aligned} \tag{9}$$

The results of Eq. 9 reveal that a large amount of the different rooms tested for airborne flanking transmission will fulfill the new legislation and that the difference on the two floors performance is less than it was indicated in Fig. 4.

$$\begin{aligned} P\left(L'_{nw,1} \leq 53\,\mathrm{dB}\right) &= 92.3\,\% \\ P\left(L'_{nw,2} \leq 53\,\mathrm{dB}\right) &= 57.3\,\% \\ P\left(L'_{nw,3} \leq 53\,\mathrm{dB}\right) &= 99.3\,\% \\ P\left(L'_{nw,4} \leq 53\,\mathrm{dB}\right) &= 79.6\,\% \end{aligned} \tag{10}$$

As expected, the floors have a much larger influence on the impact flanking transmission, as Eq. 10 reveals. Floor 1 and 3 demonstrates good results

and have almost no requirements to the flanking partitions in order to obtain a good performance. It is worth noticing, that the only difference between floor 1 and 2, the thin layer of filt is having such a large influence on the impact flanking transmission results.

$$\begin{array}{lll} P\left(R'_{w,1} + x_{R'w,1} \geq 55\,\text{dB}\right) & \geq 95.0\,\% & \Rightarrow \quad x_{R'w,1} > 1.5\,\text{dB} \\ P\left(R'_{w,4} + x_{R'w,4} \geq 55\,\text{dB}\right) & \geq 95.0\,\% & \Rightarrow \quad x_{R'w,4} > 0.9\,\text{dB} \end{array} \tag{11}$$

In Eq. 11 it is shown, that in order to obtain a probability of 95 % of the super-light slab element will be obeying legislation for an arbitrary room in airborne flanking transmission, it is needed to increase its single number rating by 1.5dB for floor 1 and by 0.9dB for floor 4. Compared to the standard room setup, a smaller improvement is needed of R'_w (1.5 dB and 0.9 dB compared to 3.7 dB) in order to satisfy legislation, despite the uncertainties are larger for the parametric study compared to the uncertainties in the analysis of the standard room. This is caused since the means of the single number ratings of the parametric study in airborne flanking transmission are 58.1 dB and 59 dB for the two floors, while the single number rating of the standard room in airborne flanking transmission is 54.6 dB.

$$\begin{array}{lll} P\left(L'_{nw,1} - x_{L'nw,1} \leq 53\,\text{dB}\right) & \geq 95.0\,\% & \Rightarrow \quad x_{L'nw,1} > 0.5\,\text{dB} \\ P\left(L'_{nw,2} - x_{L'nw,2} \leq 53\,\text{dB}\right) & \geq 95.0\,\% & \Rightarrow \quad x_{L'nw,2} > 3.2\,\text{dB} \\ P\left(L'_{nw,3} - x_{L'nw,3} \leq 53\,\text{dB}\right) & \geq 95.0\,\% & \Rightarrow \quad x_{L'nw,3} > -1.7\,\text{dB} \\ P\left(L'_{nw,4} - x_{L'nw,4} \leq 53\,\text{dB}\right) & \geq 95.0\,\% & \Rightarrow \quad x_{L'nw,4} > 1.8\,\text{dB} \end{array} \tag{12}$$

In Eq. 12 the influences of the various floors used is shown, only in the room with floor 3 will there be no need to improve the sound insulation in order to obtain a probability of 95 % to obey legislation.

For a mass production on a daily cycle, i.e., casting, curing and prestressing of the super-light slab element, the lightweight aggregate concrete is to fragile to act as a formwork for the normal concrete without risking the geometry of the lightweight aggregate concrete to be compromised. In order to increase the early stiffness and strength of the lightweight aggregate concrete, it is proposed to increase the density from 600 kg/m^3 to 800 kg/m^3. This corresponds to an increase of the surface density of 7 %, which in terms of the mass law is translated into an increase of 0.6 dB, estimating that R'_w for the standard room will be above 55 dB.

However, in order to obtain $P\left(R'_w\right) \geq 95.0\,\%$ an increase of 3.7 dB is needed corresponding to an increase of the surface density in terms of the

mass law on more than 50 %, which is not a feasible design change for the super-light element. Instead the parametric study reveals that improving on the internal partitions, which are not load-bearing and thereby easier to change, would greatly improve the flanking sound transmission by changing it to either a light-weight double wall or installing resilient layers in the joint of the super-light floor slab.

Another solution is to choose a different flooring. This has partly been investigated here, as the improvement of floor 1 is $\Delta R_1 = 3\,\mathrm{dB}$ and floor 4 is $\Delta R_4 = 9\,\mathrm{dB}$, when measured in a laboratory. This indicates that not all floor types are optimal in combination with the super-light slab element as, e.g., it was the case of a floating floor. Therefore, if a different flooring should be used to increase the performance, special attention needs to be payed towards making sure that the combination of the floor with the super-light slab element will significant increase the improvement of the airborne sound insulation.

5. Conclusion

The study of the airborne and impact sound insulation performance of the super-light element in flanking transmission is done by two parts. The first part regarding flanking transmission has been carried out for a standard room. Here, it is shown that the single number rating of the airborne transmission loss including flanking is $R'_w = 54\,\mathrm{dB}$, this value is decreased by 1 dB compared to the laboratory measurements of airborne sound insulation of the super-light element. For impact sound insulation, including flanking transmission it is shown that the single number rating is $L'_{nw} = 50\,\mathrm{dB}$, which is a great improvement compared to the laboratory measurements and specification of the used floor. These results of single number ratings have been evaluated in relation to uncertainties regarding workmanship, measurement errors and accuracy of the flanking transmission model. In total, these uncertainties are evaluated by a standard deviation of $\sigma_{R'w} = \sigma_{L'nw} = 1.99\,\mathrm{dB}$.

In the second part of the of the flanking transmission, the performance of the super-light slab element was evaluated for a room with unknown partitions. Here, it is shown that the average airborne and impact sound insulation was $R'_w = 58.6\,\mathrm{dB}$ and $L'_{nw} = 50.1\,\mathrm{dB}$

It is shown that the parametric study can be subdivided into groups depending on the floor. The single number ratings within a floor group is described by a normal distribution. For the airborne flanking transmission

the total standard deviations of the uncertainties, which include the unknown partitions, workmanship, measurement errors and accuracy of the flanking transmission model, is found as $\sigma_{R'w,1} = 2.79$ dB and $\sigma_{R'w,4} = 2.95$ dB for floor 1 and 4. Due to all flanking paths originating from the floor, the four different floor groups will have different mean, but have the same standard deviation $\sigma_{L'nw} = 2.18$ dB.

By means of Eq. 6 and the result of the parametric study the performance of the super-light element can be evaluated. In regards to obtain a 95 % probability to successfully obey with the new building code the single number rating needs to be improved for the super-light element in airborne sound insulation. This observation is valid both for the standard room and the parametric study regarding unknown partitions.

6. Acknowledgements

The acoustic technology group at the department of electrical engineering at the Technical University of Denmark is appreciated for having their staff, facilities and equipment at disposal for the measurements of the super-light slab.

The Danish Agency for Science and Technology and Innovation is also appreciated for their support to the research carried out in the above.

References

[1] K.D. Hertz, Light-weight load-bearing structures. Application no. EP 07388085.8. European Patent Office, Munich. November 2007. Application no. 61/004278 US Patent and Trademark Office. November 2007. PCT (Patent Cooperation Treaty) Application PCT/EP2008/066013, 21. November 2008. Patent January 2010.

[2] K.D. Hertz, Super-light concrete with pearl-chains, Mag Concrete Res 61, No.8. 655-663, 2009

[3] K.D. Hertz Light-weight load-bearing structures reinforced by core elements made of segments and a method of casting such structures. Application no. EP 08160304.5 European Patent Office, Munich, July 2008. Application no. 61/080445 US Patent and Trademark Office, July 2008. PCT (Patent Cooperation Treaty) Application no. PXCT/EP2009/052984, 13. March 2009. Patent January 2011.

[4] ISO 717 Acoustics – Rating of sound insulation in buildings and of building elements – Part 1: Airborne sound insulation, ISO, 1996

[5] ISO 717 Acoustics – Rating of sound insulation in buildings and of building elements – Part 2: Impact sound insulation, ISO, 1996

[6] J.E. Christensen, K.D. Hertz, J. Brunskog, Airborne and impact sound transmission in super-light structures, Proceedings INTER-NOISE 2011, 2011

[7] H.A. Metzen, Bastian Manual, DataKustik GmbH, Greifenberg, Germany, 2010

[8] EN 12354-1:2000 Estimation of acoustic performance of buildings from the performance of elements - Part 1: Airborne sound insulation between rooms, 2000

[9] EN 12354-2:2000 Estimation of acoustic performance of buildings from the performance of elements - Part 2: Impact sound insulation between rooms, 2000

[10] E. Gerretsen, Calculation of the sound transmission between dwellings by partitioins and flanking structures, App Acoust, 12, 413-433, 1979

[11] E. Gerretsen, European developments in prediction models for building acoustics, Acta Acoust, 2, 205-214, 1994

[12] T.R.T. Nightingale, I. Bosmans, Expressions for first-order flanking paths in homogeneous isotropic and lightly damped buldings, Acoustica united with Acta Acoust, 89, 110-122, 2003

[13] C. Hopkins, Statistical energy analysis of coupled plate systems with low modal density and low modal overlap, J Sound Vib, 251, 193-214, 2002

[14] L. Cremer, M. Heckl, E.E. Unger, Structure-Borne Sound, second ed., Springer-Verlag, 1973

[15] R. Szilard, Theories and applications of plate analysis, 1st edition, John Wiley and Sons, 2004

[16] Knudsen Kilen Product Sheet, http://www.knudsenkilen.dk/images/content/Brochurer/KileBrochureDK.pdf, accessed February 2013

[17] Harpun lay-up floor system, http://harpun.dk/wp-content/uploads/2009/09/Harpun-Opklodsningssystem.pdf, accessed February 2013

[18] D. Hoffmeyer, Orienterende måling af forbedring af luftlydisolation for et trægulv på strøer på kombi max kiler med lydbrik udlagt på et 140 mm betondæk, Techincal report AV 1223/11, Hørsholm, Denmark, Delta 2011

[19] D. Hoffmeyer, Måling af trinlyddæmpning for et trægulv på strøer på kombi max kiler udlagt på et 140 mm betondæk, Techincal report AV 1166/11, Hørsholm, Denmark, Delta 2011

[20] D. Hoffmeyer, Måling af trinlyddæmpning for et trægulv på strœer på kombi max kiler med lydbrik udlagt på et 140 mm betondæk, Techincal report AV 1165/11, Hørsholm, Denmark, Delta 2011

[21] D. Hoffmeyer, Orienterende målinger af trinlyddæmpning for strøegulvkonstruktion på harpun grøn opklodsning, Techincal report AV 1264/25, Hørsholm, Denmark, Delta 2005

[22] A. Osipov, G. Vermier, Sound transmission in buildings with elastic layers at joints, App Acoust, 49, 141-162, 1996

[23] R. Johnson, Miller and Freund's Probability and statistics for engineers, seventh edition, Pearson Prentice Hall, ISBN 0-13-127840-1, 2005

[24] R.J.M Craik, J.A. Steel The effect of workmanship on sound transmission through buildings: Part 1 - airborne sound, App Acoust, 27, 57-63, 1989

[25] R.J.M Craik, D.I. Evans The effect of workmanship on sound transmission through buildings: Part 2 - structure-borne sound, App Acoust, 27, 137-145, 1989

[26] J. Mahn, J. Pearse, On the uncertainty of the EN12354-1 estimate of the flanking sound reduction index due to the uncertainty of the input data, Building Acoustics, 16, 199-231, 2009

[27] DS/ISO 140-2:1992 Acoustics Measurement of sound insulation in buildings and of building elements Part 2: Determination, verification and application of precision data, ISO, 1992

[28] Generel building code 2008 Denmark(Bygningsreglementet 2008 in Danish), Energi styrelsen, 2008

[29] B. Rasmussen, Sound insulation between dwellings - Requirements in building regulations in Europe, Appl Acoust, 71, 373-385, 2010

Table 1: Overview of the parametric study and the choices of different partitions.

Flooring			
No.	Description	$\Delta R/\Delta L$, [dB]	Ref.
1	Knudsen kilen with a layer of filt	3/24	[20, 18]
2	Knudsen kilen without a layer of filt	-/21	[19]
3	Harpun lydbrik	-/26	[21]
4	Swimming floor, 22 mm chipboard on 30 mm rockwool	9/23	[7]
Facade walls			
No.	Description	ΔR_w,[dB]	Ref.
1	150 mm concrete wall with insulation and masonry 200 kg/m^2	54	[7]
2	150 mm concrete wall with insulation and masonry 200 kg/m^2 with gypsum cladding	54+20	[7]
3	13 mm gypsum - 145 mm rockwool - 9 mm gypsum - 28 mm air - 28 mm wooden panel	48	[7]
External partitions			
No.	Description	ΔR_w,[dB]	Ref.
1	200 mm concrete wall	59	[7]
2	3×13 mm gypsum - 190 mm rockwool - 80 mm air - 3×13 mm gypsum	73	[7]
Internal partitions			
No.	Description	ΔR_w,[dB]	Ref.
1	100 mm lightweight aggregate concrete wall 1350 kg/m^3	42	[7]
2	13 mm gypsum - 30 mm rockwool - 90 mm air - 13 mm gypsum	49	[7]
Room size			
No.	Description	-	-
1	Normal size room $5 \times 4 \times 2.5$ m		-
2	Large room $8 \times 5 \times 3$ m		-
Connections			
No.	Description	-	-
1	No specific detail connection	-	-
2	Resilient layer with $t = 12$ mm and stiffness $E = 3$ GPa	-	-

Table 2: Overview of the parametric study and the choices of different partitions.

	μ [dB]	σ [dB]	χ^2 [-]	DoF [-]	α [-]	χ^2_α (DoF) [-]	Hypothesis [-]
R_w	58.6	2.08	16.7	6	0.05	12.6	Rejected
L_{nw}	50.1	2.11	21.2	7	0.05	14.1	Rejected
$R_{w,1}$	58.1	1.91	4.1	2	0.05	6.0	Accepted
$R_{w,4}$	59.0	2.18	9.0	2	0.05	6.0	Rejected
$L_{nw,1}$	49.9	0.88	4.0	3	0.05	7.8	Accepted
$L_{nw,2}$	52.6	0.86	1.4	3	0.05	7.8	Accepted
$L_{nw,3}$	47.7	0.91	3.2	3	0.05	7.8	Accepted
$L_{nw,4}$	51.2	0.90	7.3	3	0.05	7.8	Accepted

Paper III

"Super-light concrete decks"

K.D. Hertz, J.E. Christensen & N.A. Castberg

Submitted to: *ACI Structural and Materials Journals, 2013*

SUPER-LIGHT CONCRETE DECKS

Kristian Dahl Hertz, Jacob Ellehauge Christiensen, Niels Andreas Castberg

Biography:

Kristian Dahl Hertz is a Professor, M.Sc. Ph.D. Struct. Eng. at the Department of Civil Engineering of the Technical University of Denmark (DTU) has a background as a consulting engineer and has made research in fire exposed concrete structures, anchorage, explosive spalling, and BIM, and he has invented the super-light structures.

Jacob Ellehauge Christensen is a M.Sc. Structural Engineering is an industrial Ph.D. student on super-light structures from Grontmij Consulting Engineers Inc. Denmark.

Niels Andreas Castberg is a M.Sc. in Architectural Engineering is a Ph.D. student on super-light structures in cooperation with BIG Architects Inc. Denmark.

ABSTRACT

The paper presents initial investigations on a prototype series of a new super-light prestressed concrete deck element designed by Abeo Inc. called the SL-Deck to investigate its performance with respect to load-bearing capacity, fire safety, and acoustical insulation.

The intension is that the new deck structure should have a low weight compared to the sound insulation, a sufficient fire resistance, and a possibility of establishing fixed-end supports to obtain long spans and flexible floor plans.

In addition, the design aims at resource savings in terms of consumption of raw materials, energy for production and transport, and need for supporting structures.

Full-scale tests and theoretical investigations show that the deck structure performs as intended, and that it is possible to assess by calculation the load-bearing capacity in bending

and shear, the pull-out strength of prestressing reinforcement, the fire resistance, and the acoustical insulation.

Keywords: super-light structures, deck structures, precast concrete, lightweight concrete, prestressed concrete, structural design, testing structural elements.

INTRODUCTION

Super-light structures consist of an ordinary strong concrete placed, where the designer wants compression forces interacting with a light-aggregate concrete stabilizing the strong parts and filling out the shape Hertz[1,2,3]. The concept won the Clean Tech Open Global Ideas competition in San Francisco November 2010, because super-light structures with their application of more than one type of concrete in structural elements allows minimization of the weight of the elements as well as the amount of cement. A result of this is a reduction of 20-50% of the embodied energy and produced CO_2 compared to normal concrete structures, and a larger reduction compared to similar steel structures (Hertz and Bagger[4]).

The SL-deck is a result of a holistic design process aiming at simultaneous fulfilment of a multitude of functional requirements for decks in domestic- and office buildings (Christensen and Hertz[5], Castberg and Hertz[6]).

This means that the deck should not only be able to carry sufficient dead- and live load, but at the same time it should have a sufficient fire resistance and acoustical insulation for airborne and impact noise. The fulfilment of the many requirements leads to a quite different structural solution than if separate parts take care of them one at a time. For example, we often see a load-bearing construction protected against fire by a cladding and providing noise insulating

by separate layers of flooring leading to a more complex and expensive total structure with a larger production of CO_2 from the construction process.

RESEARCH SIGNIFICANCE

The present paper deals with investigations made on a series of prototypes of the first super-light structural element intended for mass-production: the SL-Deck.

Because it is a result of a holistic design process the research must be multi disciplinary, showing how this load-bearing structure at the same time fulfils a multitude of functional requirements. Since the SL-deck is a first example of a super-light structure, the research also gives an idea of the possibilities of this new patented technology, and especially it unveils if super-light structures based on two widely different concrete materials may cause unforeseen problems.

SL-DECK TEST SPECIMENS

A SL-Deck specimen contains blocks of light aggregate concrete of density 600 kg/m^3 (37.5 lb/ft^3) and compressive strength 3 MPa (435 psi) with a curved surface (Fig. 1). A block stone factory produced the light aggregate blocks for the prototypes and a concrete element factory produced the pre-tensioned SL-Deck elements on a 100 m (328 ft) track (Fig. 2), where they placed the blocks with prestressed wires and slack cross reinforcement between them (Fig. 3) (Tassello[7]). Then plastic concrete of 50 MPa (7.25 ksi) was cast to the final thickness of the deck. A diamond saw has cut the elements in lengths leaving a zone of massive concrete in the end of each element in order to improve the anchorage of the prestressing wires and the

stress distribution at the supports. The time interval between new castings on the same track was 24 hours, and curing takes place at a storage facility.

At a construction site the intension is that a contractor will place reinforcement in grooves between the elements and cast out these grooves without application of additional mould pieces.

If the structural design applies a fixed-end support of an element, the contractor places additional reinforcement in grooves in the top of the element (Fig. 4) between the internal light blocks. The factory has made the grooves and the contractor casts them out at the construction site together with the grooves around the element. Alternatively, a long element is placed continuously over the supports.

MOMENT RESISTANCE

The research group at the Technical University of Denmark tested prototypes of the SL-Deck mechanically in order to investigate whether the deck will break in a tough and ductile manner with a reasonable warning or not and to unveil any unforeseen effects, when the structure is loaded to its ultimate capacity, and to indicate whether it is reliable to apply commonly accepted methods for estimating the load-bearing capacity.

Each of two test specimens for moment resistance tests are 215 mm (8.5 in) thick and 1.2 m (3.94 ft) wide SL-elements with 3 light aggregate blocks of 400 mm (15.8 in) across the width.

The span width of the elements was 4 m (13.1 ft) between the centre lines of the supports and they were reinforced by 6 prestressing wires of diametre 12.5 mm (0.5 in) and characteristic

strength 1860 MPa (270 ksi). The strong concrete has a characteristic compressive strength of 50 MPa (7.25 ksi), and the compressive strength of the light-aggregate concrete is 3 MPa (435 psi). The deck has a weight of 300 kg/m^2 (61.4 lb/ft^2) and the moment from dead load at midpoint is 7.0 kNm (5.2 kip*ft).

Two jacks apply the load at the midpoint of the span through a steel beam distributing the stresses across the width of the deck element.

Mechanical and electronic gauges measure deflections at the midpoint (Fig. 5).

An ordinary plastic design calculation gives a characteristic failure moment of 132.6 kNm (97.8 kip*ft).

The measured ultimate failure moments were inclusive dead load 153.3 (113) and 154.8 kNm (114 kip*ft). The test results are therefore approximately 17% safe compared with a calculation (Tassello[8], Lauricina[9], Halldorsson[10]).

The fracture was ductile with a gradual crack formation during the last part of the loading period (Fig. 6). This proves that the specimen responded as a coherent structure and no sign of separation occurred between strong- and light-aggregate concrete.

In Figure 7 is shown the relation between deflection and applied moment load (exclusive dead load and measured by electronic gauges) for the first 40 mm of deflection, where the ultimate moment resistance occurred at a deflection of approximately 200 mm (measured mechanically). A linear behaviour is seen up to approximately half of the ultimate applied moment load.

SHEAR RESISTANCE

A SL-Deck element has no shear reinforcement. The structure therefore transfers shear forces by means of compression- and tension stresses in the strong- as well as in the light-aggregate concrete and across the interfaces between the two materials.

We made a shear resistance test to investigate whether the structure can transfer a calculated ultimate shear force in a zone, where anchorage does not reduce the capacity.

The specimen was therefore loaded relatively close to a support with a relatively long anchorage zone extending from the support (Fig. 8). The distance between the load and the support was chosen in order to make space for a shear transfer mechanism consisting of inclined compression and to some extent tension and in order to have a representative cross section with light-aggregate blocks and strong concrete. Because we needed this distance, we knew that we could probably not obtain a pure shear failure without having a bending failure too.

A 215 mm (8.5 in) thick and 1.2 m (3.94 ft) wide SL-element with a span width of 1.985 m (6.51 ft) and reinforced by 6 prestressing wires of diametre 12.5 mm (0.5 in) was loaded at a point 0.485 m (1.59ft) from the centre of the nearest support. The distance from the centre of the support to the end of the element was 0.35 m (13.8 in) of which 0.10 m (3.9 in) at the end consists of massive concrete without light-aggregate concrete blocks.

As foreseen, the failure mode was combined bending and shear. Still, a shear force of 269 kN (60.5 kip) was measured and the test therefore shows that this force can be transferred in a zone, where light aggregate blocks are in the cross-section (Halldorsson[10]).

The shear capacity obtained by calculation (according to the Eurocode) is 215 kN (48.3 kip). The test therefore indicates that it is safe to calculate the shear resistance. By comparison with the moment resistance, the test shows that shear failure of the cross-section only

becomes decisive for theoretical span-widths of less than 1 m (3.28 ft), which means that shear resistance seldom decides the dimensions in practise.

PULL-OUT RESISTANCE

Although SL-Deck elements allow fixed-end supports and continuous slabs, it is still possible to apply a simple support, which until now is the most common for prefabricated deck elements. Often a simple support has a small bearing-depth because a wall or a console, on which the element is placed, has a limited width. The anchorage of the pre-tensioned prestressing wires is therefore of interest.

The author gives in Hertz[11] a general design method for assessing anchorage capacity as a minimum of splitting strength and bond strength. Splitting develops cracks radial from the reinforcing bar to one or more surfaces and it depends on the cross-section. Bond-failure means that the bar is pulled out of a round hole and it depends on the concrete and the corrugations on the bar. The paper describes how to calculate the maximum bond resistance for deformed bars as an ultimate shear stress on the surface of the bar of 0.65 times the compressive strength of the concrete.

This theoretical value is calculated from plain strain crushing under 45° to the bar axis and it fits with results of the bond test ("Cuff-test") described in the paper.

If the reinforcing bar does not have sufficient corrugations, the bond capacity is smaller.

It is measured by the test, and the paper shows values for common bars at normal- and at fire conditions. However, prestressing wires were not included in this test series.

A later special project (Fig. 9) therefore tested bond strength of prestressing wires Hertz[12] showing a factor of approximately 0.40 instead of the theoretical maximum of 0.65 for deformed bars.

A pull-out test is made for a SL-Deck element in order to investigate whether the anchorage capacity and thereby the ultimate reaction of a small support can be calculated.

A 215 mm (8.5 in) thick and 1.2 m (3.94 ft) wide SL-element with a span width of 1.995 m (6.54 ft) and reinforced by 6 prestressing wires of diametre 12.5 mm (0.5 in) was loaded in a point 0.500 m (19.7 in) from the centre of the support (Fig.10). The distance from the centre of the support to the end of the element was 0.040 m (1.6 in). The outmost 0.10 m (3.9 in) of the element was massive concrete without light aggregate blocks. A crack developed as foreseen from the load to the edge of the support (Fig. 11), and the ultimate failure mode was in bending due to bond failure of the prestressing lines at a reaction at the support of 132 kN (29.7 kip). This proves that no splitting failure occurs and that bond failure, which is the maximum anchorage capacity for the prestressing wires in any cross-section, was observed. The bond failure was in the 0.10 m (3.9 in) long massive part of the slab, since the crack had a thickness equal to the sliding measured from the end of all the wires of 20 mm (0.8 in).

This gives a bond strength equal to the anchorage strength for the 6 wires of 501 kN (113 kip) at 0.10 m (3.9 in) or a bond strength factor of 0.425 for a 50 MPa (7.25 ksi) concrete. It confirms that the anchorage capacity can be calculated on the safe side as the bond strength equal to 0.40 times the characteristic compressive strength of the concrete times the perimeter of the wires. This also determines a magnitude and angle of a compressive force in the deck at the support and thereby an ultimate reaction.

ACOUSTICAL PROPERTIES

In the SL-Deck, the strong concrete constitutes a series of vaults over the curved light-aggregate blocks. Since a vault is stiffer than a plane plate, the eigenfrequency of it is higher,

which is beneficial because the most difficult frequencies to make sound insulation for are in the low end of the spectrum.

Furthermore, the porous light aggregate concrete has an internal loss factor, which is 2-3 times higher than the internal loss factor of normal concrete. Additionally, the light aggregate concrete will further increase the damping as it is acting as a damping layer as described by Cremer and Heckl[13] (page 243-247).

A new method for estimating these effects is developed by Christensen et al[14].

By means of this and by full-scale tests in the acoustical laboratory of DTU-Electro (Fig.12) we found that a prototype SL-deck of 315 kg/m^2 (64.5 lb/ft^2) gives an acoustical airborne insulation of 55 dB.

This is equal to the new Danish requirement for acoustical insulation in domestic buildings. For comparison, some factories producing existing concrete deck elements decide to increase the mass of their decks to 370 - 440 kg/m^2 (75.8 - 90.1 lb/ft^2) in order to meet this new requirement.

The impact noise (or step noise) level was measured as 79 dB from which you should subtract the damping of a floor (Fig. 13). Application of a floor consisting of 22 mm (0.9 in) chipboard on 30 mm (1.2 in) mineral wool gives a damping of 29 or 32 dB for two different commercially available qualities. This leads to a step-noise level of 50 dB or 47 dB, which is less than the maximum of 53 dB allowed according to Danish standards. This shows that the step-noise level of the new SL-Deck elements is acceptable.

FIRE SAFETY

Two 6.4 m (21.0 ft) long, 1.2 m 3.94 ft) wide and 215 mm (8.5 in) thick prototype elements with 6 prestressing wires of diameter 12.5 mm (0.5 in) were placed simply supported with a fire exposed span of 6 m (19.7 ft) on a fire test oven at the Danish Institute of Fire Technology (Fig. 14). The grooves on all four edges were insulated with mineral wool, which means that the contribution to the load-bearing capacity from casting reinforced grooves did not influence this test.

The elements sustained a live- and semi-live load as required for domestic buildings of 2.5 kN/m^2 (52.2 lbf/ft^2) (in addition to the dead load of the elements of 3 kN/m^2 (62.7 lbf/ft^2)) for 120 minutes. At this time, the deck elements had a final deflection of 25 mm (1.0 in).

Then the applied load was increased to 17.6 kN/m^2 (367 lbf/ft^2), which was the limit of the jacks applied. A deflection of 200 mm (7.9 in) was measured and the deck was unloaded back to a deflection of 35 mm (1.4 in) at 135 minutes of standard fire exposure.

The elements were unharmed after the fire test. This shows that the elements have a fire resistance of at least 120 minutes. The results accord safely with calculations according to Hertz[11,12,15,16] and the Eurocode 1992-1-2[17] for example made by means of the freeware program Confire[18], where the calculated load-bearing capacity excl. dead load is found to be 15.8 kN/m^2 (330 lbf/ft^2) after 120 min standard fire, (Halldorsson[10], Rocca[19], Carstensen et al[20]).

The test indicates that the elements will also have a fire resistance of 240 minutes as you can get from the same calculations for domestic load of 2.5 kN/m^2 (52.2 lbf/ft^2).

Fire safety becomes increasingly important for load-bearing structures these years, because application of low-energy windows that do not break in fire, heavy insulation in the facades, light-weight aerated concrete walls and impact noise insulated floors means that fires become

more hot and give rise to long time exposures, which means violent damages on structures (Hertz[21]).

CONCLUSIONS

The SL-Deck is a new design of a deck structure to be made prefabricated with application of prestressed reinforcement. Mechanical tests are made of 215 mm (8.9 in) thick prototypes for bending, shear, and pull-out of reinforcement at small bearings.

The deck showed a ductile behaviour to ultimate limit conditions for all tests, and the load-bearing capacity appears to be safe compared to the calculated and can therefore be predicted by calculation.

Acoustic tests show that a SL-Deck with a weight of 315 kg/m^2 (64.5 lb/ft^2) has an airborne noise insulation of 55 dB and an impact noise level of 79 dB, which by means of standard floors may give a total impact-noise level of 47-50 dB. The SL-Deck should therefore be able to fulfil the recent Danish noise requirements for domestic buildings of maximum of 53 dB impact noise and minimum 55 dB airborne sound insulation.

A standard fire test demonstrated a load-bearing capacity of 17.6 kN/m^2 (367 lbf/ft^2) after 135 minutes standard fire exposure and it confirms calculations indicating a resistance of 240 minutes for a domestic live- and semi live load of 2.5 kN/m^2 (52.2 lbf/ft^2).

The test series indicates that some of the most important properties of a deck can be estimated by calculation for the SL-Deck, and that the holistic design of the construction seems to have a fair chance to meet the many different requirements for modern building structures.

ACKNOWLEDGMENTS

The authors wish to express their gratitude to the Danish Institute of Fire Technology for participating in the fire test, the institute DTU Electro for participating in the acoustical tests, Karlshoej and Kähler concrete element factories for producing block stones and test elements, the universities of Iceland, Padua and Rome La Sapienza and the Polytechnic of Nantes for supporting with partial projects and the company Abeo Inc. for offering the SL-Deck design for investigation.

REFERENCES

1. Hertz, K. D., “Super-light concrete with pearl-chains,” *Magazine of Concrete Research*, Vol. 61, No. 8, Thomas Telford Ltd. October 2009, pp.655-663.

2. Hertz, K. D.:, “Light-weight load-bearing structure,” *PCT (Patent Coroperation Treaty)* Application no. PCT/EP2008/066013, November 2008. PCT Patent, January 2010.

3. Hertz, K. D., “Light-weight load-bearing structures reinforced by core elements made of segments and a method of casting such structures,” *PCT (Patent Coroperation Treaty)* Application no. PCT/EP2009/052987, March 2009. PCT Patent, October 2010.

4. Hertz, K. D., and Bagger, A., “CO2 emission from super-light structures,” *Proceedings of the IABSE-IASS Symposium*, London, September 2011.

5. Christensen; J. E., and Hertz, K. D., “Super-Light Prefabricated Deck Element Integrated in Traditional Concrete Prefabricated Element Construction,” *Proceedings of IASS-APCS Symposium in Seoul*, Korea, May 2012.7 p.

6. Castberg, N. A., and Hertz, K. D., “”The Battery” Designed with Super-Light Decks”, *Proceedings of IASS-APCS Symposium in Seoul*, Korea May 2012.7 p.

7. Cornement, K., “SL-Deck. Load-bearing capacity,” Report, Département Génie Civil, Polytech Nantes, August 2012. 46 p.

8. Tassello, A., “Load-bearing capacity of super-light slabs,” M.Sc. Project. Department of Civil Engineering, DTU and University of Padova, 2011.

9. Lauricina, D., “Analisi di elementi strutturali superleggeri in c.a.p. ai fini della sostenibilità: utilizzo del codice di calcolo DIANA,” (“Analyses of structural elements at ultimate limit state by means of DIANA”) Università degli studi di Roma, La Sapienza, Facoltà di Ingegneria. 2010. 354 p.

10. Halldorsson, E., “Load-bearing capacity of super-light decks,” Faculty of Civil and Environmental Engineering, University of Iceland. Reykjavik January 2012. 60p.

11. Hertz, K. D., “The anchorage capacity of reinforcing bars at normal and high temperatures,” *Magazine of Concrete Research*, Vol.34, No. 121, Thomas Telford Ltd. December 1982, pp. 213-220.

12. Hertz, K. D., ”Vedhæftningsstyrke af spændliner ved brandpåvirkning” (“Bond strength of prestressing wires in fire”),Department of Civil Engineering, Technical University of Denmark, Report SR 05-12, August 2005, 10p.

13. Cremer, L., and Heckl, M., and Ungar, E. E., “Structure-Borne Sound,” Second edition Springer-Verlag 1973, 528p.

14. Christensen, J. E., and Hertz, K. D., and Brunskog, J., “Airborne and impact sound transmission in super-light structures,” *Proceedings of Inter-Noise 2011*. Osaka September 2011.

15. Hertz, K. D., “Concrete strength for fire safety design,” *Magazine of Concrete Research* Vol. 57, No. 8, Thomas Telford Ltd. October 2005, pp. 445-453.

16. Hertz, K. D., “Reinforcement data for fire safety design,” *Magazine of Concrete Research* Vol. 56, No. 8, Thomas Telford Ltd. October 2004, pp. 453-459.

17. EN1992-1-2: Eurocode 2. “Design of concrete structures- Part 1.2 General rules – Structural fire design,” CEN Brussels. September 2004.

18. Hertz, K. D., “Confire Users Guide,” 2. Edition, and “Confire,” freeware program. Department of Civil Engineering, Technical University of Denmark. 23 p. (Available from the publication and software part of the homepage of the dept.) Kgs. Lyngby. February 2012.

19. Rocca, N., “Risposta al fuoco di elementi strutturali superleggeri e in C.A.P.: Modellazione termo-meccanica con il codice de calcolo DIANA,” (“Response to fire of super-light structures. Thermo- mechanical modelling by means of DIANA,”) Università degli studi di Roma, La Sapienza, Facoltà di Ingegneria. 2010. 269 p

20. Carstensen, J. V., and Giuliani, L., and Hertz, K. D., “Fire Resistance of a Super-Light Deck Element: Finite Element Investigation and Related Modelling Issues,” 2nd Fire Safety Day, University of Lund, Lund, Sweden, April 2012.

21. Hertz, K. D., “Parametric fires for structural design,” *Fire Technolog,*. Vol. 48, No. 4 pp 807-823. Springer Science 2012.

FIGURES

List of Figures:

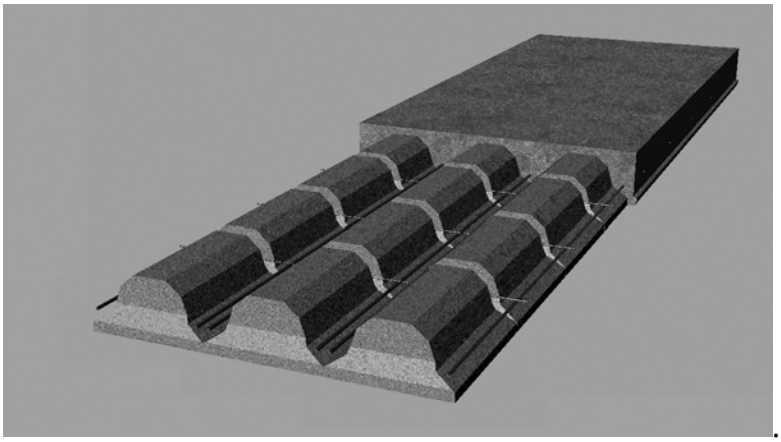

Fig. 1- Principle for a 215 mm (8.5 in) thick, 1.200 m (3.94 ft) wide prototype.

Fig. 2- Casting of SL-deck prototype test elements.

Fig. 3- Close-up of block stones and reinforcement before casting strong concrete.

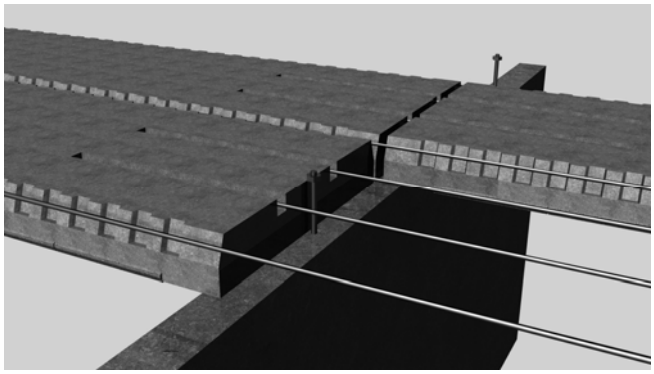

Fig. 4- Fixed end support of SL-Deck elements at a load-bearing wall.

Fig. 5- Bending test rig with a SL-Deck element.

Fig. 6- Ultimate bending failure of a SL-Deck element.

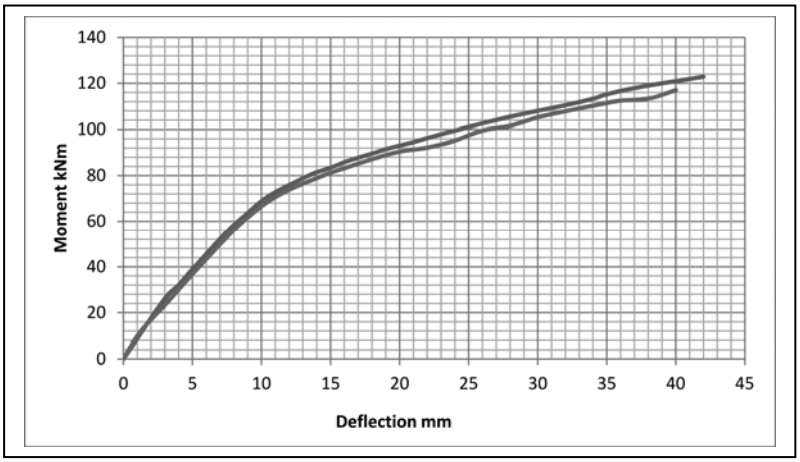

Fig. 7- Applied moment load vs. deflection.

Fig. 8- Shear resistance test with a SL-Deck element.

Fig. 9- Conical bond test specimen with prestressing wire and cracks from fire exposure.

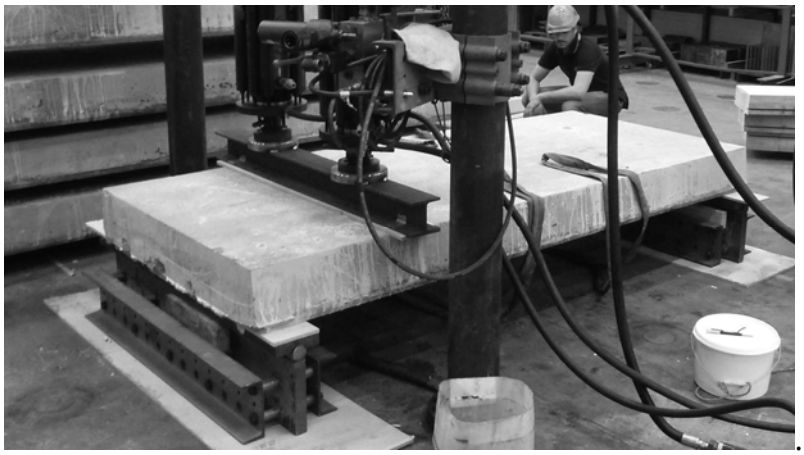

Fig. 10- Pull-out test with a SL-Deck element.

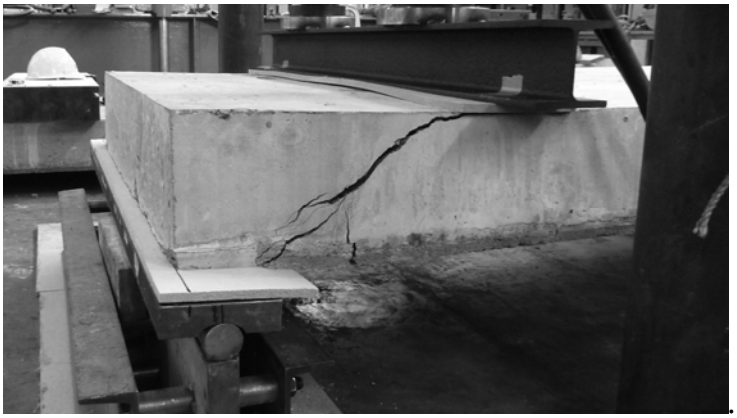

Fig. 11- Crack formation at pull-out test with a SL-Deck element.

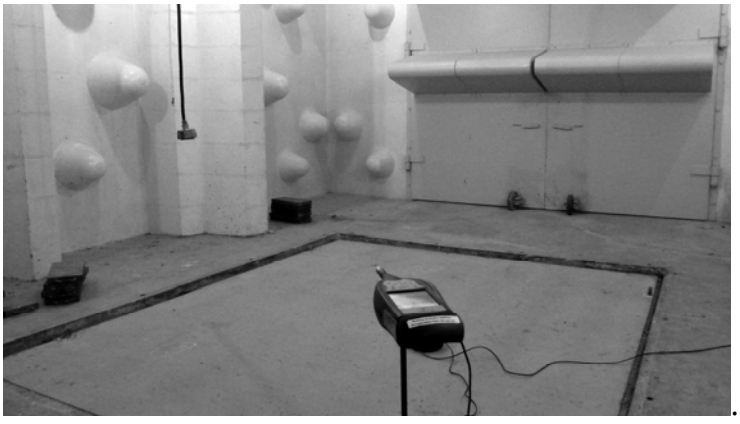

Fig. 12- SL-Deck exposed to a white noise in the floor of a sound-hard room. Noise transmission is measured to another sound-hard room below.

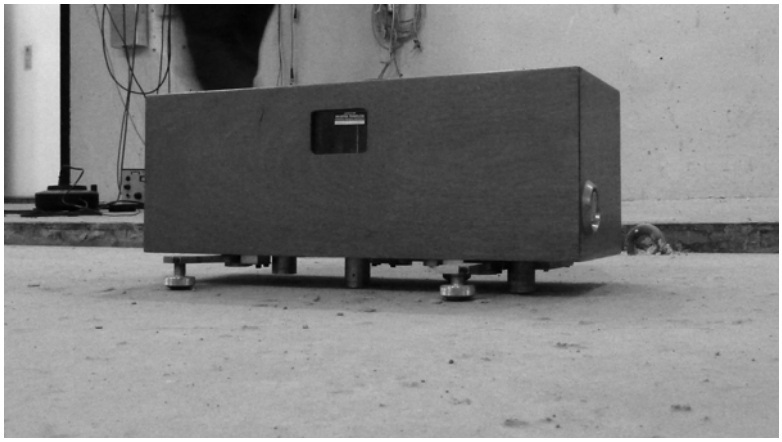

Fig. 13- Impact-noise machine on a SL-Deck.

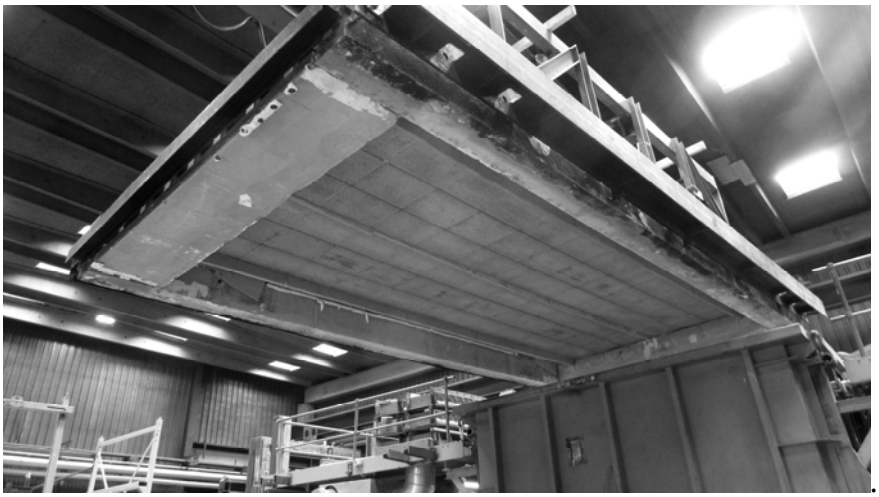

Fig. 14- Unharmed SL-Deck after 135 min standard fire exposure with 17.6 kN/m^2 (367 lbf/ft^2) load.

Paper IV

"Super-light precast deck elements integrated in a traditional concrete precast element construction."

J.E. Christensen & K.D. Hertz

Submitted to: *Engineering Structures, 2013*

Super-light precast deck elements integrated in a traditional concrete precast element construction

Jacob E. Christensen[a,*], Kristian D. Hertz[a]

[a] *Building Design, Department of Civil Engineering, Technical University of Denmark, DK-2800, Kongens Lyngby, Denmark*

Abstract

Super-light structures and pearl-chain reinforcement are recently developed concepts for creating concrete structures and elements. It is based on combining two concretes, namely a normal or high-strength concrete with a lightweight aggregate concrete. In the present study the emphasis is placed on a precast super-light slab element, which in a customized form has been used for the first time in a construction as a demo project. The super-light deck element is created by combining precast blocks of lightweight aggregate concrete with normal reinforced concrete.

The super-light slab elements are used in an indoor pedestrian bridge with a maximum span of 5.5 meters as slack reinforcement has been used. Examples of the versatility of the super-light slab element in this construction are given. This include variations in element size, integrated details in the element, such as a framework for beams and beam reinforcement and connection details to adjacent structural elements integrated in the super-light element.

The project has shown some of the advantages of the super-light slab elements compared to other precast elements, the weight is reduced and the total amount of elements is minimized. In addition, the connections between the super-light elements and adjacent elements are carried out with a minimum need for working hours, additional materials, and curing time.

Keywords: Super-light Structures, Precast concrete elements, Floor elements

*Corresponding author

Email addresses: jacoc@byg.dtu.dk (Jacob E. Christensen), khz@byg.dtu.dk (Kristian D. Hertz)

1. Introduction

The concept of super-light structures was invented in 2007 [1, 2]. Super-light structures are based on combining two different concretes in order to utilize the good properties of both concretes. For the super-light structures the concretes that have been used are a porous lightweight aggregate concrete (LWAC) with a density of 600 kg/m^3 and a normal or, if possible, a high-strength concrete with a density of 2300 kg/m^3. A super-light structure is typically constructed by placing the load-bearing concrete, i.e. the normal or high-strength concrete, where it is needed. A typical way of implementing this is by shaping the super-light structure so that the load-bearing concrete is in compression arches. The super-light structure is completed by combining the normal concrete with LWAC and its good properties. In relation to a super-light structure they include, low weight, high heat insulation, high loss factor, and good sound absorption [3, 4]. The LWAC is applied to a super-light structure for three main reasons: to stabilize the compression arch against buckling, to utilize its high thermal insulation in order to improve fire safety by protecting reinforcement or, for high-strength concrete, protect against explosive spalling as reported in [5] and [6], the third main reason is to create the final shape of the super-light structure determined by e.g. architecture or design requirements.

The principle of super-light structures is enhanced by the invention of the pearl-chain reinforcement technology [7]. The pearl-chain reinforcement is made from post-tensioned segments of concrete and a prestressed wire. By shaping the segments with e.g. inclined ends, it is possible to easily create and assemble curved shapes of the load-bearing concrete as an alternative to construct them by expensive and time-consuming formwork or scaffolding. An example of a pearl-chain reinforcement is shown in Fig. 1, where an arch is combined from easy to cast straight segments.

A super-light slab element is designed by some of the principles of super-light structures. Due to the desire of having a limited height (215 mm) of a floor structure and due to the production cost, it is not feasible to use pearl-chain reinforcement or arches spanning from support to support within a super-light slab element, which is intended for mass production. Instead smaller arches are established within the element through the use of LWAC as a mould for the normal concrete as shown in Fig. 2. Here, it is also

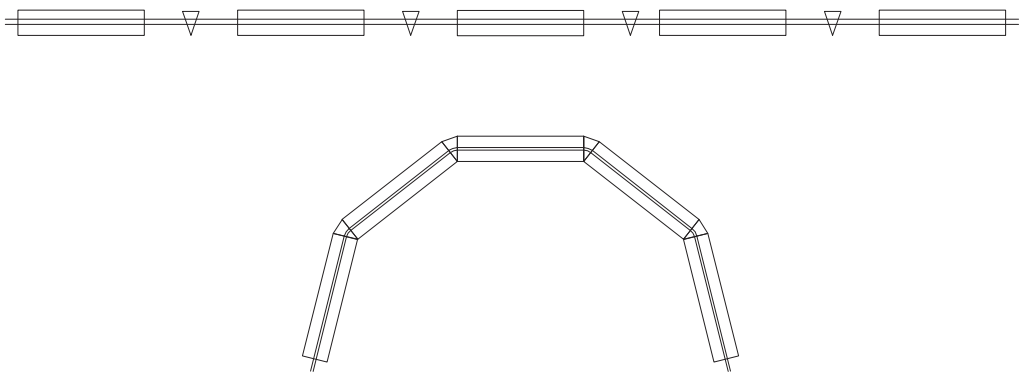

Figure 1: Principle of pearl-chain reinforcement

indicated, that for the super-light slab element, the lightweight aggregate concrete is cast as blocks. The element is 1.2 m wide, which supports the use of three LWAC blocks across the width. The LWAC blocks are covering the majority of the bottom of the slab; there they act as a thermal insulator for the reinforcement significantly increasing the fire resistance of the element. The shape of the LWAC blocks and the connection between them and the normal concrete benefits the acoustic properties of the element for airborne and impact sound insulation [9, 10]. Reinforcement has been placed in the cavities between the blocks in both directions. Prestressed reinforcement is used in the main direction and slack reinforcement is used in the secondary direction. Slack reinforcement is applied to stabilize the element against longitudinal cracking and to take horizontal forces coming from the arches. At the ends of a element full sections of normal concrete are placed for increased anchorage capacity of the prestressed reinforcement and optimal conditions at the bearings.

The super-light slab element used for the indoor pedestrian footbridges are a variation of the super-light element. The footbridge and overall plan of the building are described in Sec. 2. As the pedestrian bridges are used for access routes. A minimum width of 1.5 m is specified as a requirement due to accessibility by the Danish building code [11], but also the architectural design has influence the width of the bridge. For the production of prestressed concrete elements the prestressing of the strands is done in a custom built formwork with a width of 1.2 m. Therefore it was not possible to prestress the elements for the bridges. The solutions and design in regards to these limitations is described in Sec. 3 and 4.

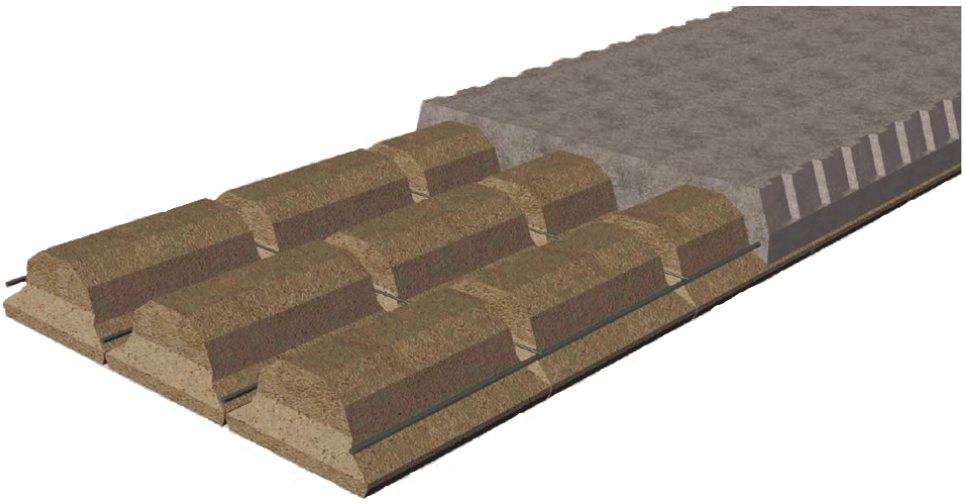

Figure 2: A super-light slab element

Some of the benefits by using super-light structures is to obtain material savings, lower the weight of elements, and minimize the emission of CO_2 during the production of the elements as shown by Hertz and Bagger [8]. Numerous studies and designs for improving monolithic concrete slabs have been carried out. One of the most widely used precast concrete elements is the precast hollow-core slab. The hollow cores are placed where the concrete would be inactive in the bending resistance design. In [12] it is concluded that two fire safety of test hollow-core slabs are worrying, fire safety of 21 and 26 minutes are measured in the tests. In the super-light element, the reinforcement is protected by the lightweight aggregate concrete and a fire safety of more than two hours has been observed [13], where the temperature of the reinforcement was 150 °. This comes at an expense of a shorter internal lever arm for the prestressed reinforcement with regards to the moment calculations, since the bottom of the element is covered by lightweight aggregate concrete.

The surface density of a concrete floor slab is generally determined by the requirements to airborne and impact sound insulation. The surface density is the most important property when obtaining airborne and impact sound insulation [14]. Secondary factors, which influence the sound insulation are the critical frequency, which is dependent on the ratio between the bending stiffness and the surface mass [15] and the loss factor. An acoustic design

of monolithic concrete elements cannot be lightweight as it is shown in [10], where the sound insulation properties are determined of a 328 kg/m^2 heavy super-light slab, this slab has the same acoustic properties, in terms of insulation ratings, as a 372 kg/m^2 heavy hollow-core slab [16].

The aim of the present work is to describe the implementation of super-light slab elements for the first commercial project involving a super-light structure. Modifications have been made to the original design of a super-light slab element in order to comply with the architectural features of the footbridge, several known technologies have been implemented in the design of the precast super-light footbridge elements.

2. Indoor Pedestrian Bridge

The super-light slab elements have been used in a 3-storey tall building with a plan area of 2000 m^2. The building consists of eight towers as it is indicated in Fig. 3, where the plan of the bridges is shown. The bridges have an area of 200 m^2 at each of its two storeys.

The indoor pedestrian bridges have a rather irregular design as it is twisting through the building while connecting all towers. Several different purposes of the bridges exist. The elements marked as two and three, provide two open floor spaces with sizes 10×5 m and 8×5 m. The elements marked four, are part of cantilevered office space. The elements marked one and five are in general used as access space only.

The individual super-light elements have been designed to fit the geometry of the indoor bridge, only the open spaces are subdivided into more elements as indicated by Fig. 3. This is done since size and weight is limited by laws of public road transportation and the availability of cranes at the construction site. In general, four different kinds of supports have been used for the bridges, three point supports, and one line support. These support points are predetermined by the structural system of the building, e.g. hangers from the ceiling can only be applied where beams in the roof exist. These limitations and conditions lead to the introduction of steel beams as a secondary support structure for the elements in the open space to secure the stability of the footbridge shown in Fig. 3 as SL-B01-4.

3. Super-light Slab Element

The super-light slab elements used for the footbridges are made from two different concretes. The normal concrete is a self compacting plastic concrete

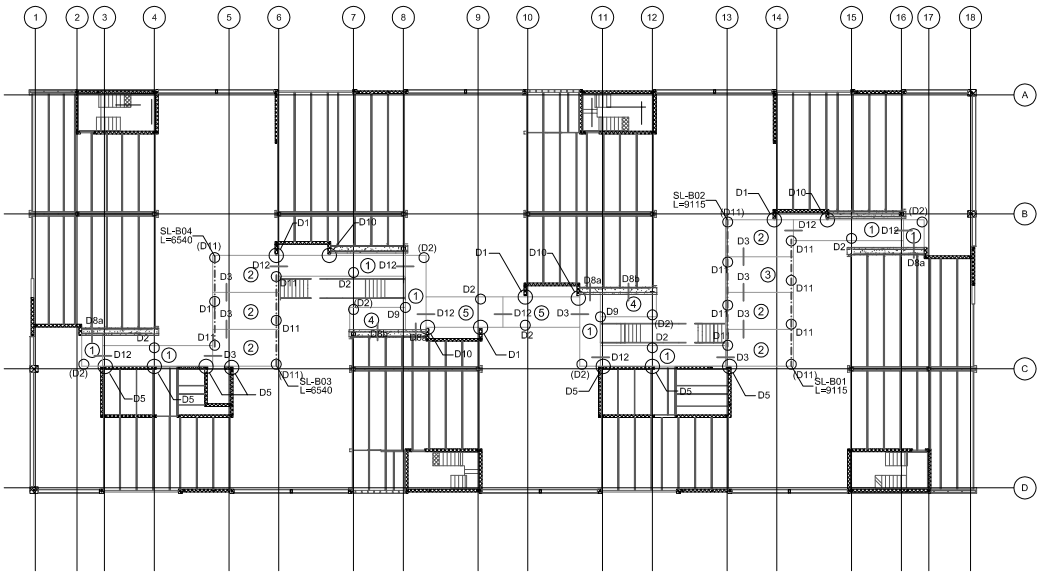

Figure 3: Plan of the building with the eight towers, which the super-light element has been integrated in along with the slab plan of the indoor pedestrian bridge

with a maximum aggregate grain size of 16 mm. The normal concrete has a compression strength of 55 MPa and an E-modulus of 38 GPa. The LWAC blocks are made from expanded clay aggregate with a compression strength of 3 MPa and an E-modulus of 3 GPa. The contribution from the LWAC blocks in regard to static calculations is not utilized in the ultimate limit state calculations, but is included in the calculations for the serviceability limit state.

The super-light slab element has been modified in size to fit the geometry of the building. The LWAC blocks are cast with a fixed box dimension of $400 \times 500 \times 185$mm, (they are not actually shaped as a box Fig. 2). The width of 400 mm is not aligned with any widths of the pedestrian bridge, which are 1500, 1750 and 2200 mm. The same goes for the length of the majority of the elements. Edge-, end- and cross-beams have been integrated into the elements to obtain the necessary custom widths and lengths. Examples of these internal beams are shown in Fig. 4 and Fig. 5.

As indicated in Fig. 6, the span between the supports and the general size of elements does not always align with the geometry of the LWAC blocks. This means that the area, where a full section of concrete is present can be significantly larger than needed. This is especially the case for the elements

Figure 4: Beam reinforcement placed in order to create edge and end beams in a super-light element

constituting the open floor space (element 2 and 3 Fig. 3), where the spacing of the pre-determined hanger supports does not fit the geometry of the LWAC blocks very well. Here, for the most extreme cases, the surface density is up to 30% larger than for the elements where the geometry is more aligned.

In Fig. 6, a typical production drawing is shown containing a number of typical details for the bridge elements. In Fig 4 and Fig. 5, the preparation of the elements prior to normal concrete being cast, is shown with the LWAC blocks, reinforcement and connection details prepared and arranged. In Fig. 7 several of cast super-light slab elements are shown along with the integration of the details regarding the modified super-light slab element,

3.1. Load-bearing, deflections and vibrations

The performance of the super-light element is described for its design requirements in the ultimate and the serviceability limit state (ULS and SLS). All the calculation methods applied here have been verified by experimental work [13]. For all calculations, the element shown in Fig. 6 has been used, its static system is explained by Fig. 8. This is the element with the longest span of 5.5 m, where $q_d = 3.8\,\mathrm{kN/m^2}$ is the dead load, $q_s = 1\,\mathrm{kN/m^2}$ is the supplemental deadload and $q_i = 5\,\mathrm{kN/m^2}$ is the imposed load.

The beam is subjected to both positive and negative moments in the special case with continuous supports. The super-light slab element is in general

Figure 5: Super-light element with LWAC blocks and reinforcement prior to normal concrete being cast

not optimal for negative moments, but inclusion of edge beams makes it possible to constitute a larger compression zone in the bottom of the slab when, it is subjected to a negative moment. For calculation of the moment capacity an ordinary plastic calculation has been applied for normal reinforced concrete [17].

$$M_{rd,+} = F_{s,+} z_+ = 135.6\,\text{kNm} \tag{1}$$

$$M_{rd,-} = F_{s,-} z_- = -66.0\,\text{kNm} \tag{2}$$

where the subscript $+$ is related to positive moment resistance and $-$ for negative, F_s is the steel yield force and z is the internal lever arm. Here the moment capacities are shown for a 1500 mm element with the amount of reinforcement as the production drawing in Fig. 6 show in the section cuts B-B and C-C. The maximum positive and negative moment design load in Fig. 8 are $M_{ed,+} = 38.0\,\text{kNm}$ and $M_{ed,-} = -43.7\,\text{kNm}$.

Calculation of the shear resistance of the super-light slab is based on the method the eurocode [19] for beams without shear reinforcement. The contribution of the lightweight aggregate concrete is ignored as its tensile strength is low. Experimental work show that this method underestimate the shear capacity of the element by approximately 20 % [13]. The shear

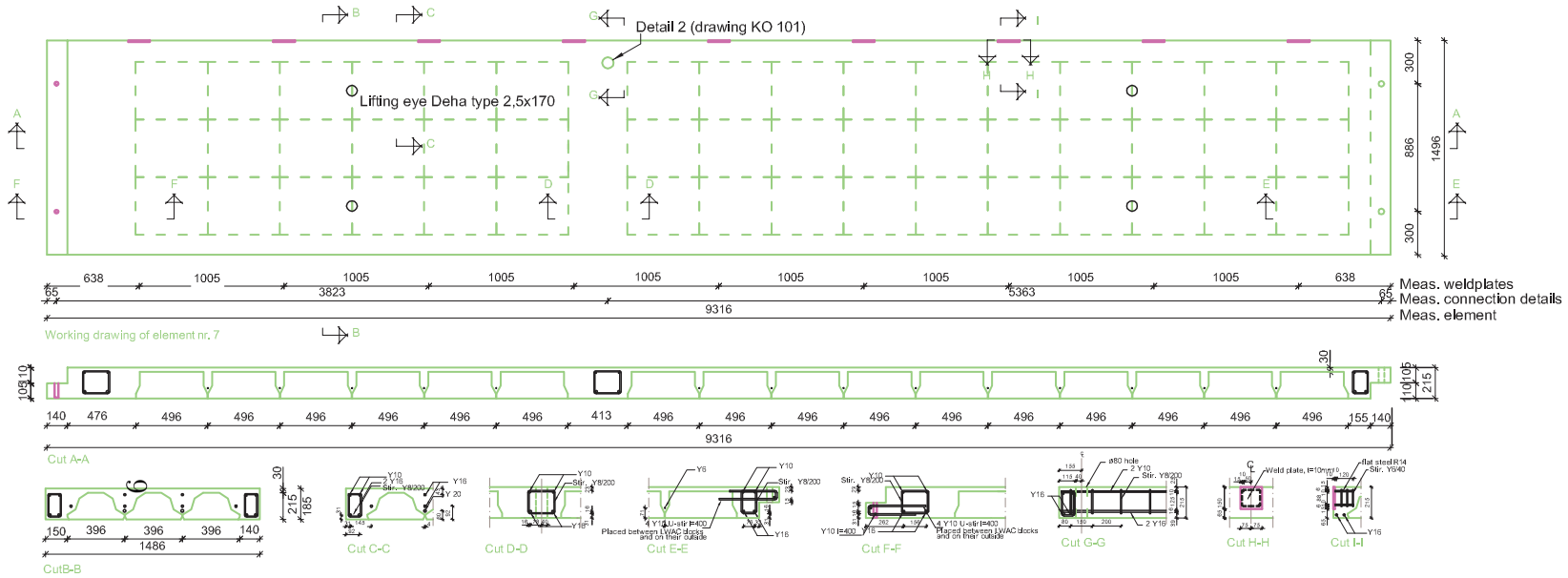

Figure 6: Production drawing of a super-light element used as a pedestrian bridge

Figure 7: Examples of several super-light slab elements.

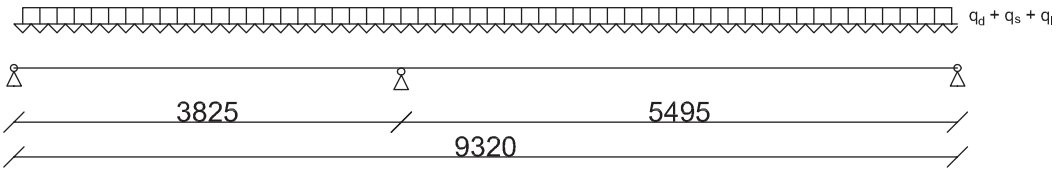

Figure 8: Static system of super-light slab element 7

design resistance is

$$V_{Rd} = \left(C_{R,c} k \left(100 \rho_l f_c \right)^{1/3} + k_1 \sigma_{cp} \right) A_{cn} = 144 \, \text{kN} \tag{3}$$

where $C_{R,c} = 0.18$, $k = 1 + \sqrt{200/d} \leq 2$ is the scale effect and $\rho_l = A_{sl}/bd$ is the degree of longitudinal tensile reinforcement in the element. The last term in the bracket is the influence from a normal force. It is zero for the slack reinforced slab. A_{cn} is the area of normal concrete in the rectangular area specified by the width and internal lever arm. Again the element in Fig. 6 has been used as a reference for calculations. The largest shear force is 88 kN at the continuous support, where a full section of normal concrete is present.

The super-light bridge elements are produced without pre-stressing. However, large deflections are avoided because the span widths are short. This is a powerful alternative as the deflection is dependent on the span length to the power of four. The expected maximum deflection is found to be $u_{max} = 14.7$ mm for the load-case in the statical system in Fig. 8, when the imposed load is only applied between the second and third support.

In general the level of vibrations is an important design requirement for footbridges. However, the super-light slab elements have short spans so their dynamic performance have been controlled as were they floor slabs, this is done by the simplified model in [20], showing that their natural frequencies f_n are high compared to the first four harmonic frequencies associated with walking. This means that the design criteria is reduced to $f_1 \geq 8$ Hz. This is verified by a simplified static system with a simply supported beam spanning 5.5 m [18]. In reality, the support conditions of the super-light slab element will have some degree of restraining moment causing the natural frequency to be higher than for the case with simple supports.

$$f_1 = \frac{\pi^2}{L_b^2} \sqrt{\frac{EI}{\mu}} = 8.65 \, \text{Hz} \tag{4}$$

where EI is the bending stiffness and μ is the mass pr. length of the beam including 20 % of the imposed load.

4. Details

Several details constituting the support for the precast super-light elements have been incorporated. The technologies used all are well-known

and have been used with concrete structures, but never in relation with a super-light structure.

4.1. Internal beams

The edge beams have widths between 75 mm and 150 mm. The beam reinforcement consists of longitudinal tension, compression bars and stirrups, which create strong frames in the elements. The reinforcement in the end beams is utilized for example in the connection detail between the super-light element consoles. The introduction of a solid section of concrete in the edge- and end-beams also makes it possible to create strong support and connection details for the point supports.

Cross beams have been applied in the super-light slab elements. They are present at continuous supports and like end beams they are supplied with beam reinforcement and hey are integrated into the element by adding space between the LWAC blocks, see Fig. 6.

4.2. Hanger connection

The most common support of the super-light slab bridges are hanger supports. An example is shown in Fig. 9. Steel rods are suspended from the ceiling at pre determined points throughout the building, D2 and D11 Fig. 3.

All hanger supports have been placed in a intersection between edge beams and cross beams or between end beams and cross beams, so that the point support force acts on a full section of normal concrete. Furthermore, the hole through the element constituting the connection is situated in a nest of beam reinforcement

A rather stiff steel support plate distributes the concentrated force ensuring that the risk of punching shear is eliminated. This would have been critical if the point support force had been applied at a lightweight aggregate block. Additionally, it increases the anchorage of the four main rebars in the edge and cross- or end beam.

4.3. Insert connection

Inserts embedded in the super-light slab elements have been used to exchange forces with adjacent walls by means of steel parts over a small gap between the wall and the pedestrian bridge see Fig. 10 for this detail. Application of embedded steel parts is possible because the edge beams provide

Figure 9: Hanger supports of super-light indoor pedestrian bridge at an element end, on the left production drawing, in the middle setup prior to casting, on the right connection in-situ

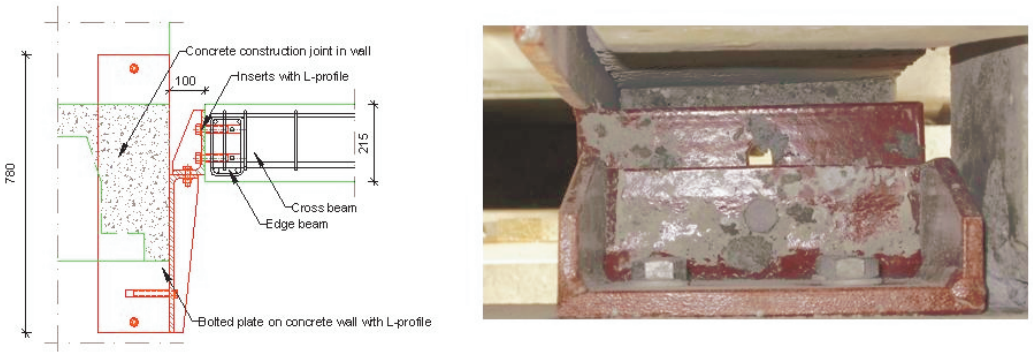

Figure 10: Insert supports of super-light indoor pedestrian bridge, on the left production drawing, on the right connection in-situ

the space necessary. Here, a sufficient amount of ordinary concrete is present to ensure that the inserts are fully anchored.

As it was the case for the hanger connection end- or cross beams are present in the element at the point connection in order to stabilize and strengthen it.

4.4. Blade connection

Elements are connected to each other by a blade connection solution as shown in Fig. 11. The connection is made sequential throughout the building with regards to the mounting of the elements. The sequence of mounting is from right to left in the plan of the building shown on Fig. 3.

The connection between the two elements is further ensured by a post-tensioned steel rod. This applies a degree of fixing providing a restraining

Figure 11: Console connection between super-light indoor pedestrian bridge, on the left production drawing, on the right connection in-situ

moment and preventing any horizontal displacement between the two elements.

No extra reinforcement or bedding material is needed to complete the connection between the two precast elements.

5. Conclusion

It is shown that the technology of super-light structures has been applied to develop a deck element, which as a first application has been used for indoor pedestrian bridges.

It is shown how the super-light elements have been slightly modified in order to accommodate custom widths of the pedestrian bridge throughout the building. This includes the introduction of edge beams being integrated into the element, which eliminate the limits caused by the fixed dimensions of the LWAC blocks.

Several special details to create the right boundary conditions of the super-light elements have been developed and implemented. These details depend on the possibility of having strong solid sections of normal concrete in the element. For this purpose concept of cross and end beams have been included in the super-light slab element design. Together with the edge beams they form the sections of normal concrete needed in order to establish the connection details.

6. Acknowledgements

For aiding of design of the Super-light pedestrian bridge and general ideas Field Project Manager Per Alan Olsen of Grontmij A/S is thanked. For aiding the study and design of the indoor pedestrian super-light bridge ABEO

A/S as owner of the technology is thanked along with Kähler A/S for production and design ideas. The Danish Agency for Science Technology and Innovation is appreciated for their support to the research in Super-light Structures.

References

1. Hertz KD, Light-weight load-bearing structures. Application no. EP 07388085.8. European Patent Office, Munich. November 2007. Application no. 61/004278 US Patent and Trademark Office. November 2007. PCT (Patent Cooperation Treaty) Application PCT/EP2008/066013, 21. November 2008. Patent January 2010.

2. Hertz KD, Super-light concrete with pearl-chains, Mag Concrete Res 61, No.8. 655-663, Thomas Telford Ltd, 2009

3. Chandra S, Berntsson L, Lightweight Aggregate Concrete Science Technology and Applications, William Andrew publishing, Norwich New York, 2002

4. FIP, FIP manuel of lightweight aggregate concrete 2nd edition, Surrey University Press, London, 1983

5. Hertz KD, Limits of spalling of fire-exposed concrete, Fire Safety J 38, 2, 103-116, 2003

6. Sanjayan G, Stocks LJ, Spalling of high-strength silica fume concrete in fire, ACI Mater J 90, 2, 170-173, 1993

7. Hertz KD, Light-weight load-bearing structures reinforced by core elements made of segments and a method of casting such structures. Application no. EP 08160304.5 European Patent Office, Munich, July 2008. Application no. 61/080445 US Patent and Trademark Office, July 2008. PCT (Patent Cooperation Treaty) Application no. PXCT/EP2009/052984, 13. March 2009. Patent January 2011.

8. Hertz KD, Bagger A, CO2 emissions from Super-light Structures, Proceedings of IASS 2011.

9. Christensen JE, Hertz KD, Brunskog J, Airborne and impact sound transmission in super-light structures, Proceedings of Inter-Noise 2011.

10. Christensen JE, Hertz KD, Brunskog J, Simulation of flanking transmission in super-light structures for airborne and impact sound, Proceedings of Inter-Noise 2012.

11. Generel building code 2008 Denmark(Bygningsreglementet 2008 in Danish), Energi styrelsen, 2008

12. Andersen NE, Lauridsen DH, Danish Institute of Fire Technology Technical Report X 52650 Part 2Hollow Core Concrete Slabs, DIFT, Denmark, 1999, http://www.dbi-net.dk/media/2d18a8346b6c4006b1e4accb3871a9b6.pdf

13. K.D. Hertz, J.E. Christensen and N.A. Castberg, Super-light concrete decks, To be published, Department of Civil Engineering at the Technical University of Denmark, Kgs Lyngby, Denmark,

14. I.L. V'er, C. I. Holmer, Interaction of sound waveswith solid structures, in: L.L. Beranek, Noise and vibration control, INCE, 1988, pp. 270-357

15. L. Cremer, M. Heckl, E.E. Unger, Structure-Borne Sound, second ed., Springer-Verlag, 1973

16. B. Christensen, BEF Bulletin No 1 - July 2012 Lydisolation for tungt byggeri af beton- og letbetonelementer - eksempelsamling (Sound insulation for heavy construction of concrete and lightweigth concrete elements - collection of examples), Betonelementforeningen, 2012 http://www.bef.dk/files/DanskBeton/%C3%98vrige%20publikationer/Bulletin%20no%201%20-%20med%20beregningsbilag.pdf

17. M.P. Nielsen, L.C. Hoang, Limit analysis and concrete plasticy, third edition, CRC Press Taylor & Francis group, 2010

18. Teknisk Ståbi 18. udgave, Nyt Teknisk Forlag, 2004

19. Eurocode 2: Design of concrete structures - Part 1-1: General rules and rules for buildings, CEN, 2004

20. Eurocode 1: Design of concrete structures - Part 1-1: General rules and rules for buildings, CEN, 2004